Development of Criteria for Flameholding Tendencies within Premixer Passages for High Hydrogen Content Fuels

Final Report

Reporting Period: 10/1/2011—12/30/2014

Prepared By: Elliot Sullivan-Lewis and Vincent G. McDonell

Date of Report: December 2014

DOE Award #: DE-FE0007045

University of California

Irvine, CA 92697-3550

DISCLAIMER

ABSTRACT

Due to increasingly stringent air quality requirements stationary power gas turbines have moved to lean-premixed operation, which reduces pollutant emissions but can result in flashback. Flashback can cause serious damage to the premixer hardware. Curtailing flashback can be difficult with hydrocarbon fuels and becomes even more challenging when hydrogen is used as the fuel. The two main approaches for coping with flashback are either to design a combustor that is resistant to flashback, or to design a premixer that will not anchor a flame if flashback occurs. Even with a well-designed combustor flashback can occur under certain circumstances, thus it is necessary to determine how to avoid flameholding within the premixer passageways of a gas turbine. To this end, an experiment was designed that would determine the flameholding propensities at elevated pressures and temperatures of three different classes of geometric features commonly found in gas turbine premixers, with both natural gas and hydrogen fuel.

Experiments to find the equivalence ratio at blow off were conducted within an optically accessible test apparatus with four flameholders: 0.25 and 0.50 inch diameter cylinders, a reverse facing step with a height of 0.25 inches, and a symmetric airfoil with a thickness of 0.25 inches and a chord length of one inch. Tests were carried out at temperatures between 300 K and 750 K, at pressures up to 9 atmospheres. Typical bulk velocities were between 40 and 100 m/s. The effect of airfoil's angle of rotation was also investigated. Blow off for hydrogen flames was found to occur at much lower adiabatic flame temperatures than natural gas flames. Additionally it was observed that at high pressures and high turbulence intensities, reactant velocity does not have a noticeable effect on the point of blow off due in large part to corresponding increases in turbulent flame speed. Finally a semi empirical correlation was developed that predicts flame extinction for both natural gas and hydrogen flames.

TABLE OF CONTENTS

LIST OF FIGURES

LIST OF TABLES

EXECUTIVE SUMMARY

Strict air quality requirements have driven stationary power gas turbines towards lean-premixed operation, where the fuel and air at a fuel-lean fuel to air ratio are mixed prior to entering the combustor. However, mixing the fuel and air prior to the combustor creates the possibility of flashback, which is when the flame propagates upstream of the combustor into the premixing zone. This often results in severe damage to the engine. While preventing flashback is challenging when engines are operated on traditional fuels, like natural gas, much higher reaction rates mean that preventing flashback becomes even more difficult when engines are operated on fuels with a high hydrogen content. The major goal is to develop criteria for the flameholding tendencies of high hydrogen content fuels in the wakes of features typical of a gas turbine premixer at elevated temperatures and pressures, thus mitigating damage associated with flashback. For this experiment, four flameholders have been tested: a 0.25 inch diameter cylinder, a 0.5 inch cylinder, a symmetric airfoil with a frontal width of 0.25 inches and chord length of 1.0 inch. Tests were carried out at temperatures between 80°F (300 K) and 900°F (755 K), though the majority were performed between 500°F (533 K) and 800°F (700K). Experiments were between three and nine atmospheres. For each temperature-pressure combination, tests were typically conducted with free stream velocities between 40 and 100 m/s. The effect of airfoil's angle of rotation was also investigated. Laser Doppler velocimetry was used to measure the velocity profile at the entrance to the test section and verify that the flow was fully developed. Also, turbulence levels were quantified and compared to empirical correlations. Generally, it was observed that all of the test features had similar flameholding propensities. The results of the reacting experiments were compared against existing blow off correlations. All of correlations that were investigated were found to be inadequate in one way or another. The most prominent discrepancy was the inability of any one correlation to accurately predict the behavior of both natural gas and hydrogen flames. Based on the poor agreement between the data of this experiment and existing correlations a new correlation was developed based on turbulent flame propagation rates that accurately describes the current experimental data and captures the stochastic nature of blow off. The major conclusions of this study are as follows.

Adiabatic flame temperature should be used as the characteristic temperature to describe blow off. Changes in inlet temperature will affect the equivalence ratio at blow off. Increasing inlet temperature results in lower equivalence ratios at blow off. Decreasing inlet temperature has the opposite effect. However, in this experiment, for a given flame holder and fuel type, the point of blow off occurs at a specific adiabatic flame temperature, regardless of combination of inlet temperature and equivalence ratio used to achieve that particular flame temperature.

Velocity doesn't affect equivalence ratio at blow off when pressure or turbulence magnitudes are high. Turbulent flame speeds correlations are generally composed of a laminar flame speed term and a turbulence magnitude term, typically taking the form: $S_T=S_L+ku'$. As pressure increases, laminar flame speeds decrease along with the contribution of laminar flame speed towards turbulent flame speed. As velocity increases, the magnitude of the turbulent velocity fluctuation increases along with the contribution of the turbulent component of turbulent flame speed. When turbulent flame speeds are high, any changes in the velocity of the flow is compensated by an increase in turbulent flame speed, which allows the flame to stay stable. When turbulent flame speeds are low, and at lower pressures this is not the case due to the much larger role of laminar flame speed. When velocity increases, the increase in turbulent flame speed solely due to turbulence is not enough to maintain stability, so laminar flame speed must increase in order to maintain a stable flame. This can only be achieved by shifting the reactant mixture closer to stoichiometric.

Hydrogen flames can anchor in boundary layer of streamlined bodies. This is a fundamentally different mechanism than for bluff bodies with recirculation zones. Despite the lack of an appreciable recirculation zone, streamlined bodies can still have flame anchoring. If the length is long enough the boundary layer can grow larger than the quenching distance. When there are regions outside of the quenching distance with velocities lower than the flame propagation rate, a flame can be stabilized. Hydrogen flames are especially capable of this due to hydrogen's much higher flame propagation rates and narrower quenching distances Flameholding can be prevented on streamlined bodies by keeping the length as short as possible to minimize boundary layer growth.

Product of ST, dilation ratio, and (1-B) correlates well with bulk velocity at blow off. The wake serves as a point where hot combustion products can be stored for a long enough period of time to and provide an ignition source for the incoming reactants. The amount of heat transferred is proportional to the temperature in the wake and also to the amount of time that the reactants spend adjacent to the wake. The heat transfer rate from the wake to the free stream is captured by the dilation ratio. While (1-B) term captures the residence time effect.

Flame extinction is stochastic event. While the majority of work on the subject of flame holding and blow off seem to characterize blow off as an exact, repeatable point. The results of this study show that the exact point of blow off cannot usually be predicted exactly due to the interaction of the many variables that influence the behavior of the flame. Rather, blow off can be analyzed statistically with a probability density function. In this experiment the onset of blow was found to occur when the product of turbulent flame speed, dilation ratio, and one minus the blockage ratio is less than 0.375 times the bulk reactant velocity. Blow off becomes increasingly more likely as that product approaches 0.150 times the bulk velocity.

Turbulent flame regime has a significant effect on how flames respond to turbulence. In order for flame holding correlations to accurately predict the behavior of flames within a gas turbine, they must be based on flames within the same turbulent flame regime. Unlike data from most other studies on flameholding, the data obtained during this study was from the thin-reaction-zones regime, which is representative of gas turbine flames, and thus can be used to predict flame behavior within a gas turbine.

NOMENCLATURE

$A_{Channel}$	Area of test channel
$A_{Feature}$	Frontal area of test features
A_L	Laminar flame sheet surface area
A_T	Turbulent flame sheet surface area
ATM	Atmosphere
B	Blockage Ratio
D	Bluff body characteristic diameter
Da	Damköhler Number
D_H	Hydraulic diameter
LDV	Laser Doppler Velocimetry
L_T	Turbulence length scale
P	Absolute pressure
Re	Reynolds Number
S_L	Laminar Flame speed
S_T	Turbulent Flame Speed
t_{Res}	Wake residence time
T_{Static}	Temperature of static gas
T_{Total}	Temperature of gas at stagnation point
T_{Burned}	Temperature of combustion products
$T_{Unburned}$	Temperature of reactants
U	Average velocity
u’	Root mean square turbulent velocity fluctuation magnitude
δ	Boundary layer momentum thickness
δ_{Flame}	Flame sheet thickness
Θ	Flame front angle

Chapter 1 -Introduction

1.1 Overview

Strict air quality requirements have driven stationary power gas turbines towards lean-premixed operation, where the fuel and air at a fuel-lean fuel to air ratio are mixed prior to entering the combustor. Lean-premixed operation maintains low combustion temperatures for the same combustor exit temperature, resulting in decreased pollutant emissions while maintaining engine efficiency. However, mixing the fuel and air prior to the combustor creates the possibility of flashback, which is when the flame propagates upstream of the combustor into the premixing zone. This often results in severe damage to the engine. Furthermore, in order to increase engine efficiency, current gas turbines are being operated at higher combustor inlet temperatures and pressure ratios. Both increases in pressure and temperature are known to increase flashback propensity. While preventing flashback is challenging when engines are operated on traditional fuels, like natural gas, much higher reaction rates mean that preventing flashback becomes even more difficult when engines are operated on fuels with a high hydrogen content. Hydrogen containing fuels are gaining significant interest because they can be generated from a variety of sources, including both conventional sources like natural gas and coal, as well as renewable sources, such as biomass gasification, and renewable powered electrolysis of water. Consequently, efforts must be undertaken to cope with the possibility of flashback. The two main approaches for coping with flashback are either to design a combustor that is resistant to flashback, thus preventing flashback from occurring, or to design a premixer that will not anchor a flame if flashback occurs.

Even the best combustor design is still prone to flashback under certain circumstances. Therefore, in order to prevent flashback related engine damage, premixing passageways should be designed to avoid flame stabilization. There is currently a high need for guidelines that can be used in the development of

premixers that do not allow flames to anchor. However, before such guidelines can be developed, it is necessary to quantify the conditions that promote flameholding under conditions relevant to gas turbines. While a considerable amount of work has been done in the past to quantify flameholding, the vast majority of these studies was not done at conditions relevant to gas turbines, end even fewer studied hydrogen as a fuel.

1.2 Goals and Objectives

The aim of this project is to address gaps in knowledge that are critical for expanding the use of hydrogen as a fuel in gas turbine power systems. The major goal is to develop criteria for the flameholding tendencies of high hydrogen content fuels in the wakes of features typical of a gas turbine premixer at elevated temperatures and pressures, thus mitigating damage associated with flashback.

The experiment focuses on characterizing the effects of five major factors on the flameholding propensities of hydrogen and natural gas. Three of these factors, pressure, temperature, and velocity, are systems factors that are controlled by the balance of the engine, and are not controlled by a combustion engineer. As a result, in this study experiments have been carried out across a wide range of pressures, temperatures and velocities, in order to provide useful data for the greatest number of engine configurations. Another factor is fuel composition and fuel-air ratio. Often, it is required to design a combustion system that will operate reliably over a range of fuel types and fuel-air ratios, however, this becomes increasingly challenging as hydrogen is introduced to the fuel. In this experiment, natural gas was tested alongside hydrogen in order to act as a control. Experimental data was also compared against existing data from the literature. Finally, the geometry of the flameholding feature was investigated. This is a factor that is entirely within the control of a combustion system engineer. Four feature types were studied for their flameholding tendencies: a 0.25 inch diameter cylinder, a 0.5 inch diameter cylinder, a reverse facing step, and an airfoil. In an engine these features

would provide the necessary turbulence to ensure complete mixing of the fuel and air. Because of this, they are very likely to provide wakes capable of stabilizing a flame.

The major goal of this project was achieved by carrying out the following tasks:

Objective 1: Build experiment apparatus

Objective 2: Obtain data from the entire experimental design space

Objective 3: Investigate validity of current predictive expressions

Objective 4: Correlate results and develop design guidelines

In the following chapters each of these objectives will be addressed. Chapter 2 will discuss background information and look at previous work that is relevant to this dissertation. Chapter 3 describes the approach that was used to carry out this experimental study. Chapter 4 outlines the experimental setup and procedure. Chapters 5 and 6 contain the results of the experiment, and the analysis of the data, respectively. Chapter 7 summarizes the findings of the dissertation.

Chapter 2 - Background and Motivation

Ground based gas turbines are a significant source of electric power generation and also provide mechanical power for a variety of applications. This is due to their high efficiency, high power density, high reliability, and ability to operate on a wide range of fuels. The move to lean-premixed operation of gas turbines in order to comply with air quality requirements results in low NOx emissions while minimizing emissions of carbon monoxide and hydrocarbons. In addition to this, to increase overall cycle efficiency, engines are being operated at higher pressure ratios and higher combustor inlet temperatures, which further exacerbates flashback for both conventional fuels and hydrogen.

Combustion of traditional fossil fuels is the most significant cause of increasing concentrations of carbon dioxide in the atmosphere, ultimately leading to climate change. Replacing fossils fuels with fuels derived from renewable sources will reduce the net emission of carbon dioxide in the atmosphere. Biomass is a renewable fuel source that can be consumed in a gas turbine engine once converted to a high-hydrogen gaseous fuel through gasification. Additionally, the increasing cost of petroleum and natural gas has made opportunity fuels more attractive. Opportunity fuels are fuels that might otherwise be considered a waste product and might include fuels like blast furnace gas, which is high in hydrogen. Alternately, coal can be gasified to form a high hydrogen fuel that can be burned in a gas turbine or gas turbine combined-cycle power plant, which have higher efficiencies than Rankine cycle plants.

As mentioned earlier, flashback is a primary concern when operating a gas turbine on a high hydrogen fuel. A significant amount of work has been done to characterize the mechanisms behind flashback, particularly for high hydrogen fuels. Increasing preheat temperature is known to increase laminar flame speeds, which correlates with turbulent flame speeds, and leads to a higher flashback propensity. In addition to this, increasing temperature decreases the quenching distance, also increasing flashback

likelihood. Because higher temperature and pressure are necessary for increased system efficiency, it is unlikely to see a reversal of this trend. Consequently, efforts must be undertaken to cope with the possibility of flashback. As mentioned before, the two main approaches for coping with flashback are either to design a combustor that is resistant to flashback, or to design a premixer that will not anchor a flame if flashback occurs. In practice both approaches are used together.

A combustor that is designed to resist flashback can be successful the majority of the time. However, even with a well-designed combustor, certain circumstances can result in flashback. These include an autoignition in the premixing section due to an unexpected change in fuel composition, or the presence of a drop of lubricating oil which may be more prone to autoignition (see Figure 2-1). Additionally, during the initial light off of the engine, pressure pulses caused by ignition can result in momentary flow reversals that cause the flame to propagate upstream to the premixing section (Koseki 2002).

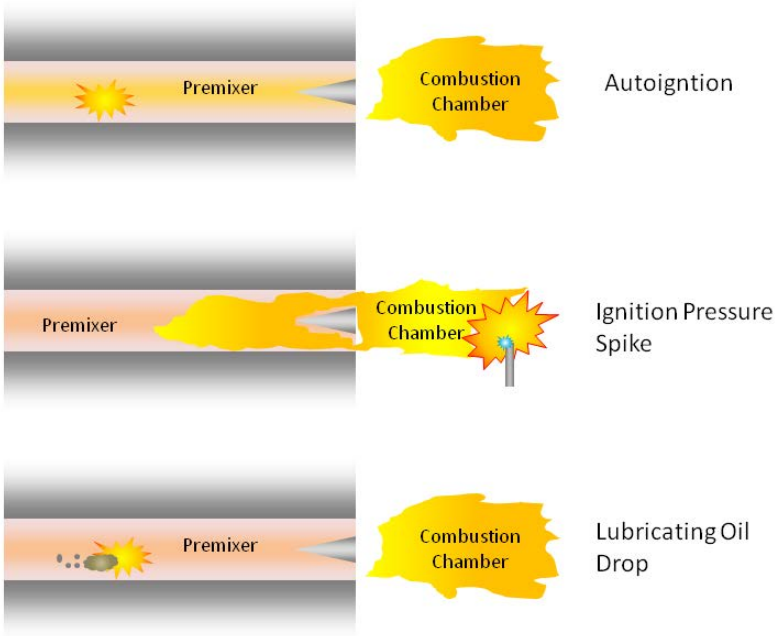

Figure 2-1: Non-Steady State Sources of Flashback

When any of these situations occur with hydrocarbon fuels, the flame is usually disgorged from the premixing section. However, the high reactivity of hydrogen can result in the flame anchoring within the premixer (see Figure 2-2). In order to design a gas turbine premixer that will not allow a flame to anchor within it, it is necessary to characterize the factors that promote flameholding under realistic gas turbine conditions, and particularly for hydrogen.

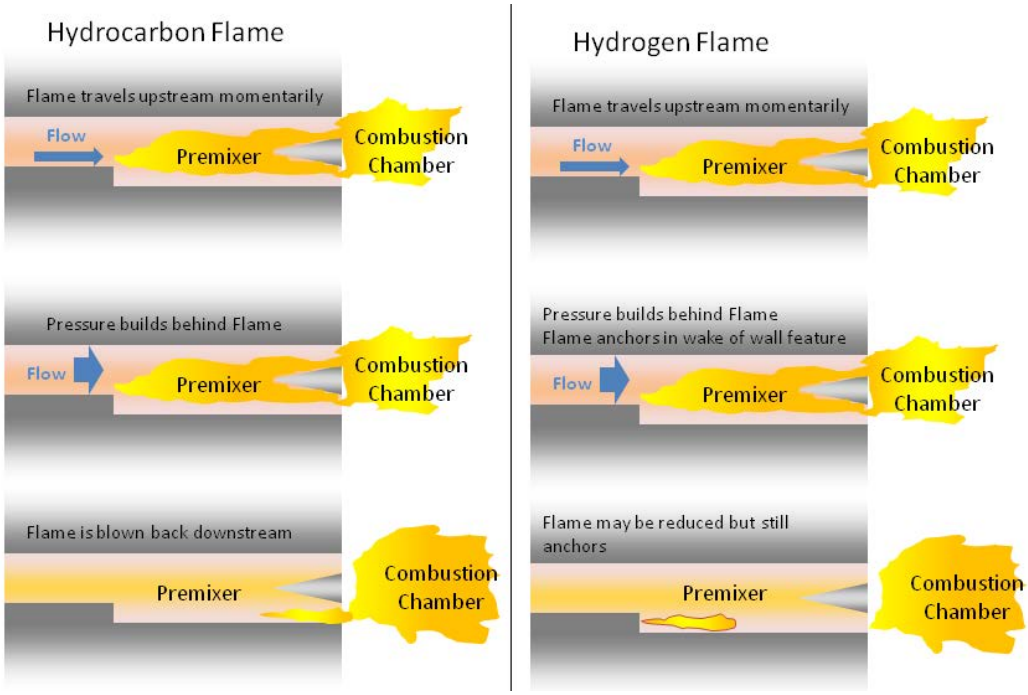

Figure 2-2: Flashback and flame anchoring of hydrocarbons and hydrogen

Current gas turbines operate at pressures between 6 and 35 atm and combustor inlet temperatures between 520 and 850K. Table 2-1 summarizes the conditions within combustors of a number of current engines. In spite of this fact, the majority of research conducted on flame holding, or even combustion

in general, within gas turbines has been done at atmospheric pressure, and much of that has been done without preheat.

Table 2-1: Gas Turbine Pressures and Temperatures (GE Energy, Solar Turbines, Siemens Gas Turbines, Alstom Gas Turbines)

Engine	Pressure Ratio	Approximate Inlet Temp (K)	Mass Flow (kg/s)
GE 6FA	15.6	667	212
GE 7FA	16.2	675	436
GE 9FA	17	684	641
GE 7EA	12.7	629	299
GE 9E	12.6	627	418
GE 6B	12.2	621	141
GE 6C	19.6	713	122
Solar Saturn 20	6.7	522	6.53
Solar Centaur 40	10	586	18.9
Solar Centaur 50	10.6	596	19.1
Solar Taurus 65	15	660	21
Solar Taurus 70	17.6	691	26.9
Solar Mars 100	17.7	692	42.6
Solar Titan 130	17.1	685	49.8
Solar Titan 250	24	756	68.2
Siemens SGT-100	14	647	20.6
Siemens SGT-200	12.2	621	29.3
Siemens SGT-300	13.7	643	30.2
Siemens SGT-400 (12.90 MW)	16.8	682	39.4
Siemens SGT-400 (14.33 MW)	18.9	706	44.3
Siemens SGT-500	13	633	97.9
Siemens SGT-600	14	647	81.3
Siemens SGT-700	18.7	703	95
Siemens SGT-750	23.8	755	114.2
Siemens SGT-800 (47.5 MW)	20.4	721	132.8
Siemens SGT-800 (50.5MW)	21.1	729	134.2
Alstom GT26	35	844	692
Alstom GT24	35.4	847	505
Alstom GT13E2 (185 MW)	16.9	683	565
Alstom GT13E2 (188 MW)	17.5	690	548
Alstom GT13E2 (203 MW)	18.2	698	624
Alstom GT11N2	15.9	671	400
Range	6.7-35.4	522-847 K (479-1065 F)	6.53-692 kg/s (14.4-1520 lb/s)

The premixing section of a gas turbine has several important roles. The primary role is to establish a homogeneous mixture of the fuel and air before entering the combustion chamber. The premixer also establishes the necessary flow structure to create a stable flame within the combustion chamber.

Premixers consist of a duct, one or more fuel injection points, mixing elements that ensure sufficient mixing of the fuel and air, and flow conditioners that stabilize the flame inside the combustor. In addition to enhancing mixing and conditioning the flow for the combustion chamber, geometry also plays a significant role in whether or not a flame can be anchored within the premixer. An effective premixer will provide rapid mixing of the fuel and air while simultaneously preventing flames from anchoring in the event of flashback. Unfortunately the geometric features that enhance mixing by increasing turbulence tend to promote flameholding by increasing the turbulent flame speeds of the reactant mixture as well as providing large recirculation zones where flames can stabilize. Features commonly found in premixers include steps, cylinders, flat struts/vanes, and airfoils. Steps are often found where two piece of metal are joined in a lap joint. Because this is usually a result of the designer's choice of construction rather than a necessary feature for effective operation of the premixer, these features can be avoided relatively easily. Cylinders have traditionally been used either as points of fuel injection or for internal structural support. Because cylinders tend to have large wakes behind them, at the present time cylindrical supports and fuel injection points have largely been phased out of engines where flashback is of concern. While flat struts/vanes and airfoils may seem like obvious choices for premixer internal structures due to their narrow profile and limited recirculation zones, these features are often somewhat long. This can lead to non-trivial boundary layer growth, which can also allow a flame to anchor. One example of a premixer with many of these features is from a Solar Turbines engine (Figure 2-3). It contains three of these types of features (cylinders, airfoils and steps) and thus, is likely to have flames anchor in the event of flashback.

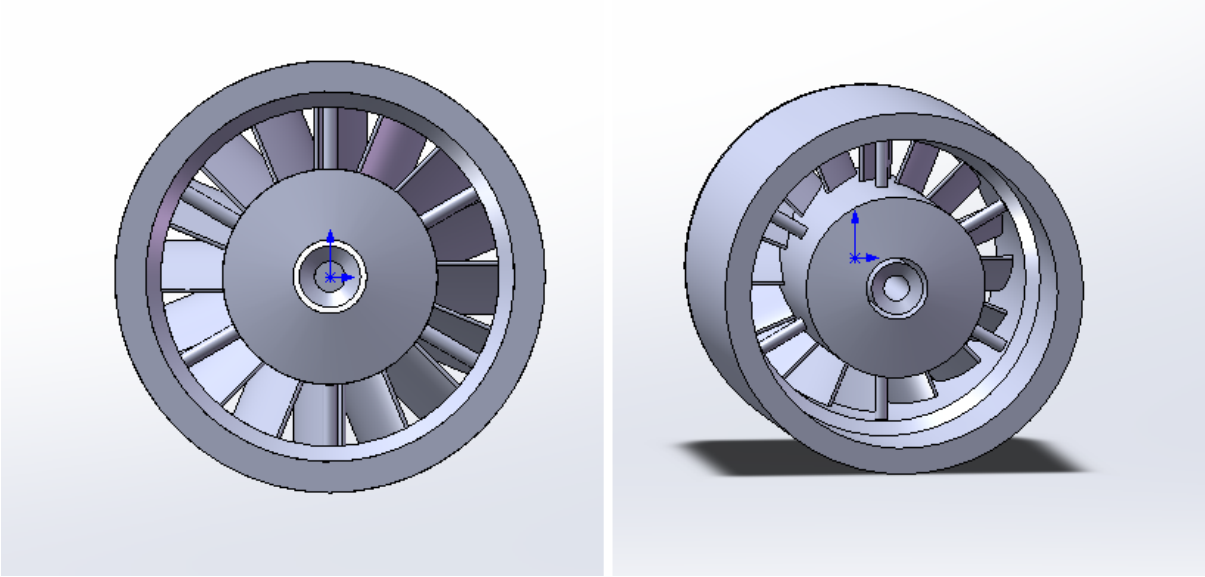

Figure 2-3: Rendering of Solar Turbines premixer showing step, cylinders and airfoils

Other manufacturers have premixing passages with fewer geometric features. These are less likely to anchor a flame. One example is from the GE DLN 2.6+, which contains only airfoils (Figure 2-4). This design is likely less prone to flame anchoring due to the lack of steps and cylinders, which have large recirculation zones in their wakes.

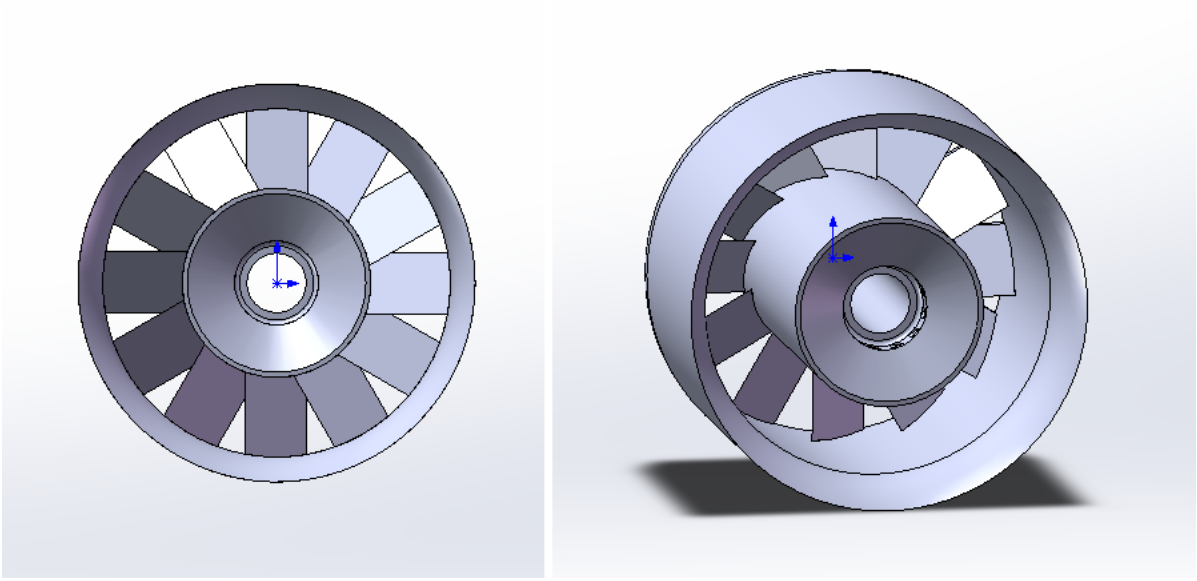

Figure 2-4: Rendering of GE premixer showing airfoils

It is worth noting that these premixers were designed for use with hydrocarbon fuels, which are significantly less prone to flashback. As a result, some of the features most likely to anchor flames can be tolerated. If these premixers were operated with hydrogen there would be a greatly increased chance of engine damage. In order to cope with much greater reactivity of hydrogen, some premixers have been developed specifically for use with hydrogen, such as the GE multi-tube injector (Figure 2-5).

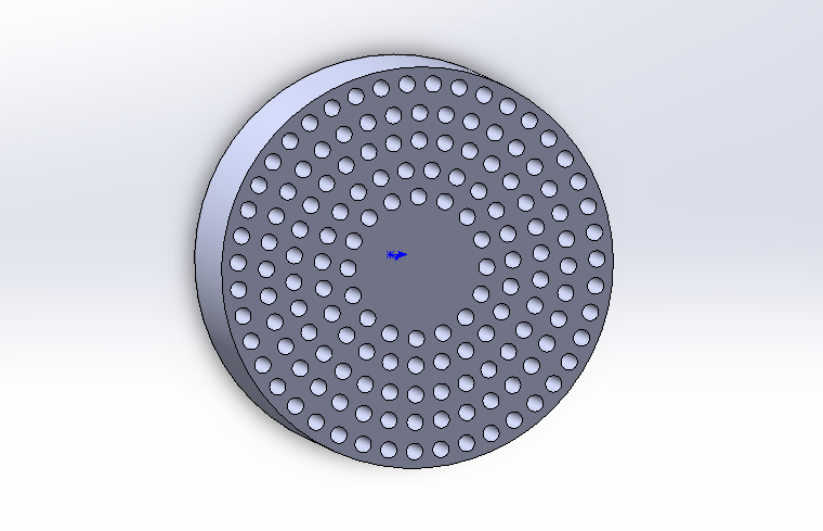

Figure 2-5: Rendering of GE multi-tube premixer

As can be seen in Figure 2-5, this design mixes the fuel and air by directing the air through narrow passages where the fuel is injected. The narrow diameter of the passages ensures proper mixing without the need for additional turbulence. Furthermore the diameter of the passages is smaller than the quenching distance of the hydrogen and air mixture, limiting the likelihood of flashback and subsequent flameholding. While this design is successful for use with hydrogen, due to the lack of flow conditioning (i.e. swirl vanes to create a center recirculation zone) it is not necessarily the most practical for use with hydrocarbon fuels. Thus, there still exists the need for a single premixer design that can be used for both hydrogen and hydrocarbon fuels. An ideal premixer would promote rapid mixing with geometries that do not have large wakes, provide sufficient flow conditioning to allow hydrocarbon flames to be stable

within the combustion chamber, while not providing so much hydrogen flames are prone to flashback In order to achieve this, the effect of geometry on flameholding must be more thoroughly understood.

2.1 Flame Properties

Flames can be anchored in several ways. If the flame propagation speed is greater than the local flow velocity, the flame will propagate upstream until it either reaches a point where the flame propagation speed is less than the flow velocity or until the flame reaches a surface that quenches the reaction. The most common means of stabilizing a flame in gas turbine combustors is to create a recirculation zone, such as in the wake of a bluff body (Figure 2-6).

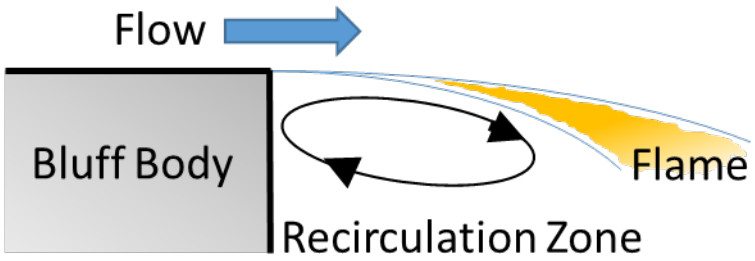

Figure 2-6: Flame stabilized by recirculation zone of bluff body

In the recirculation zone the flow, and the flame, move backwards, bringing the hot reacting mixture in contact with and igniting the fresh reactants. Flames can also be anchored within a boundary layer. Typically a flame will be quenched when it comes near a wall. The minimum distance that a flame can be to a wall without being quenched is called the quenching distance. If the velocity boundary layer grows to be larger than the quenching distance, then the flame will propagate within the boundary layer. It will continue to propagate until it there is no region outside of the quenching distance with a velocity below the flame propagation speed (Figure 2-7).

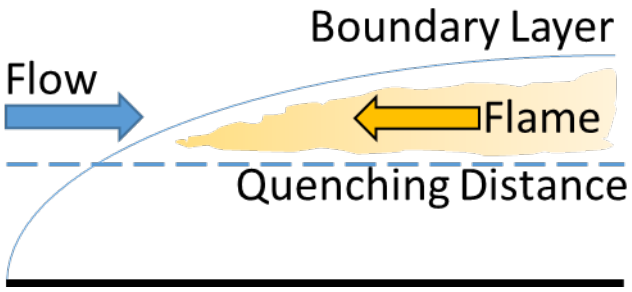

Figure 2-7: Flame stabilized in velocity boundary layer

This method is a common source of flashback in engines. When a flame anchored by another means (e.g. bluff body stabilized flame) radiates enough heat to the surface the quenching distance can be reduced until it is below the velocity boundary layer, at which point the flame can propagate upstream. This is referred to as boundary layer flashback.

Recently, low swirl burners have been developed that stabilized flames purely by matching the flow velocity to the flame propagation speed. This is achieved by creating a diverging flow field where the axial velocity decreases with distance from the burner exit. Because of this velocity decay, the flame will anchor at the point where the flow velocity is equal to the flame propagation speed (Figure 2-8). This type of flame stabilization less prone to boundary layer flashback because the flame is stabilized away from the burner rim.

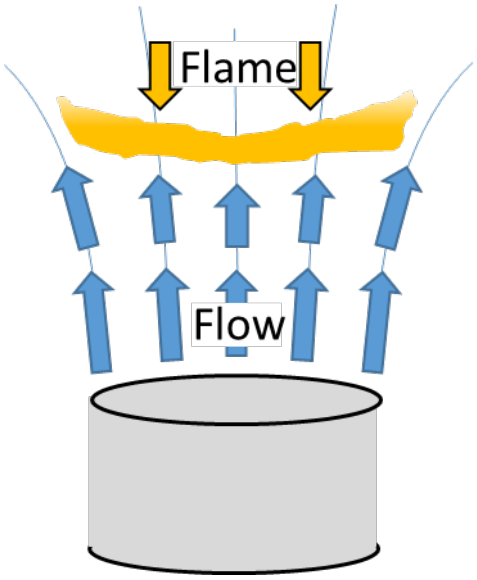

Figure 2-8: Flame stabilized with low swirl burner where flow velocity equals flame propagation speed

While these three methods have been presented here as entirely different, in practice most gas turbine combustors use a combination of all three types of flame stabilization to achieve a stable reaction.

Premixed flames can be classified in a number of ways. One of the most common is to employ a turbulent combustion regime map. Slight variations exist in the exact layout of this diagram (Figure 2-9), most notably the version by Borghi (1985) and Peters (1999).

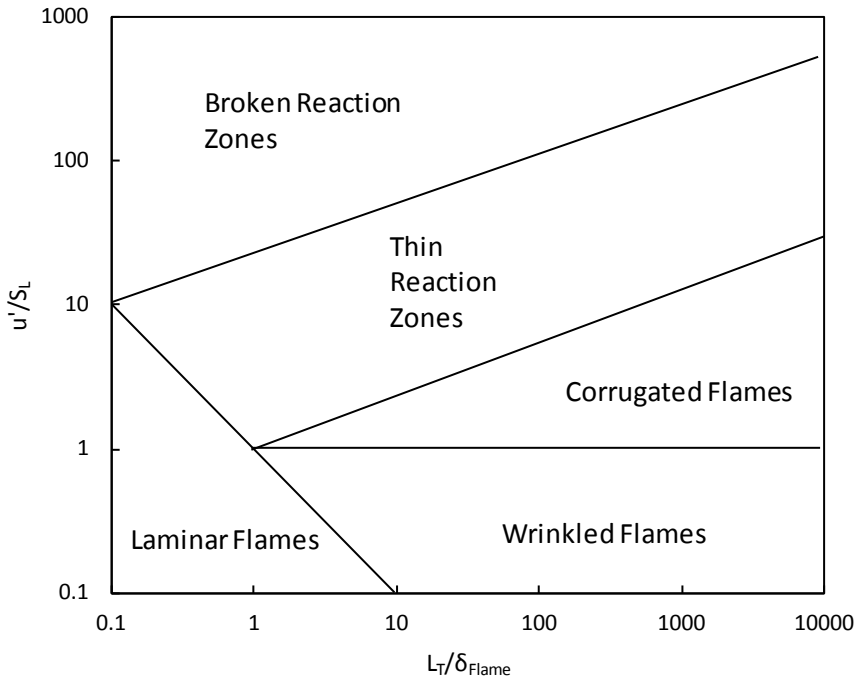

Figure 2-9: Turbulent flame regime diagram

In this diagram, the ratio of turbulence magnitude to laminar flame speed (u'/S_L) is plotted against the ratio of turbulent length scale to flame sheet thickness (L_T/δ_{Flame}). Essentially, flames can be categorized into five different regimes. In the laminar flame regime, there is very little turbulence and the flame front is smooth. This regime is separated from all others by the line where the turbulence Reynolds number is equal to one. In the wrinkled flame regime, turbulence exists, but the laminar flame speed is much greater than the turbulent fluctuation magnitude, which means that the flame front may be wrinkled slightly but remains overall unaffected. Above this is the corrugated flame regime, where the flame front is stretched and contorted due to turbulent eddies that are much larger than the thickness of the flame front. The reaction zone changes shape but the internal structure remains the same. Above this region is the thin reaction zones regime. This is the region where gas turbines tend to operate (Griebel 2005). In this region the smallest turbulent eddies can penetrate the reaction zone, altering the transfer of heat and the mixing of reactants and products. Finally, above this is the broken reaction

zones regime. In this region turbulent eddies are small enough to enter and break down the reaction zone. Local extinctions of the flame front can ultimately lead to extinction of the flame due to excessive heat loss to the reactants.

One significant factor that is relevant to flameholding is the flame propagation speed. The flame propagation speed is affected by fuel type, fuel to air ratio, temperature, pressure, and turbulence level. An important distinction must be made between the laminar flame speed and the turbulent flame speed. Both laminar and turbulent flame speeds are used as a measure of reactivity of the fuel-air mixture. Laminar flame speeds are a function of the reactant mixture properties are widely quantified for a variety of different fuels and conditions. Turbulent flame speeds are a strong function of the turbulence intensity, and a much weaker function of the reactant mixture properties. Furthermore there exist several methods of defining the turbulent flame speed: Global and local displacement speeds and global and local consumption speeds. Turbulent flame speeds are more relevant measure of mixture reactivity at gas turbine conditions. Turbulent flame speeds are much more sparely quantified at the current time.

Only two of these methods, local displacement speeds, and local consumptions speed, are suitable for bluff body stabilized flames, which do not have discreetly defined boundaries. Global consumption speeds, which are the averaged value of local consumption speed, are defined as the volumetric flow of reactants divided by the average flame front area. Because a flame area must be defined, global consumption speeds are only defined for fully enveloped flames such as jet burners (Lieuwen 2010). Global displacement speeds are defined as the averaged values of the local displacement speeds. It also requires a closed expanding flame with a defined a flame area, such as an expanding flame kernels. Never the less, even when a particular flame speed cannot be directly measured for a flame, each type of flame speed can be defined for any premixed flame as a function of measurable properties if there

exists a correlation. These flame speeds need not necessarily have similar values, nor would they be expected to. As mentioned earlier each flame speed method is simply a method of characterizing the reactivity of flame.

While there are several means of defining turbulent flame speed that can be applied to bluff body stabilized flames, the local displacement flame speed and global consumption flame speeds have been has been extensively investigated at conditions representative of a gas turbine combustor, and for both natural gas and hydrogen fuels. Bluff body flameholders are typically used for direct measurement of local displacement flame speed. By measuring the flame angle of rod stabilized, "V", flames (Figure 2-10), the local displacement flame speed can be inferred by determining the flow velocity normal to the flame front:

$$S_{T,LD} = |U| \, Sin\Theta$$

Where $|U|$ is the free stream velocity, and Θ is the angle of flame front relative to the direction of flow (Figure 2-10). While this method does allow for direct measurement of the flame speed, it is somewhat ambiguous, as the angle of the flame front is not constant.

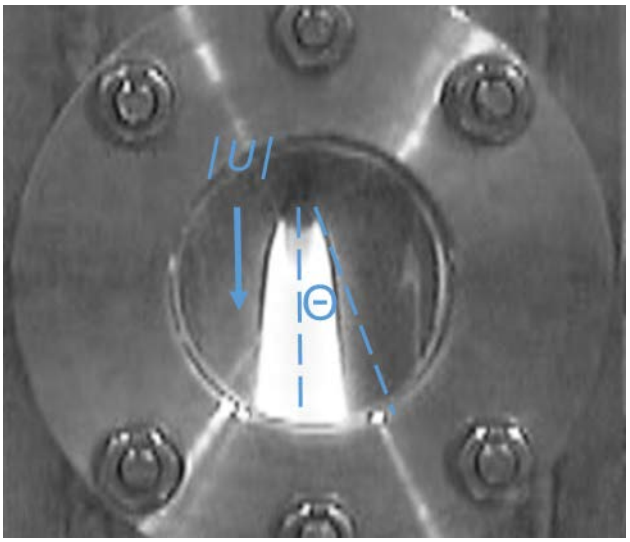

Figure 2-10: V-Flame with dimensions for determining local displacement turbulent flame speed

Early work on turbulent flame propagation by Damköhler, outlined in Driscoll (2008), suggested that for the flamelet regime where the flame front structure remains distorted but intact, the ratio of turbulent to laminar flame speed was controlled by the turbulent stretching of the flame front:

$$S_T/S_L \propto A_T/A_L$$

Where S_T and S_L are the laminar and turbulent flame speeds, and A_T and A_L are the flame front areas for turbulent and laminar flames, respectively. Taking S_L and A_L to be constants, the turbulent flame speed is proportional to the turbulent flame front area. Turbulent fluctuations stretch the flame front so that the turbulent flame area is proportional to the root mean square of the turbulent velocity fluctuation, u'. This leads to the conclusion that turbulent flame speed is proportional to turbulent velocity fluctuation magnitude:

$$S_T \propto u'$$

Two studies by Cheng et al. (2008, 2008) observed that the turbulent local displacement flame speed for both methane and hydrogen are linearly dependent on the turbulent fluctuation magnitude of the flow. The relationship

$$S_T = S_L + K \cdot u'$$

Where S_T is the turbulent local displacement flame speed, respectively, K is an empirical constant, and u' is the root mean square turbulent fluctuation magnitude. It was observed that the value for K was approximately 2.1 for hydrocarbon flames, and 3.15 for hydrogen flames. At low turbulence levels, the flame speed simply becomes the laminar flame speed. Note that there was no observed effect of inlet pressure, temperature, or fuel to air ratio outside of their effect on laminar flame speed, which at high turbulence levels contributes somewhat negligibly to the turbulent flame speed.

Beerer et al. (2012) attempted to extend the correlation of Cheng (2008) to elevated pressures. It was found that while turbulent flame speed remained linearly dependent on turbulent fluctuation magnitude, that the experimental data was not consistent with the Cheng's correlation. Once again, the only relevant factor affecting turbulent flame speed was the turbulence level, and not temperature, pressure or fuel to air ratio.

Beerer et al. investigated turbulent local displacement speeds for premixed hydrogen and methane fuel mixtures at elevated temperatures and pressures using a low swirl burner. In this study, it was observed that turbulent flame speed was not significantly affected by pressure, inlet temperature of fuel to air ratio. It appears that the turbulent displacement flame speed was only a function of turbulence levels; flame speed was found to be linearly proportional to the root mean square of the turbulent velocity fluctuation magnitude. Hydrogen flames were found to have a turbulent flame speed of approximately twice that of methane. Mixtures of 90% (by volume) hydrogen and 10% methane consistently had flame speeds of 4.2 times the turbulent fluctuation magnitude, while methane flames had flame speeds of 2.1

times the turbulent fluctuation magnitude. The correlations did not include a term for the laminar flame speed, indicating that there may exist significant error at low turbulence levels. However, such low turbulence levels are not of interest at conditions relevant to gas turbines.

Venkateswaran et. al (2011) studied the turbulent global consumption speeds for mixtures of hydrogen and carbon monoxide as well as methane. It was also observed that there was a linear dependence between turbulent consumption speed and turbulence intensity. Venkateswaran et. al (2014) extended the turbulent consumption speeds for high hydrogen fuels for pressures up to 20 atm not only concluding that the linear relationship between turbulence intensity and global consumption speed still held, but also finding that the effect of pressure is to increase turbulent consumption speed.

2.2 Previous work

A considerable amount of work has been done to assess the flameholding ability of features specifically designed to hold flames. Early work performed on bluff body flame stabilization was compiled by Longwell (1953). The general conclusions of Longwell's study were that increasing bluff body size, and any changes that increase laminar flame speed tend improve flameholding. Later work by Williams (1957) investigated the effects of boundary layer growth of the entrainment of a propane-air mixture into the wake of a semi-circular bluff body. In this study, the boundary layer was removed by means of a vacuum source within the trailing edge of the bluff body. It was determined by measuring the composition of the bluff body wake that flame anchoring was achieved by recirculation of hot combustion products into the wake. It was also observed that increasing the boundary layer thickness improved flame stability, implying that the length of a bluff body can promote flameholding, as can the width.

Barrère and Mestre (1954) identified that the aerodynamic width is just as important to flameholding as the geometric width of a flameholder. In their study the lean extinction limits were found for three V-

gutter flameholders with different included angles but with the same width. It was found that with by increasing the included angle that the flameholding propensity was increased, due to an increase in the size of wake, which increases residence time and allows for flames with lower chemical times (i.e. leaner mixtures) to be stabilized. This was one of the earliest studies to suggest the effect of wake size was the dominating factor for flameholding, rather than simply the geometric width. However, for a given shape of flameholder, the wake size will be proportional to the geometric width.

The size of wake is also controlled by the mixture velocity. Roberds et al. (1989) investigated the effect of flow velocity on the residence time in the wake of bluff body in free stream at atmospheric pressure and velocities from 45 to 95 m/s. In their study, carbon dioxide was used as a tracer gas injected upstream of the bluff body. They carbon dioxide flow was shut off and an infrared laser and detector were used to measure the time for the carbon dioxide to disappear from the wake region of the bluff body. It was observed that residence time within the wake region decreased with velocity, but not inversely (Figure 2-11). Implying that the wake length increases, but not linearly, with velocity.

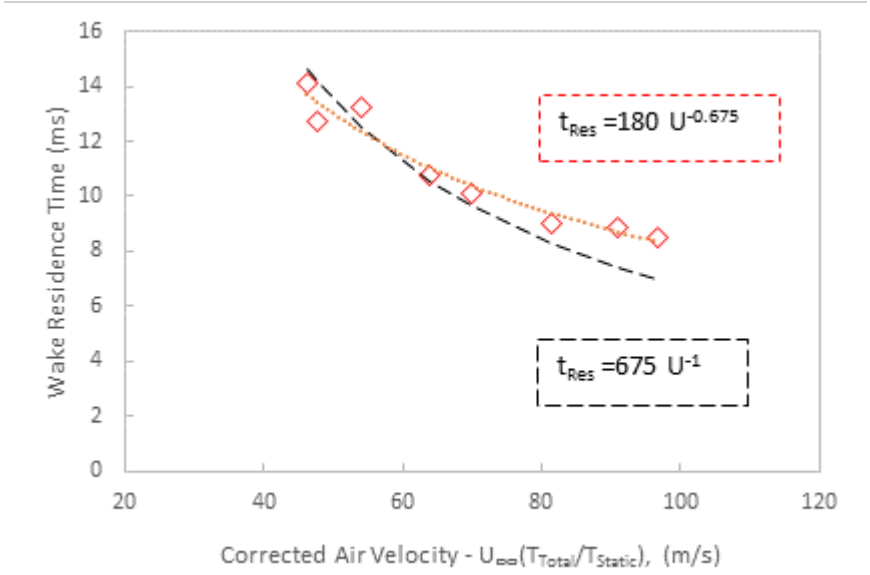

Figure 2-11: Wake residence time as a function of air velocity. Reproduced from Roberds et al. (1989)

Potter and Wong (1958) studied the effects of pressure on the blow off velocity for stoichiometric propane-air flames at room temperature stabilized in the wake of cylindrical flameholders in rectangular ducts. In this study pressure was varied from 0.3 to 0.7 atm. Velocities ranged from 30 to 130 m/s. Four flameholder diameters, ranging from 9.5mm to 25mm, were studied. Two rectangular ducts were studied, a 25mm by 76mm duct, and a 76mm by 76mm duct. Potter and Wong found that blow off velocity was proportional to flameholder diameter, and that blow off velocity generally increases proportionally to pressure raised to a power between 1.3 and 2.5. In all cases increasing pressure increased the velocity at blow off.

Roffe and Venkataramani (1978) investigated several different types of V-gutter, perforated plate, and reverse cone flameholders with the aim of quantifying the emissions, lean blow off limit and flashback limit for each. In this experiment propane was used as the fuel and velocities were varied from 20 to 35 m/s. Inlet temperatures were around 800K and pressure was 10 atm. Most of the flameholders were tested at two blockage ratios of 70 and 80%. It was observed that the lean blow off limit did not change with velocity or bluff body type; lean blow off consistently occurred around an adiabatic flame temperature of 1700K. The fact that lean blow off did not vary with velocity is contrary to many other studies on flameholding conducted at lower pressure, implying that pressure does have a measurable effect of flameholding.

Later work by Rizk and Lefebvre (1983) investigated reverse cone flameholders as well as wall mounted angled struts for flameholding ability. It was found that the wall mounted baffles of the same blockage ratio had greater flameholding abilities, attributed to higher residence times (lower velocities) in the boundary layer. Additionally Stwalley and Lefebvre (1987) investigated different configurations of V-gutter flame holders. It was found that the flameholding was decreased by removing material from the

trailing edge of the bluff body; irregular bluff body shapes producing less stable recirculation zones than regularly shaped bodies.

Yamaguchi (1985) measured the blow off limits for rod stabilized propane-air flames. These experiments were performed at room temperature and atmospheric pressure. Flow was contained within a 22mm by 60mm rectangular test section. Three flameholder arrangements were studied: a single cylinder with a diameter of 24mm, two cylinders with diameters of 12mm, and three cylinders of 8mm. Each configuration maintained a blockage ratio of 0.4. Yamaguchi observed that increasing the number of rods lead to slightly higher blow off velocities at very lean and very rich conditions, while severely lowering blow off velocities for fuel-air mixtures near stoichiometric.

Regarding flameholding of wall features, some of the most relevant work done on this subject was done by Choudhury and Cambel (1962) who investigated the flameholding of wall recesses. This study suggests that the mechanisms behind wall recess flameholding are the same as that for a bluff body. A Damköhler type function was developed relating to free stream velocity at blow off, flame front thickness. When the free stream velocity normal to the flame front exceeded a calculated turbulent flame speed, the flame would blow off. Unfortunately, this method requires knowledge of the flame front angle and flame front thickness a priori, making it impractical for predictive applications. Furthermore, this experiment gives no specific dimensions are given for the wall recess flameholders that were studied.

Fetting et al. conducted a study of comparing the flameholding abilities of cylindrical and streamlined bodies. Propane was used as the fuel and was fully premixed with air well upstream of the flameholders. In their experiments cylindrical flameholders with a frontal width of 5mm and three streamlined bodies with frontal width of 5mm were compared for their flameholding abilities. It was observed that when the length of the streamlined body was short (the included angle of the trailing edge was large), that the

streamlined bodies behaved similarly to the cylinder. When the streamlined body was long (the included angle of the trailing edge was small) that the streamlined bodies performed much worse than the cylinder. This study confirms the role of flow separation in the stability of the flame. When the flow is separated (cylinder and short streamlined body), recirculation zones occur which transfer hot products forward to ignite the fresh mixture. With the long streamlined body, flow separation does not occur, removing the large recirculation zones, instead barely stabilizing the flame due to the growth of the boundary layer.

Filippi and Fabbrovich-Mazza (1960) conducted almost identical tests to Fetting et al., but in addition to testing propane, also performed tests with methane. Tests conducted with the exact same flameholder configuration, that methane and propane had significantly different stability curves. While it is usually taken for granted that all hydrocarbon fuels have similar flame characteristics, the data from this experiment show that for shorter chain hydrocarbons (C1-C3) that this might not be the case. This is shown in Figure 2-12 It is worth noting is that there is not complete agreement between the data of Fetting et al. and the propane data of Filippi and Fabbrovich-Mazza. This suggests a measurable degree of uncertainty that exists in data from this time period, which is likely a result of measurement limitations either in fuel/air flow rates, or possibly in fuel composition.

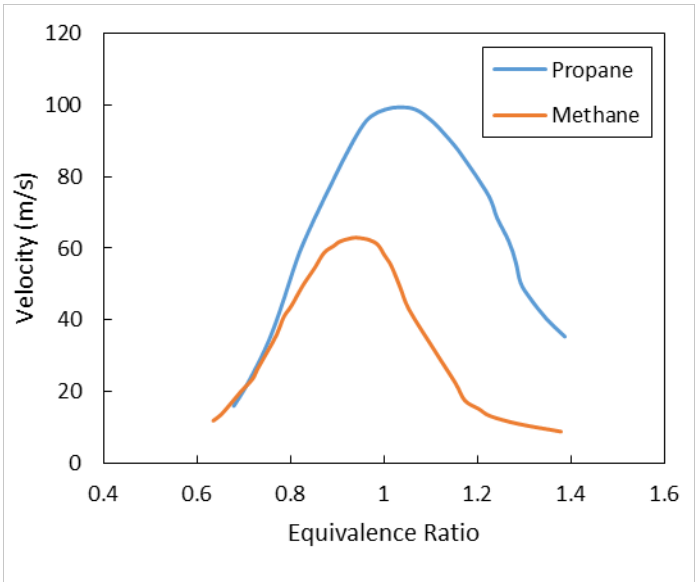

Figure 2-12: Blow off velocity as a function of equivalence ratio for methane and propane. Reproduced From Filippi and Fabbrovich-Mazza (1960)

Lefebvre and Ballal (1976) investigated the effects pressure, turbulence intensity and fuel type on quenching distance. Quenching distance was determined by igniting the reactant mixture with varying levels of spark energy and distance between the electrodes. The distance corresponding to the minimum ignition energy was defined as the quenching distance. Lefebvre and Ballal found that increasing turbulence intensity tended to increase the quenching distance due to increased turbulent thermal diffusion (Figure 2-13). Furthermore, they found that quenching distance decreased with increasing pressure and any changes that increased laminar flame speed. This has implications for wall-recess flameholders, which, unlike bluff body flameholders, transfer a significant amount of energy to the wall; It implies that if all else is held constant, at higher turbulence intensities a wall-recess flameholder may have significantly worse performance than a bluff body flameholder with similar sized wake.

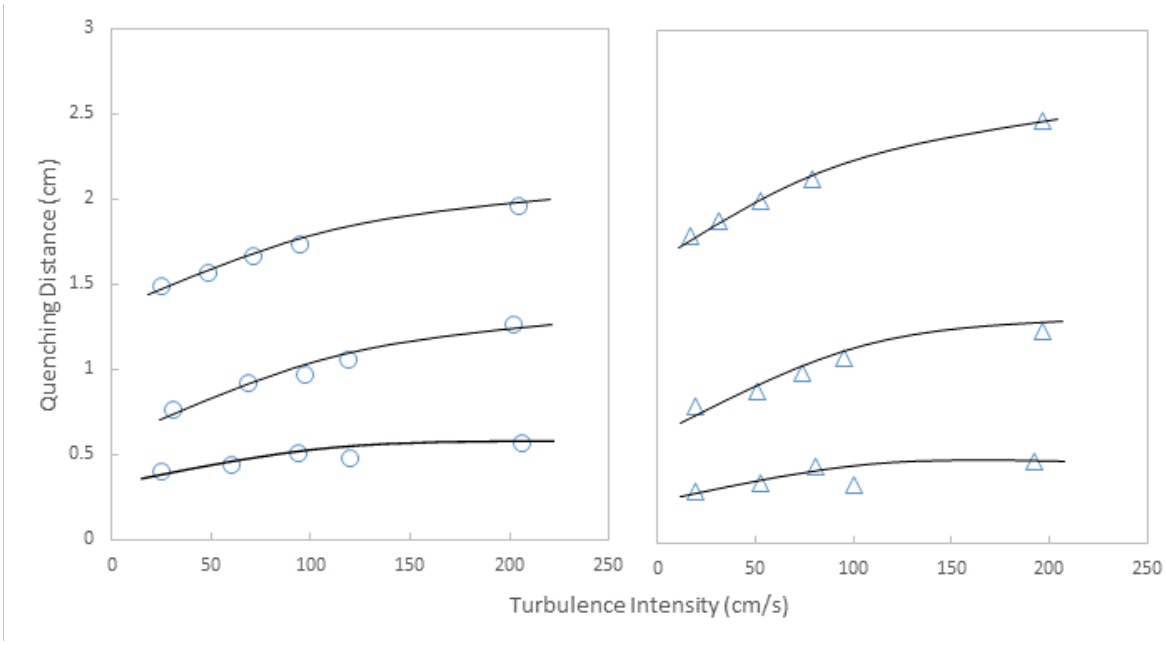

Figure 2-13: Quenching distance as a function of turbulence intensity. Reproduced from Lefebvre and Ballal (1976)

Egolfopoulos et al. (1997) investigated the effects of heat loss on the extinction strain rate of methane and air mixtures at atmospheric pressure. In their experiment, the extinction strain rates of opposed jet flames were compared with single jet flames strained against a flat wall. It was found that when strained against a wall, the single jet flames had significantly lower extinction strain rates due to the heat loss to the wall. Furthermore, it was found that the temperature of the wall had little effect unless the wall's temperature was very high. In addition, these results were compared with numerical simulations and found to be quite close. This study has implications for flames stabilized near walls; Flames stabilized in wall recesses may perform differently than flames stabilized by traditional bluff bodies due to heat loss to the wall.

Recently, studies focusing on avoiding flameholding have been conducted. Samuelsen, McDonell and Couch (2004) studied flameholding of premixed natural gas flames, stabilized in the wake of step expansions at elevated temperatures and pressures. It was found that at these conditions, the height of the step expansion was not significant, but did note that step heights of less than 3mm did not tend to

anchor flames. It was also noticed that there was significant variation in the equivalence ratio at blow off, which is consistent with the wide range between the onset of instabilities and total extinction. Finally, it was observed that for large step heights (6 mm) that there was decent agreement between measured lean blow off values and predictive equations developed for bluff body flame holders by Ballal and Lefebvre (1979). A recent thesis from Pennsylvania state university describes a study done on the flameholding tendencies of airfoils designed to provide swirl at elevated temperatures and pressures (Marzelli 2010). Several variants of natural gas were used for fuel and only a single airfoil shape was tested. Temperature, pressure and fuel to air ratio were varied. In this study free stream velocities were reasonably high (60 m/s). Flameholding was never observed during this experiment.

Based on a study of fully premixed propane-air flames at pressures between 0.2 and 0.9 atm, 10 and 100 m/s and inlet temperatures of 300-600K, Ballal and Lefebvre (1979) suggest the following empirical correlation for the equivalence ratio at blow off for hydrocarbon flames:

$$\text{Equivalence Ratio} \propto \left[\frac{\mathrm{U}}{\mathrm{P}^{0.25}\mathrm{T}\exp(\mathrm{T}/150)\mathrm{D}(1-\mathrm{B})}\right]^{0.16}$$

Where U is the free stream velocity (m/s), P is the absolute pressure (N/m^2), and T_0 is the unburned mixture temperature (K). B is the blockage ratio (ratio of flameholder cross sectional area to the area of the duct) and D is the characteristic dimension (m) of the flameholder. To be valid for any fuel Ballal and Lefebvre suggest the more general correlation

$$\text{Equivalence Ratio} = \left[\frac{\mathrm{a}[1+0.4\mathrm{U}(1+\mathrm{u}'/\mathrm{U})]}{\mathrm{P}^{\mathrm{n}-1}\mathrm{T}_0\exp(\mathrm{T}_0/\mathrm{b})\mathrm{D}(1-\mathrm{B})}\right]^{\mathrm{c}}$$

Where u' the RMS value of the velocity fluctuations (m/s), and a, b, c, and n are empirical constants. Some of the more important things to take away from these equations is the relatively small effect that pressure has on the weak extinction limit, and that increasing bluff body width does tend to decrease

the equivalence ratio at blow off, unless the increase in width also increases the blockage ratio (i.e. increasing the buff body width in a fixed width duct), which still improves flameholding, but to a much lower extent up to a certain value, at which point flameholding is worsened. This is likely due to increased flame stretch in the shear layers of the wake, which increases with velocity as blockage ratio increases. Ju et al. (1997) conducted a numerical study of stretched methane-air flames and determined that flame stretch can improve flammability limits. For mixtures with Lewis number less than unity (e.g. lean H2-air and CH4-air mixtures), moderate levels of stretch extended the lean flammability limit, while excessive levels of stretch caused earlier flame extinction.

Yamaguchi (1985) studied the mechanisms behind blow off for rod stabilized propane-air flames by measuring pressure gradients along the rod's surface and by high speed schlieren photography. Based on observations Yamaguchi determined that the extinction of the flame occurs when the flame is strained to the point where the flame at the end of the recirculation zone is extinguished. Cool gas is then recirculated back to the front of the flame rather than hot combustion products, leading to the flame extinction.

Plee and Mellor (1979) used data obtained by Ballal and Lefebvre (1979) along with new experimental data to predict the lean blow off of fully premixed, and non-premixed, axially symmetric bluff body stabilized flames. The fully premixed data obtained from Ballal and Lefebvre (1979) was obtained for velocities from 10-100 m/s, between 0.2 and 0.9 atm, and inlet temperatures between 300 and 575K. They suggested that blow off is controlled by the competition between chemical timescales and physical time scales. Physical timescales were defined as bluff body size divided by lip velocity, while chemical timescales were defined as the product of ignition delay time and dilatation ratio ($T_{Burned}/T_{Unburned}$). Plee and Mellor found that at the lean blow off limit, the physical timescale was proportional to chemical timescale; physical time was roughly twice the chemical time.

A recent review of blow off of bluff body flames was done by Shanbhogue et al. (2009). This extensive review collected data from flameholding studies conducted over the past 60 years. Shanbhogue et al. found a correlation between Damköhler number (the ratio of physical to chemical timescales) at blow off and Reynolds number. For axially symmetric features they found that $Da \propto Re^{-0.67}$ and that for two dimensional features $Da \propto Re^{-1}$ (see Figure 2-14).

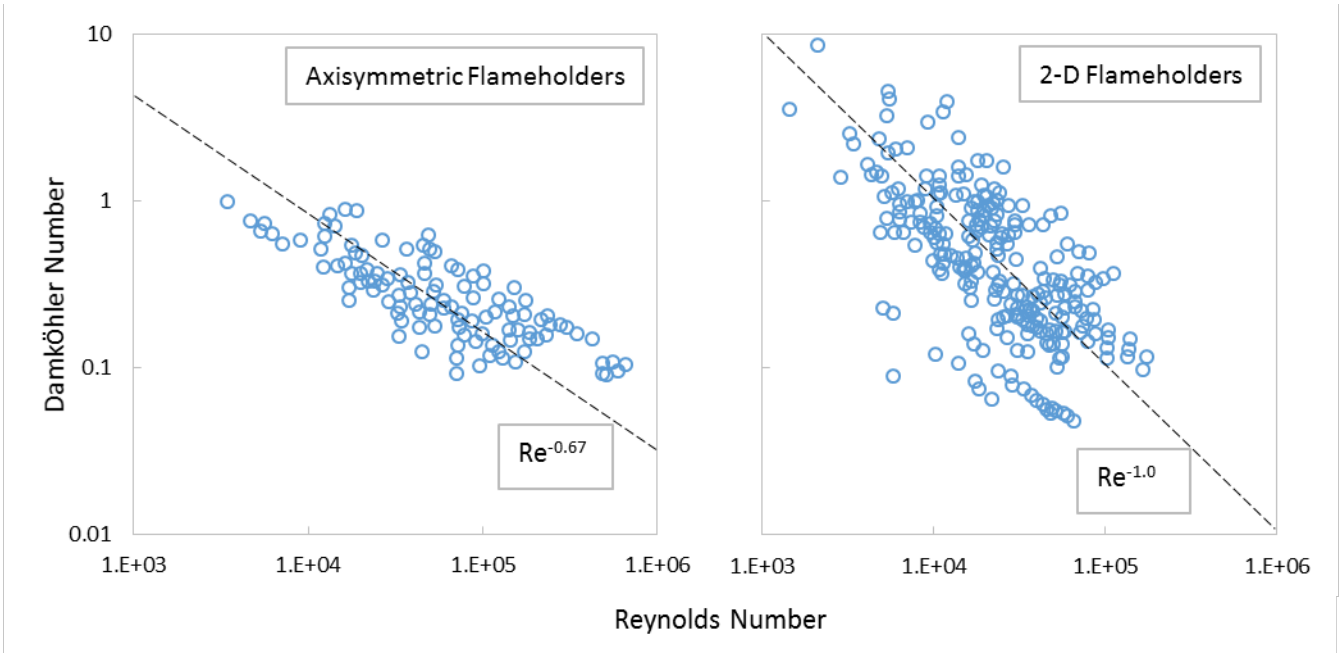

Figure 2-14: Damköhler number vs. Reynolds number for axially symmetric and two dimensional flameholders from Shanbhogue (2009)

Unfortunately, while there does appear to be a trend that generally indicates that as Reynolds number increases, Damköhler number decreases, there is too much scatter in the data to conclude that Reynolds and Damköhler numbers are the only two factors. Furthermore, all of the data obtained is exclusively from experiments on hydrocarbon fuels, conducted at atmospheric pressure or slightly below. Therefore this correlation may or may not be useful for hydrogen containing fuels or at high pressures.

Based on this review of the current work on the subject of flameholding, several conclusions can be drawn. The limits of flameholding occur at roughly the point where the characteristic chemical time is appreciably longer than and characteristic physical timescale. Both timescales can be defined in a number ways. The size of the bluff body, both the width and the length are proportional to the physical timescale. Increasing length increase the height of the boundary layer, which increases wake size. The width of the feature also increases wake size, but the aerodynamic width should be considered rather than the geometric width (i.e. more blunt flameholders will have larger wakes). Increasing bluff body size will usually increase flameholding propensity unless increasing its size will increase blockage, due to increased strain in the shear layers. Chemical timescale can be defined in a number of ways, but is generally inversely proportional to turbulent flame speed. Turbulent flame speeds, which are a measure of the reactivity of the fuel and air mixture, increase from the laminar flame speed proportionally with turbulence intensity. The effect of pressure, temperature, or fuel to air ratio is only manifested in changes to the laminar flame speed, which only has a small effect on turbulent flame speed. Fuel type also plays a significant role as different fuels respond differently to increased levels of turbulence. While studies have suggested that wall-recess flameholders hold flames in the same means as bluff bodies, a wall step may be expected to have worse flameholding than a bluff body of equivalent sixe due to heat loss to the wall. Increasing turbulence intensity also tends to increase quenching distance, which may further decrease flameholding for wall features, especially in highly turbulent flows. While low pressure (sub atmospheric) studies on the effect of pressure have identified a slight pressure effect on flameholding propensities, other studies performed at higher pressures indicate no pressure affect. This may be due to changes in the effect on laminar flame speed.

2.3 Summary

Several questions remain unanswered with respect to flameholding. While considerable work has been done to quantify blow off for large scale bluff bodies that are designed to hold flames, very little work

has been done to verify that blow off for smaller features, like those found in the premixers of gas turbine engines, which are not necessarily designed to hold flames, perform similarly. The majority of the existing work on flameholding has focused on hydrocarbon fuels, which have wider quenching distances, lower flame speeds and generally are much less reactive than hydrogen. Further, while some work exists on the effects of pressure on flameholding, it is largely limited to sub atmospheric conditions. The purpose of the research reported herein is to address these gaps in knowledge and to develop practical methods for predicting flameholding that can be effectively applied to systems at elevated temperatures and pressures, with hydrogen containing fuels and a wider selection of geometric features which are not necessarily intended to anchor a flame. With this in mind, a new test apparatus was constructed to achieve the experimental conditions that are necessary to address these knowledge gaps.

Chapter 3 - Research Approach

The objectives of this experiment were carried out in the following tasks:

3.1 Task 1: Build experiment apparatus

A new test rig was assembled that consisting of two components: a new test section, and an upgraded fuel delivery system. The high pressure facility is capable of reaching pressures up to 10 atm, and can provided air flow rates up to 1.4 kg/s. However, these two conditions are not necessarily available simultaneously. While a similar test section was developed for a previous experiment in flameholding at the UCICL, this test section has a cross sectional area too large to achieve the sufficiently high test velocities at the desired temperatures and pressures. In order to achieve the desired flow conditions, a new test section was developed that includes the ability to swap the test features, as well as have optical access both at the feature, and upstream of it. Sample ports have been included at regular intervals along the test section to allow for extractive sampling, should it prove necessary. In addition to this, the upstream section of the new test section has been tailored to produce a uniform fuel and velocity distribution. The existing fuel system in to the test facility was upgraded to be capable of providing both hydrogen and natural gas in quantities sufficient to provide a stoichiometric mixture at the highest anticipated air flow rates. A previous effort to study flameholding at UCICL revealed the need to ensure fully developed velocity and fuel distributions. This lead to significant uncertainty in measured weak extinction vs. velocity measurements. In the current experiment every effort was made to ensure that the fuel is perfectly mixed with air, and that the flow field is fully developed.

3.2 Task 2: Obtain data from the entire design space

The existing high pressure facility requires the exhaust gas from any combustion experiment to be cooled prior to coming in contact with the backpressure regulating valve. The facility has the capability of rejecting up to 400kW of thermal power continuously. The combination of preheating and

combustion of air at up to 1.4 kg/s can easily result in heat rejection requirements in excess of 400 kW. Because of this, it was necessary to conduct tests in short bursts that did not, on average, overwork the cooling system of the facility. This requirement created challenges to a reliable and consistent experiment as operating in a “steady-state” mode will not be possible. Quickly stabilizing fuel flow rates, with minimal overshoot, ensuring adequate fuel-air mixing, and quickly gathering data were the primary challenges to overcome. After the test apparatus was completed and the experimental procedure developed, testing was carried out over the range of the experiment design space. In addition to testing with hydrogen, tests with natural gas were performed as a baseline.

3.3 Task 3: Investigate validity of current predictive expressions

Presently there exist a number of correlations that have either been developed from first principles or empirically that attempt to predict blow off. Fundamental correlations such as Damköhler scaling pose blow off as a competition between fluid mechanical and chemical effects. Empirical correlations tend to predict blow off simply in terms of measurable parameters. However, empirical correlations can often be regrouped in a form similar to a Damköhler type expression. One of the aims of this study was to investigate the extent to which these expressions, which have been largely based around hydrocarbon flames, can be extended to hydrogen flames, and also to elevated pressures and temperatures.

3.4 Task 4: Correlate results and develop design guidelines

In order for the results gathered during Task 2 to be relevant towards the design of future gas turbines, they must be correlated with parameters that will be known by engine designers. Physical parameters, like temperature, pressure, and velocity, were considered. However, it is likely that when expressed solely in these terms, little insight is provide on the mechanisms behind flameholding. While this would certainly be useful, a more significant result would be to represent the data in terms of non-dimensional numbers (research has indicated the significance of non-dimensional terms like the Damköhler number,

Lewis number, and Reynolds number). By doing this the data is more widely applicable. In order to quantify results in terms of Damköhler number both physical and chemical timescales must be known. While physical time scales can be accurately known to within an order of magnitude from the known flow rates and feature geometry, chemical timescales can be defined in several different ways (Ignition delay times, minimum perfectly-stirred-reactor time, and flame sheet thickness over laminar flame speed) that are often not directly proportional to each other. In order to properly correlate results an appropriate chemical timescale must be defined.

Chapter 4 - Experiment

4.1 Facility

All experiments have been carried out in the UC Irvine Combustion Laboratory high pressure combustion facility. The test apparatus used during the current study is designed to simulate as closely as possible the conditions inside a gas turbine premixer. The high pressure combustion facility has two floors with three test rigs. The first floor contains a simulated combustor rig, which can be used for running experiments with model gas turbine combustors. The second floor contains a flow reactor used for ignition delay experiments, and also the flameholding rig, which was used in this experiment. Both the upper and lower floors use the same ancillary systems (compressed air supply, fuel supply, air heaters, heat rejection systems, and backpressure valve) and are controlled from the same control room. These can be seen in Figure 4-1 and Figure 4-2.

Figure 4-1: Flameholder test stand in the UC Irvine High Pressure Combustion Facility

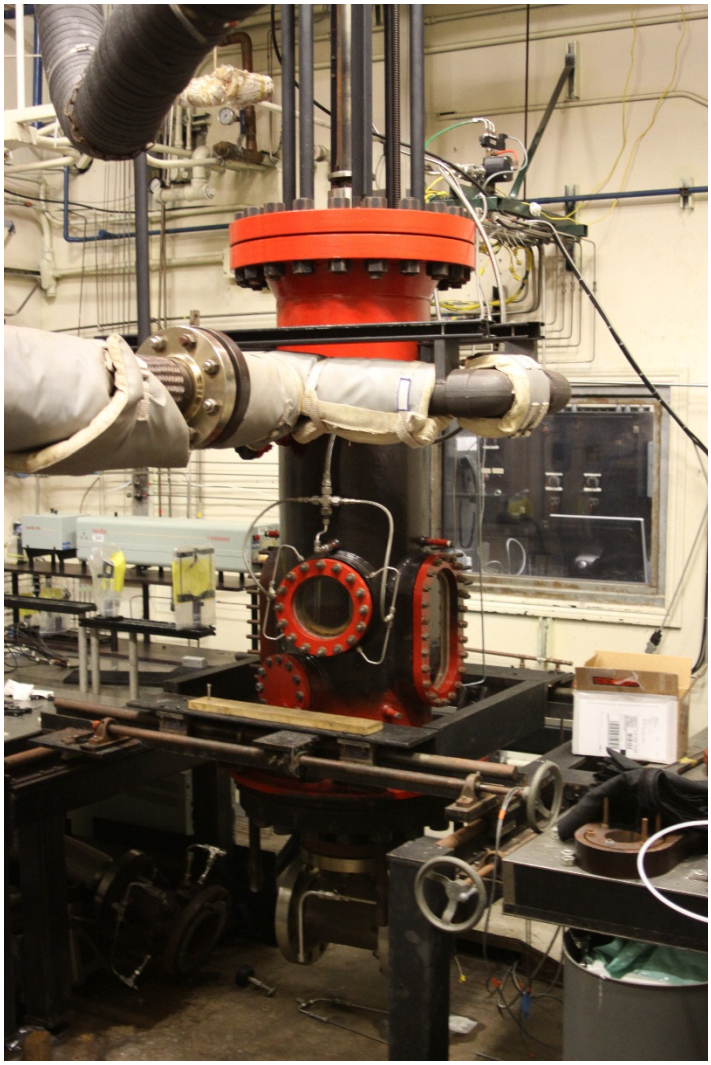

Figure 4-2: Model combustor test stand in the UC Irvine High Pressure Combustion Facility

4.2 Experiment Apparatus

The test apparatus consists of a rectangular cross section passageway that measures 2.3 meters in overall length and 45 mm by 19 mm in cross section (Figure 4-5). The apparatus is divided into a flow development section upstream and a test section downstream.

For the purposes of this experiment, a new test rig was required. While a similar test rig was constructed for a previous experiment (Samuelsen et al. 2004), its cross section was too large to achieve the velocities required for this experiment. Furthermore, the previous test rig suffered from poor flow

development, resulting in considerable ambiguity in the velocity profile and fuel and air distribution. A rendering of the initial test rig design can be seen in Figure 4-3. The majority of components were fabricated in the combustion lab machine shop. Figure 4-4 shows all of the components used in the construction of the new test rig, prior to its final assembly.

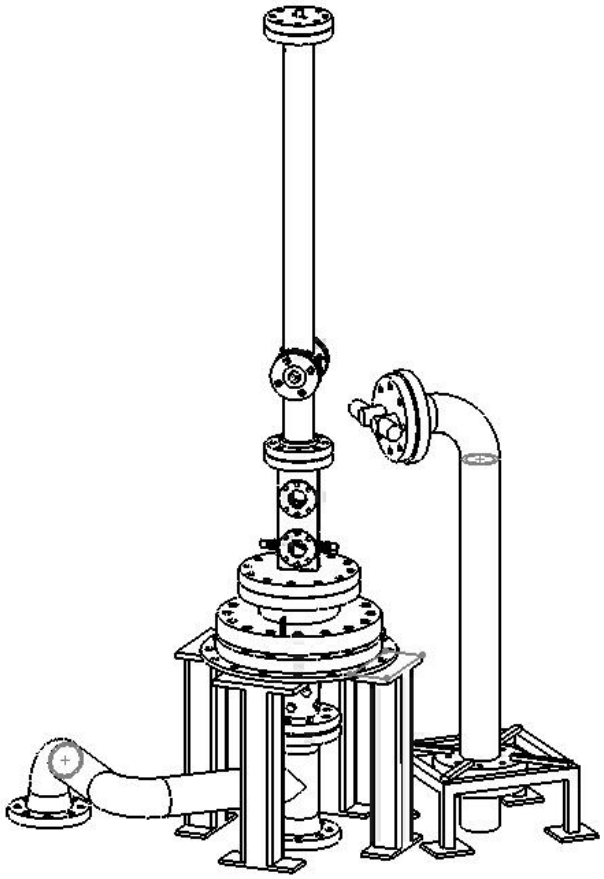

Figure 4-3: Initial rendering of flameholder test rig

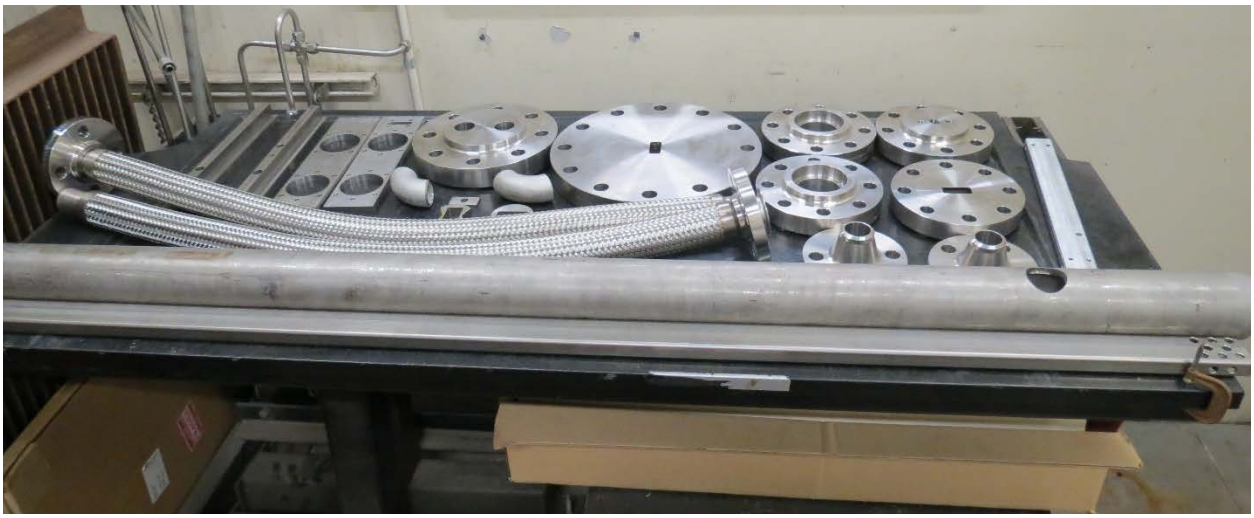

Figure 4-4: Flameholder test rig components prior to assembly

One critical component in the design of the new test apparatus was providing sufficient optical access. The windows that were selected for this experiment are made of pure silicon dioxide, which can withstand temperatures up to 1420 K. The windows are three inches (76.2 mm) in diameter and 0.5 inches (12.7 mm) thick. Care was taken to ensure that these windows could withstand pressures up to ten atmospheres (Appendix A). The test section has space for four windows, two upstream of the igniter and two downstream of the igniter. The flameholder test features to be tested are mounted on grade 304 stainless steel disks that are the same size as the windows. This allows the test feature to be placed in any of the window positions. The round base of the test features also allows them to be rotated. Design drawings of all test features used in this experiment can be found in Appendix E.

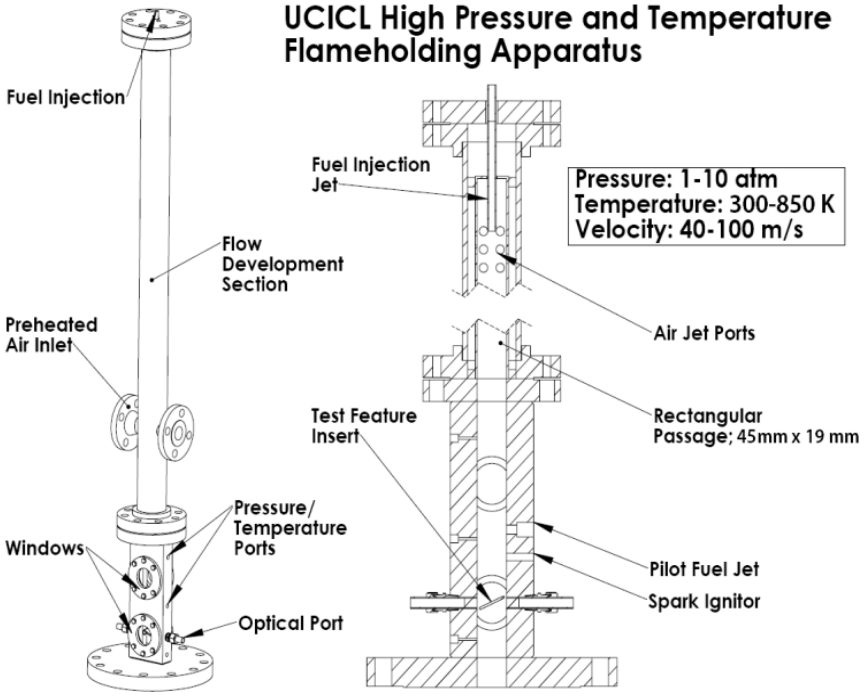

Figure 4-5: UC Irvine Combustion Lab Flameholding Apparatus

The dimensions of the test apparatus were carefully chosen to provide the best conditions for this experiment. The cross section of 45 mm by 19 mm was selected because it was similar to a section of the annular passageways found in many large gas turbine premixers. Figure 4-6 shows this cross section in comparison to renderings of actual premixers found in engines from Solar Turbines, General Electric, and Siemens-Westinghouse. 5. While similar in shape, the rectangular passageway does have limitation in its applicability to the annular passageways of premixers. The major difference being that an annular passageway has two walls rather than four. The additional walls could lead to differences in heat transfer, and velocity near these. Also, looking at a single test feature, rather than the many features (e.g swirl vanes) found in premixers may have effects on the aerodynamics around the test feature.

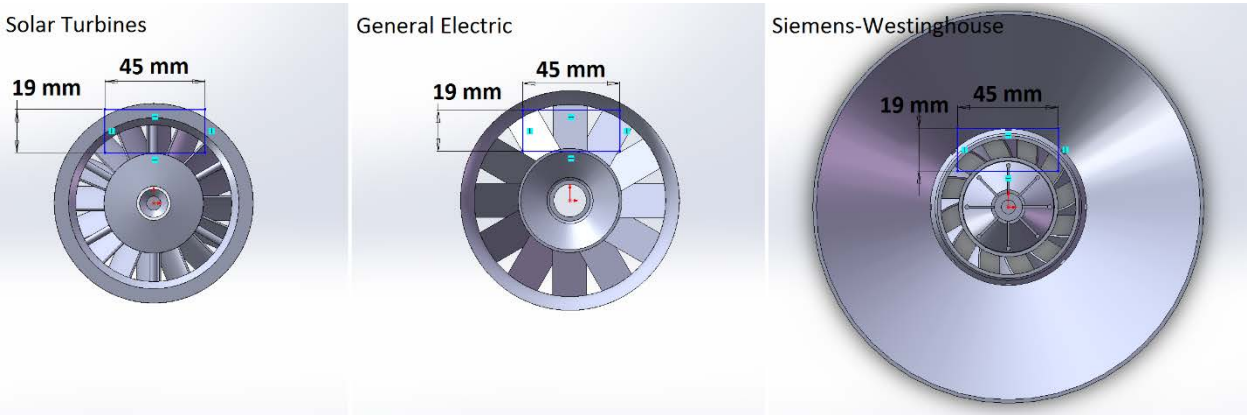

Figure 4-6: Cross section of flameholding test section projected onto renderings of production premixers

Fuel is injected through a single axial jet into the rectangular passage at the entrance to flow development section. Air enters through twelve inward pointing jets in the wall surrounding the fuel injector. The flow development section is two meters in length, guaranteeing sufficient time to produce fully developed flow and to develop a homogeneous fuel distribution. The calculations used for determining the minimum length for fully developed flow can be found in Appendix B.

Thermocouples are located at the entrance to the flow development section, at the wall of the test section, and embedded inside of each test feature. Pressure taps are located in the wall of the test section upstream and downstream of the test feature. Four round window ports are included in the test section. These round ports can either contain a quartz window, providing optical access, or the round base of a test feature insert. This allows for flexibility in the positioning of the test feature, which can be placed either on the front or back of the test section, and either upstream or downstream of the point of ignition. The flame is ignited in the wake of the test feature by momentarily bathing the feature in the flame from a hydrogen pilot torch (Figure 4-7). The hydrogen pilot is ignited with a spark igniter. Both the spark igniter and the pilot fuel injector are flush with the wall of the test section to prevent disturbances to the flow field.

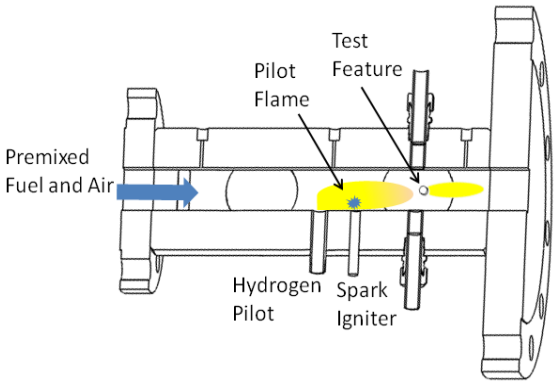

Figure 4-7: Flameholder Ignition System

Tests are conducted by first bringing the test rig to the required temperature, pressure and velocity. The pilot flame is then ignited with the spark igniter. Once the pilot flame is stabilized and touching the test feature the main fuel solenoid is opened allowing fuel to enter the flow development section. Fuel flow is adjusted to the desired flow rate. Once a flame is stabilized in the wake of the test feature the pilot fuel is turned off. The main fuel flow rate is then decreased until the pilot flame extinguishes. Fuel is allowed to continue flowing long enough to record the fuel flow rate during blow off. The reaction is observed through a 57 mm diameter quartz window using a digital video camera with a live feed to a desktop computer. A plot depicting the sequence of events for a single test is shown in Figure 4-8.

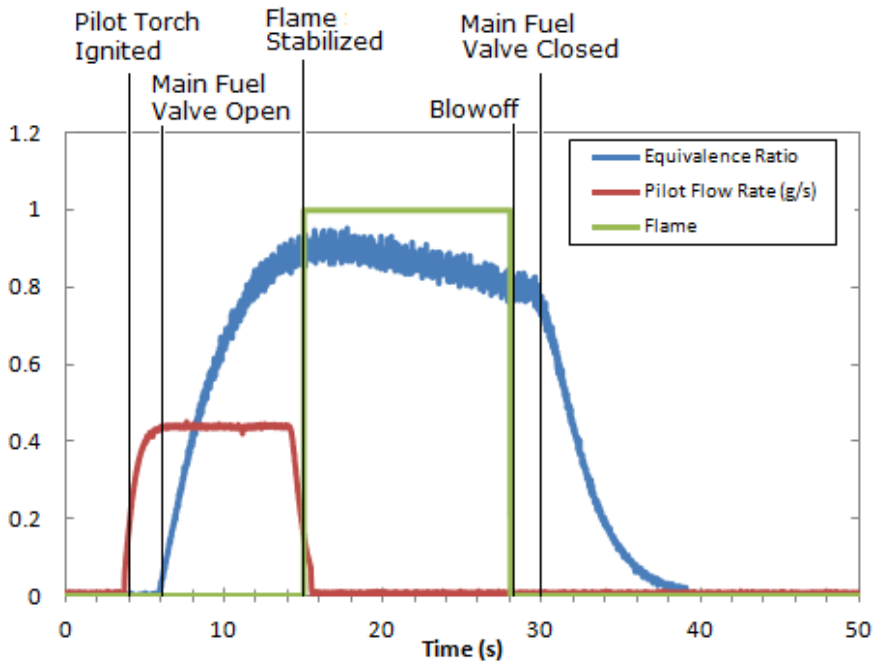

Figure 4-8: Flameholding Test Event Sequence

4.3 Ancillary Systems

In addition to the experiment apparatus, a number of subsystems contribute to the proper function of each test.

4.3.1 Air Circuit

Air is delivered to the test cell at 140 psig (10.5 atm) via a pipeline from three air compressors capable of producing a combined 3.1 lb/s (1.4 kg/s) of air. The air flow is controlled with two valves. Coarse adjustment is accomplished with a four inch pipe size butterfly valve while fine adjustment is performed by a one inch pipe size Fisher V200 remote control valve and a Sierra model 7805-NAA-NC9-32-P3-V4-NR-0 flow meter, which interact via a Fisher DPR 900 PID (proportional-integral-derivative) process controller. The set point for the air mass flow is entered into the process controller, which reads the current mass flow through the flow meter via a 4-20 mA analog signal, and then outputs a 4-20 mA signal to the remote control valve to adjust the airflow rate to the necessary value. A backpressure

valve, located downstream of the test rig maintains pressure during experiments. Two backpressure valves are used, a six inch pipe size gate valve is used to provide course adjustment of the backpressure, while fine adjustment is accomplished with a 1.25 inch pipe size Fisher V200 remote control valve. The remote control backpressure valve is also controlled by a Fisher DPR 900 PID process controller. Air can either be directed through the upper or lower floor test rigs. This is accomplished my unbolting the flexible air lines leading to and from one rig and reattaching the lines to and from the other. This process is relatively fast, taking approximately three hours, and allows two experiments to be setup concurrently.

While capable of being operated in a manual control mode, the air flow and backpressure fine control vales are typically operated automatically with the PID controllers. This is because the pressure upstream of the primary air valve does not remain constant. Air is supplied from three compressors that come online in stages. The primary air compressor provides to 0.5 lb/s (0.24 kg/s). If the pressure drops below 110 psig, the second air compressor, capable of producing approximately 1.0 lb/s (0.45 kg/s) of air, comes online and operates until the pressure increase to 140 psig. Because of the wide range in pressure set points, experiments requiring greater than 0.5 lb/s of air necessitate the use of the PID controller to provide a steady flow rate of air.

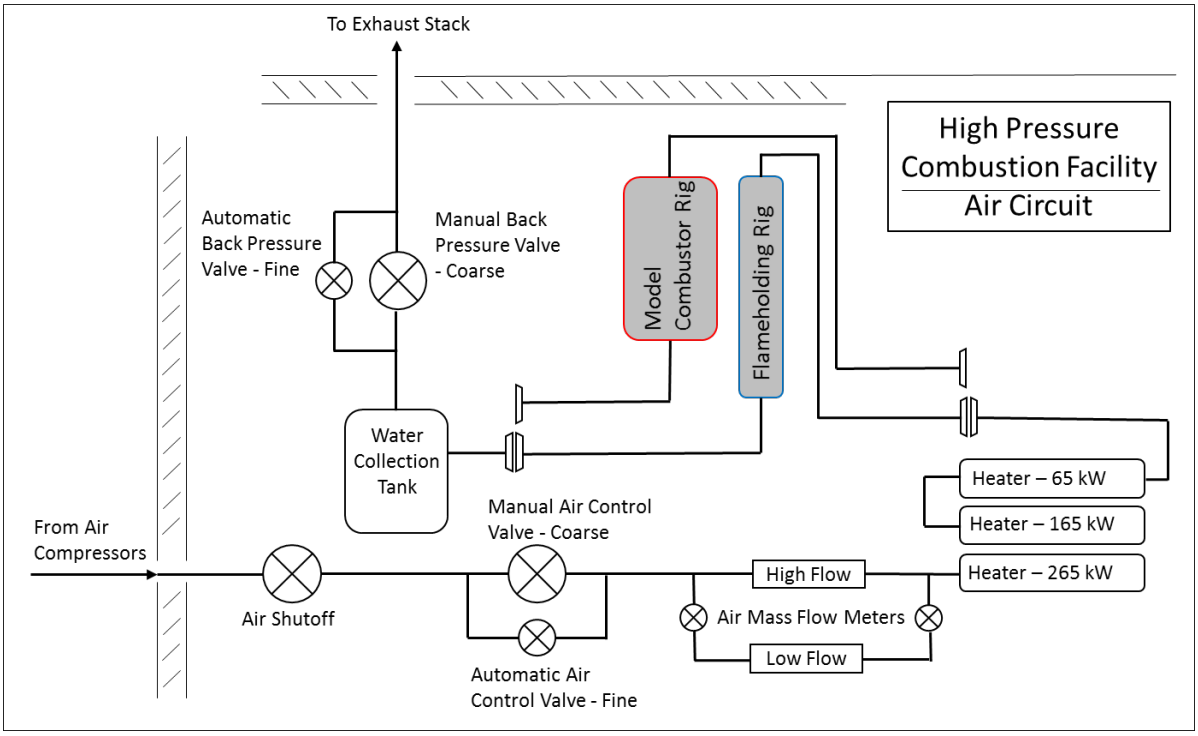

Figure 4-9: High pressure combustion facility air circuit schematic

4.3.2 Fuel Circuit

Fuel can come from one of three sources: a low pressure natural gas compressor, a high pressure natural gas compressor, and a bottled gas manifold. The low pressure gas compressor has a maximum pressure of 140 psig (10.5 atm) and the high pressure gas compressor has a maximum pressure of 400 psig (28 atm). The bottled gas manifold has the capability of providing gas at pressures up to 250 psi (18 atm). Once the fuel enters the test cell it travels through a shutoff solenoid a rotary needle valve, and a second shutoff solenoid. The final shutoff solenoid is located immediately upstream of the test rig, and allows the fuel to be immediately separated from the experiment. Upstream of the final shutoff solenoid is the rotary needle valve, which controls the fuel flow rate. Upstream of this is the first shutoff solenoid. This solenoid is used to shutoff the fuel without having to change the position of the rotary needle valve (preserving the fuel flow setting for a future experiment) or have excessive fuel flow when the fuel is turned back on (as would be the case if pressure final fuel shutoff valve was closed and pressure was

allowed to build behind it). The fuel flow rate is measured by a Micromotion CMF025, coriolis-type, flow meter. The maximum measurable fuel flow of rate is 40 g/s. Coriolis flow meters directly measure mass flow rate using the Coriolis Effect. In these instruments, fluid flows through an oscillating, eccentric portion of tubing. The momentum of the fluid deflects the outward flowing and inward flowing portion of tubing in the opposite direction. This deflection can be measured and correlated with mass flow. Directly measuring mass flow rate allows them be used with multiple fuel types without the need to recalibrate in between.

The Corken natural gas compressor is a non-variable frequency two stage compressor. Because this compressor cannot be ramped down to a lower speed, the compressor operates continuously at maximum power. In order to control the output pressure, an onboard regulator measures the pressure in the pipeline and diverts any excess pressure back to the inlet of the compressor. However, this diversion process is not instantaneous, sometimes taking as long as one minute to respond to changes in the line pressure. The result of this is that during short duration tests (such as those done for this experiment) the natural gas line pressure may drop significantly before the compressor attempts to compensate, leading to constant adjustment of the manual fuel control valve. In order to combat this problem, a storage tank was placed in the test cell immediately upstream of the first shutoff solenoid. This storage tank has sufficient volume to limit fuel line pressure fluctuations to less than ten percent.

Pilot fuel for igniting experiments is controlled in a similar manner. Hydrogen is used for pilot fuel in all experiments. The fuel is stored in gas cylinders outside of the test cell, and a pressure regulator decreases the pressure to approximately 250 psig. The pilot fuel then enters the test cell where it flows through a Micromotion CMF010 coriolis-type flow meter. After the mass flow rate of pilot fuel is measured the fuel enters the control room. In the control room the fuel flows through a manual shutoff

valve and electric fuel solenoid before finally flowing through a rotary needle valve which controls the flow rate. After this, the pilot fuel flow to the igniter system in the test cell.

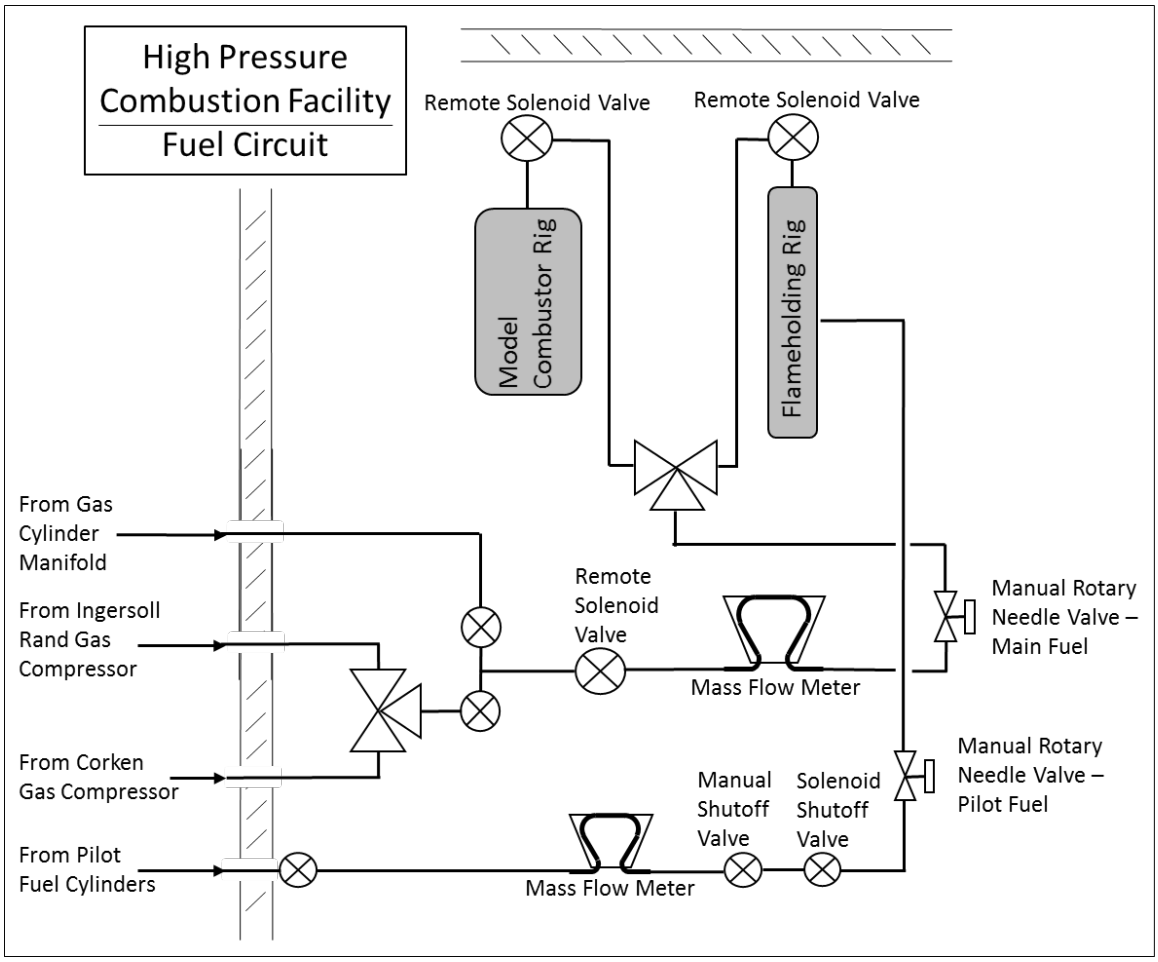

Figure 4-10: High pressure combustion facility fuel circuit schematic

4.3.3 Heaters

Preheating of the air is achieved with the use of a bank of three electrical resistance heaters with a combined output of 495 kW Figure 4-11. There are three heaters with outputs of 265, 165, and 65 kW. The first stage heater (265 kW) has a maximum exit temperature of 925° F (700 K). The second stage heater (165 kW) has a maximum exit temperature of 1100° F (865 K). The final stage heater (65 kW) has a maximum exit temperature of 1350° F (1000 K). The heated air is ducted to the test rig through four

inch insulated flex lines. Despite the insulation, there is significant heat loss between the heaters and the test rig, resulting in a maximum rig inlet temperature of approximately 1050° F (840 K). The physical size of heaters result in significant thermal inertia for the heating elements to overcome. It typically takes at least one hour for the heaters to bring the test rig to the desired temperature. Additionally, the heater exit temperature fluctuates up to twenty degrees in either direction of the set point temperature. Because of this, a heater bypass valve is used to provide faster response temperature response. Typical operation consists of setting the heaters to a temperature higher than what is required, and then bypassing air with the manual bypass valve to lower the temperature to the desired level.

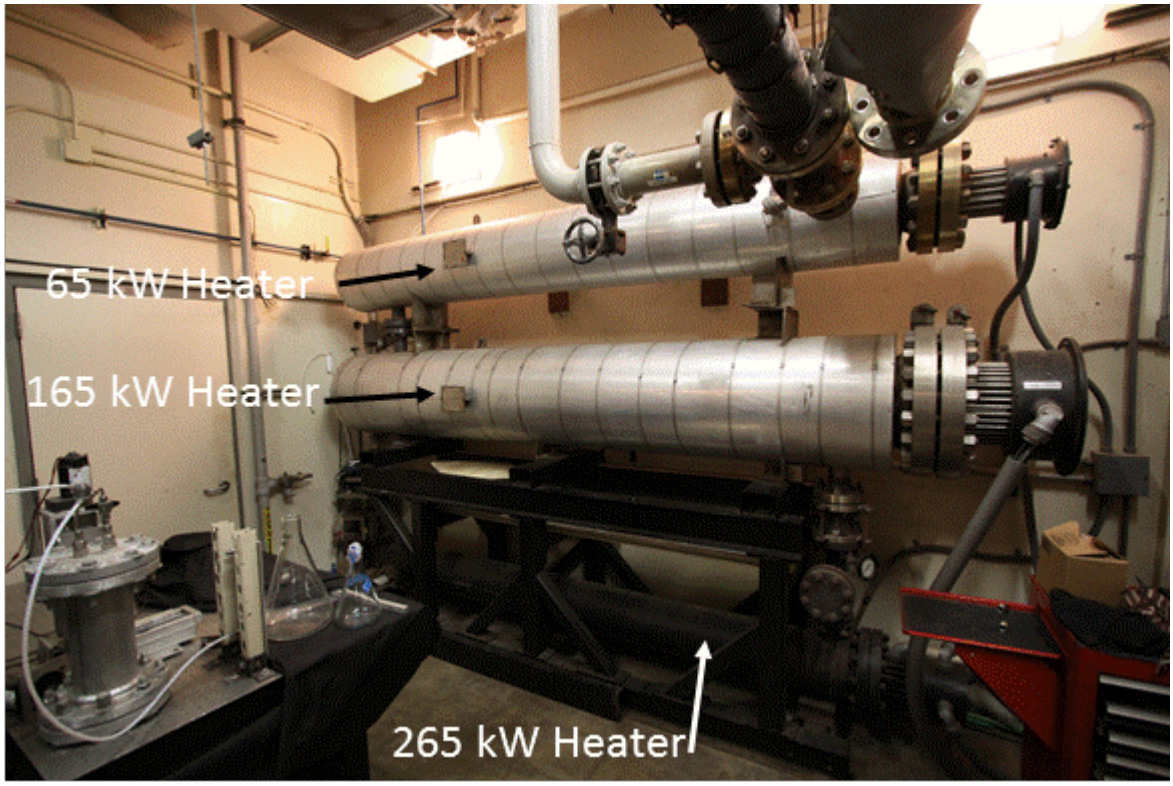

Figure 4-11: Air heaters in the high pressure combustion facility

4.3.4 Heat Rejection

In order to protect the backpressure valve and exhaust stack from excessively high temperatures the test facility is equipped with a heat rejection system (Figure 4-12).This system is designed to spray water into the exhaust of the test rig to lower the temperature of the exhaust gas. The system has the ability to expel approximately 400 kW of heat during continuous operation, but the large volume of water in the collection tank allows for the periods of higher thermal output from the rig as long as the average value is maintained below 400 kW. A schematic of the system is shown in Figure 4-12.

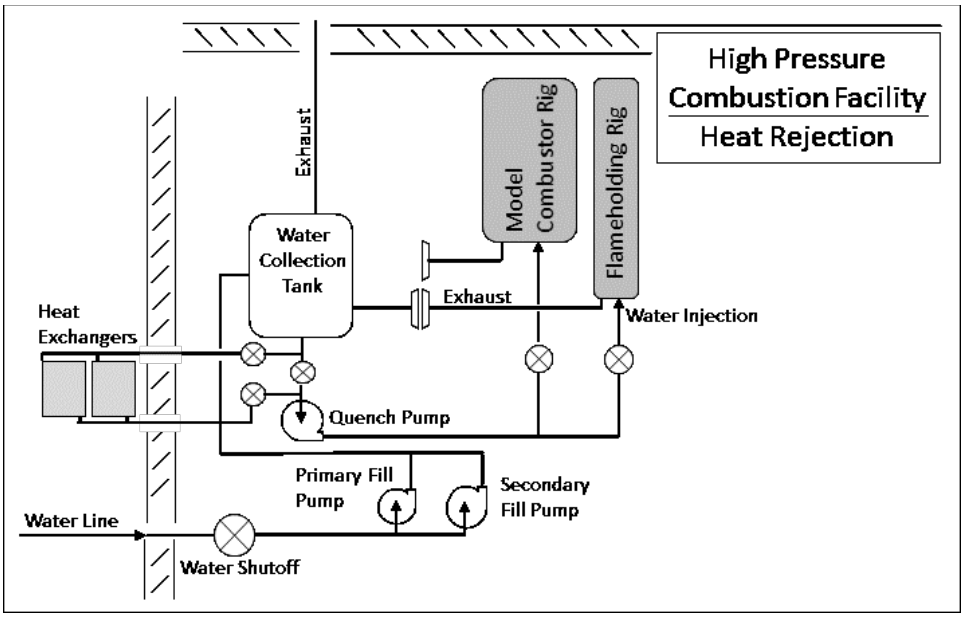

Figure 4-12: Schematic of heat rejection system

The system operates by pumping water at 400 psig with a twenty horsepower centrifugal quench pump to the water injectors Figure 4-13, which cools the exhaust. The exhaust and water spray then travel through four inch braided stainless steel flex lines to the 140 gallon water collection tank. In the collection tank gravity separates the water from the exhaust. The exhaust then travels through the backpressure valve and out through the exhaust stack. The quench water that has collected in the tank is then drawn through two forced air heat exchangers which lower the water temperature before

returning to the quench pump. The water level is maintained at a specific level within the collection tank. If the water drops below a threshold level, the primary fill pump is triggered. The primary fill pump is a 7.5 horsepower centrifugal pump which pumps water from the water lines into the collection tank at high enough pressure to overcome the pressure within the test rig. If, under extreme conditions the water level continues to drop the 15 horsepower secondary fill pump will start, and will provide additional pumping capacity to ensure that there is sufficient water for the quench pump to continue operation.

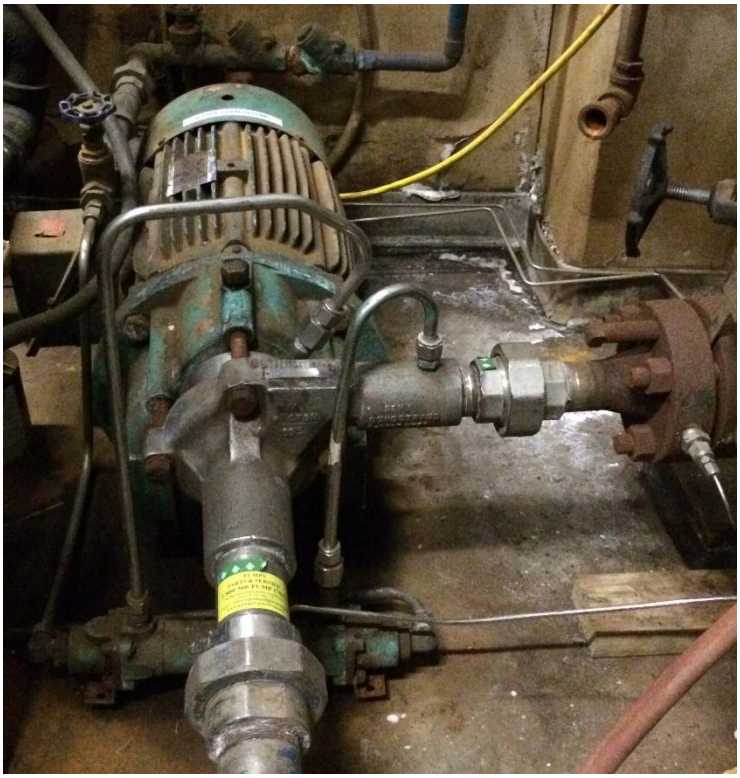

Figure 4-13: Exhaust water cooling pump

4.3.5 Video capabilities

Due to the fact that the flameholding apparatus is on the upper floor of the test cell, direct visual access to the experiment is impossible. Because of this, remote cameras are used to provide visual contact during experiment. The primary video camera is a remote CCD camera which outputs video directly to

desktop computer at 29 frames per second and 862 by 647 pixels, which can simultaneously display and record video. In addition to this camera, an additional camera is available for use during testing. The second camera is a Nikon model J1, which is capable of recording video at resolutions of 1920 by 1080 pixels at 30 frames per second, 640 by 240 pixels at 400 frames per second, and 320 by 120 pixels at 1200 frames per second. This camera is not capable of simultaneously outputting and recording video. When high speed video is required, the first video camera is used for visualizing the experiment, and a remote control activates the second camera to begin recording.

4.3.6 Computer Controller

A desktop computer running Labview software is used to display and record operating data during all experiments. The computer uses two national instruments PCI connected data acquisition boxes to record the test apparatus absolute pressure, differential pressure drop across the test feature, mass flow rates of air, fuel and pilot fuel, and the air temperature at the inlet to the test rig. Additionally the user specifies fuel type. With this data it is able to calculate equivalence ratio, average mixture velocity. The computer program also contains a flashback alarm. The inlet temperature thermocouple is located at the point of fuel injection. When flashback occurs, the thermocouple will register the rise in temperature and signal an alarm to alert the user. The alarm uses a user specified temperature, typically 100 K above the desired inlet temperature, as the threshold for what is considered flashback. If the inlet temperature rises above this value, the alarm is triggered. The graphical user interface is shown below in Figure 4-14.

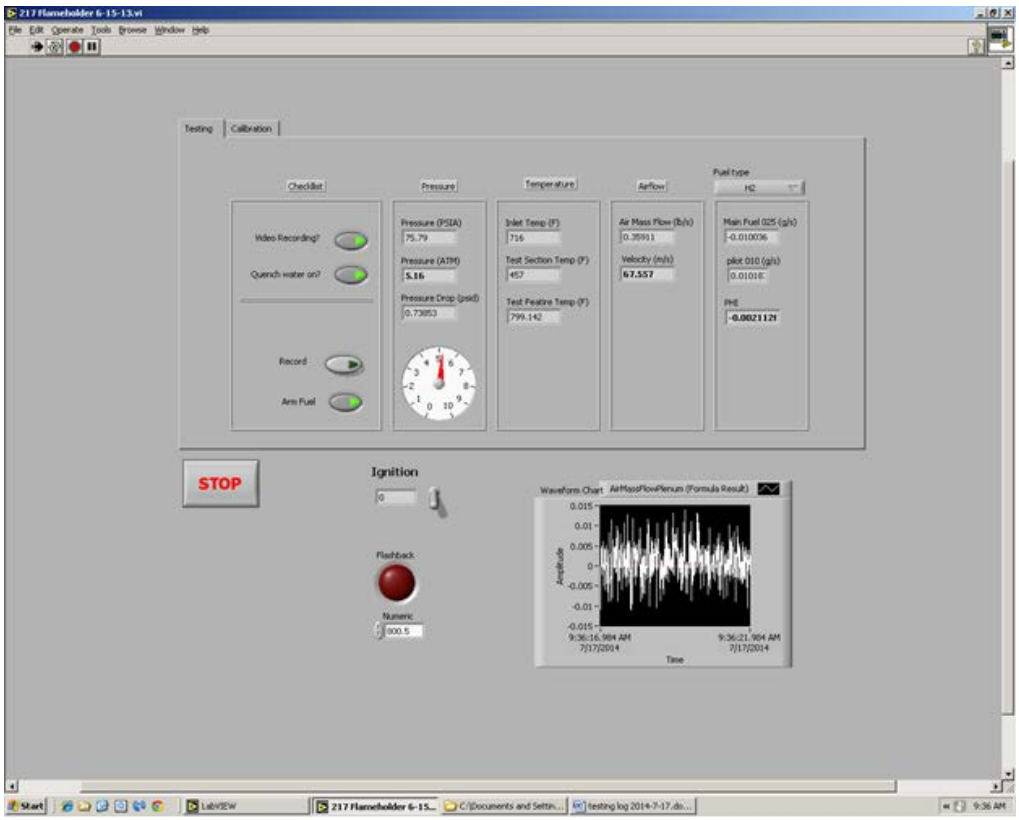

Figure 4-14: Screenshot of Labview interface

4.3.7 Data Post Processing

Data collected during testing was post processed using a MATLAB program and using Cantera subroutines. During each experiment, data is collected continuously. This program filters through the data to locate just the data corresponding to flame extinction. Cantera, an open source chemical kinetics software, was used to calculate fuel-air mixture properties (density, viscosity, temperature) as well as reacting properties (adiabatic flame temperature, ignition delay times). In addition to calling Cantera subroutines, the MATLAB program calculated mixture velocity and Reynolds number. Chemkin was used for calculating laminar flame speeds. Both Cantera and Chemkin used the GRI 3.0 chemical kinetics and transport mechanism.

4.3.8 Laser Doppler Velocimetry

Laser Doppler velocimetry (LDV) was used in order to verify that the velocity profile is fully developed and that turbulence intensity is in the expected range. LDV measures velocity by focusing two laser beams of the same wavelength on the point where velocity is to be measured. At the point where the beams cross, an interference pattern is generated from the constructive and destructive interference of the beams. To measure velocity the flow must be seeded with particles. Common particles are water or oil droplets, or alumina powder. When the particles pass through the sampling point, light from the fringe pattern will be reflected off the particles at a frequency that is proportional to the velocity of the particle and inversely proportional to the fringe spacing. A photo detector measures light reflected from the sampling point. If the fringe spacing is known, then the velocity at the sampling point can be calculated. A typical LDV setup is shown in Figure 4-15.

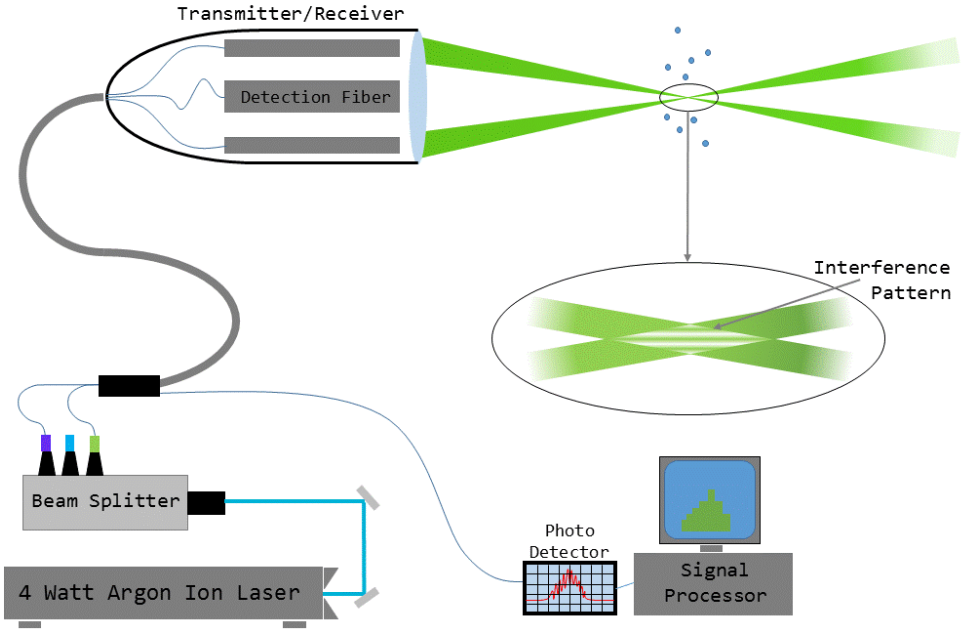

Figure 4-15: Schematic of typical Laser Doppler Velocimetry system

The setup used for this experiment consists of a 4 watt Coherent Innova 90C-A4 argon ion laser used with a TSI LDV system. The LDV system consists of an Aerometrics Fiberlight multicolor beam separator, a LDV00302 backscatter transceiver fitted with a 261 mm focal length, a PDM 1000 photo detector module, and a FSA 4000 multibit digital processor. The laser, beam separator and signal detecting and processing equipment are located in the downstairs control room (Figure 4-16). The transceiver is located in the upstairs test cell, adjacent of the test apparatus. The transceiver is mounted on a remotely controlled traverse system with digital position readouts to facilitate quick and accurate repositioning (Figure 4-17).

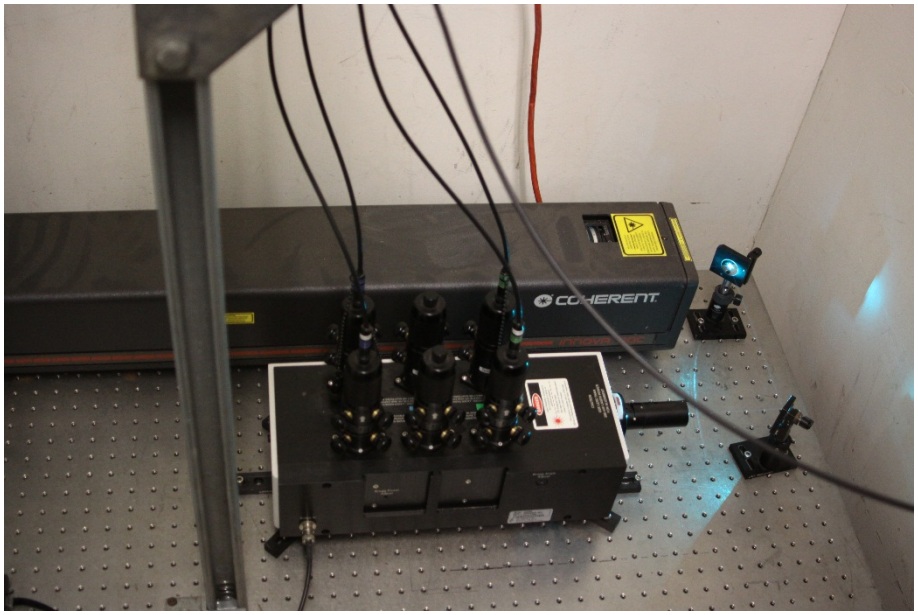

Figure 4-16: Laser and beam separator used for laser Doppler velocimetry

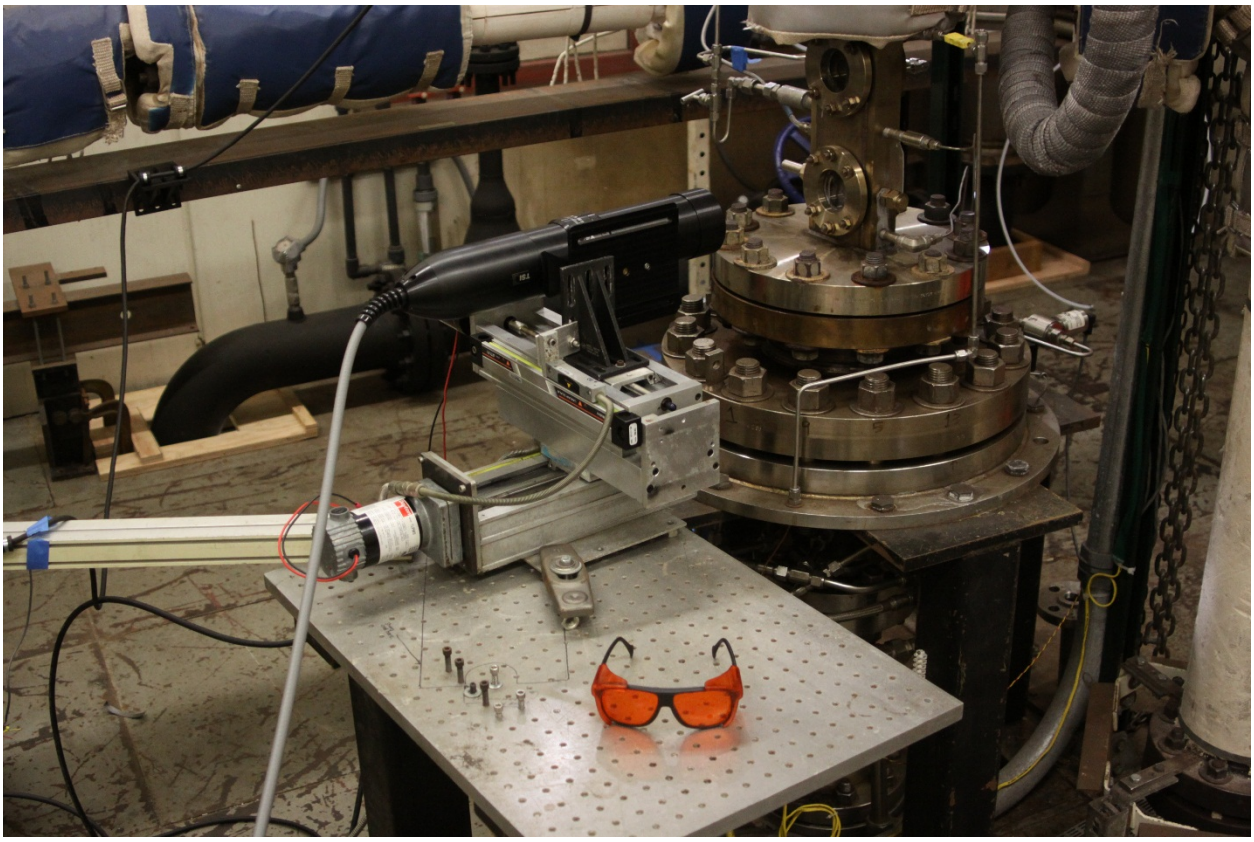

Figure 4-17: Transceiver mounted on traverse adjacent to test rig.

The flow was seeded with water droplets. The water droplets are generated with a BETE PJ10 fogging nozzle inserted into the fuel injection port on the test rig. Water is supplied from a pressurized tank and flow rate is controlled with a rotary needle valve (Figure 4-18).

Figure 4-18: High pressure water seeding tank

4.4 Testing

There are three major types of geometric features commonly found in gas turbine premixers that have the potential for anchoring flames: reverse facing steps, airfoils, and cylinders. Reverse facing steps are found where two pieces of metal are joined in a lap joint. Airfoils are typically used either as points of fuel injection or are used to provide rotation to the flow before entering the combustor. Cylinders are used either for internal structural support or as points of fuel injection. For this experiment, four flameholders have been tested: a 0.25 inch diameter cylinder, a 0.5 inch cylinder, a symmetric airfoil with a frontal width of 0.25 inches and chord length of 1.0 inch. These features are shown in Figure 4-19.

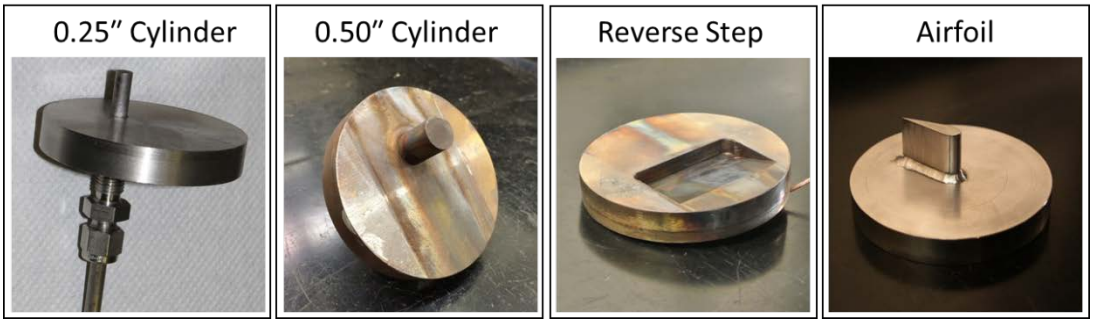

Figure 4-19: The four test features constructed for this experiment

Tests were carried out at temperatures between 80°F (300 K) and 900°F (755 K), though the majority were performed between 500°F (533 K) and 800°F (700K). Experiments were between three and nine atmospheres. For each temperature-pressure combination, tests were typically conducted with free stream velocities between 40 and 100 m/s. The effect of airfoil's angle of rotation was also investigated. A summary of the testing conditions is shown below in Table 4-1.

Table 4-1: Testing Conditions

Fuel	Feature	Nominal Inlet Temperature (K)	Reactant Temperature (K)	Nominal Pressure (atm)	Actual Pressure (atm)	Velocity (m/s)	Reynolds Number (x10^3)
Natural Gas	Cylinder 0.25"	300	295-298	3	3.04-3.27	40-60	251-412
Natural Gas	Cylinder 0.25"	530	502-523	3	2.99-3.45	53-92	128-225
Natural Gas	Cylinder 0.25"	530	500-510	5	4.88-5.22	22-56	85-221
Natural Gas	Cylinder 0.25"	530	488-510	7	6.51-7.44	24-68	128-412
Natural Gas	Cylinder 0.25"	650	600-612	5	5.02-5.46	40-79	123-247
Natural Gas	Cylinder 0.25"	650	595-612	7	6.26-7.27	42-76	166-319
Natural Gas	Cylinder 0.25"	650	596-604	9	8.59-9.35	40-64	217-353
Hydrogen	Cylinder 0.25"	530	499-512	3	2.95-3.17	55-109	119-247
Hydrogen	Cylinder 0.25"	530	500-515	5	4.90-5.22	74-84	196-315
Hydrogen	Cylinder 0.25"	650	581-616	3	2.97-3.13	84-105	136-174
Hydrogen	Cylinder 0.25"	650	540-624	5	5.02-5.14	46-86	153-217
Natural Gas	Step	530	497-508	3	3.03-3.29	54-101	115-221
Natural Gas	Step	530	501-509	5	5.05-5.37	42-90	145-319
Natural Gas	Step	530	502-507	7	6.74-7.24	42-71	200-387
Natural Gas	Step	530	503-507	8	7.82-8.31	71-81	395-434
Natural Gas	Step	530	498-506	9	8.60-9.52	39-67	255-459
Natural Gas	Step	650	580-607	3	3.03-3.24	51-97	81-162
Natural Gas	Step	650	590-606	5	4.94-5.38	50-101	136-276
Natural Gas	Step	650	596-611	7	6.98-7.33	40-76	145-285
Natural Gas	Step	650	592-611	8	7.61-8.48	44-88	187-332
Natural Gas	Step	730	643-680	5	4.90-5.41	65-94	140-217
Natural Gas	Step	730	654-684	7	6.98-7.40	49-81	145-264
Natural Gas	Step	730	652-678	8	7.54-8.32	44-73	157-242
Hydrogen	Step	530	491-513	3	2.98-3.20	64-107	123-221
Hydrogen	Step	530	497-505	5	4.83-5.34	53-101	166-336
Hydrogen	Step	530	499-510	7	6.87-7.11	54-87	234-378
Hydrogen	Step	650	591-608	3	2.95-3.17	83-106	111-153
Hydrogen	Step	650	608-613	5	4.90-5.13	58-91	128-208
Hydrogen	Step	650	591-613	7	6.77-7.10	42-89	136-336
Hydrogen	Step	650	595-605	9	8.59-9.14	65-94	276-434
Hydrogen	Step	730	620-690	5	4.92-5.23	64-114	132-221
Hydrogen	Step	730	620-622	7	6.90-7.14	64-70	200-221
Hydrogen	Step	730	696-713	9	8.70-9.24	63-100	200-293
Hydrogen	Airfoil (Neutral)	530	487-515	3	2.96-3.32	68-106	149-234
Hydrogen	Airfoil (Neutral)	530	495-513	5	4.96-5.20	63-71	157-272
Natural Gas	Airfoil (Rotated)	650	590-600	4	4.08-4.48	61-78	153-208
Natural Gas	Airfoil (Rotated)	650	587-606	5	4.89-5.45	48-84	153-247
Hydrogen	Airfoil (Rotated)	650	581-607	5	4.98-5.64	73-90	191-268
Natural Gas	Cylinder 0.50"	650	585-612	5	5.14-5.47	57-96	183-298
Hydrogen	Cylinder 0.50"	650	596-619	5	4.94-5.40	72-103	225-298

In summary, the temperatures, and velocities are representative of the majority of modern ground based gas turbines. While many current engines operate at pressure higher than this were studied here, this range of pressure, combined the realistic range of temperature and velocity means that the results of this experiment will still be of tremendous value to gas turbine designers. This is particularly true for experiments involving hydrogen, which currently has sparse data conditions that are relevant to gas turbine engines.

Chapter 5 - Results

Generally, it was observed that all of the test features had similar flameholding propensities. All of the center mounted features (cylinders and airfoil) were somewhat difficult to ignite because the spark igniter was located at the wall of the test section. The reverse facing step was much simpler to ignite. In all cases, the flame was ignited at a somewhat high equivalence ratio; approximately stoichiometric for natural gas and approximately 0.5 for hydrogen. Once ignited, it was observed that the reverse facing step tended to transfer considerably more heat to the test feature than the center mounted features. Because ignition was achieved at high equivalence ratio, the temperature of the surface just behind the reverse step could become quite high. Blow off was approached much more slowly for the reverse step so that test feature could come to thermal equilibrium, avoiding any piloting effects associated with excessively high wall temperatures. At blow off, the temperature of the test features was typically within 100 K of the reactant temperature.

However, each feature exhibited subtle differences in their behavior just prior to blow off. The blow off sequence for the 0.25 inch cylinder and the 0.5 inch cylinder are shown in Figure 5-1 and Figure 5-2, respectively. In both cases, just prior to blow off the non-luminous region of the flame just behind the bluff body stretches. Additionally, the flame brush becomes narrower. As the flame becomes leaner, the flame temperature is lowered and the heat transferred from the recirculation zone into the reactants is reduced. When the heat transfer to the reactants becomes too low, the reactants take longer to ignite, which results in the narrowing the flame brush. The wake of the bluff body has a finite recirculation zone length. If the point where the reactants ignite is sufficiently far downstream, then high temperature products will not be drawn into the recirculation zone, rather simply entering the turbulent wake region. When this occurs, the recirculation zone becomes less luminous, due to the lack of hot products. The lack of hot products in the recirculation zone further reduces the heat transfer to the reactants, ultimately leading to complete flame extinction.

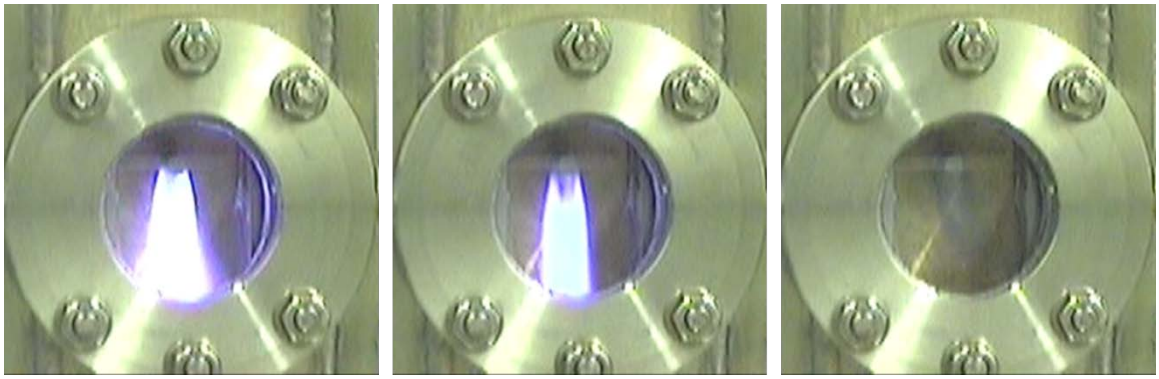

Figure 5-1: Blow off sequence for a natural gas flame with the 0.25 inch cylinder

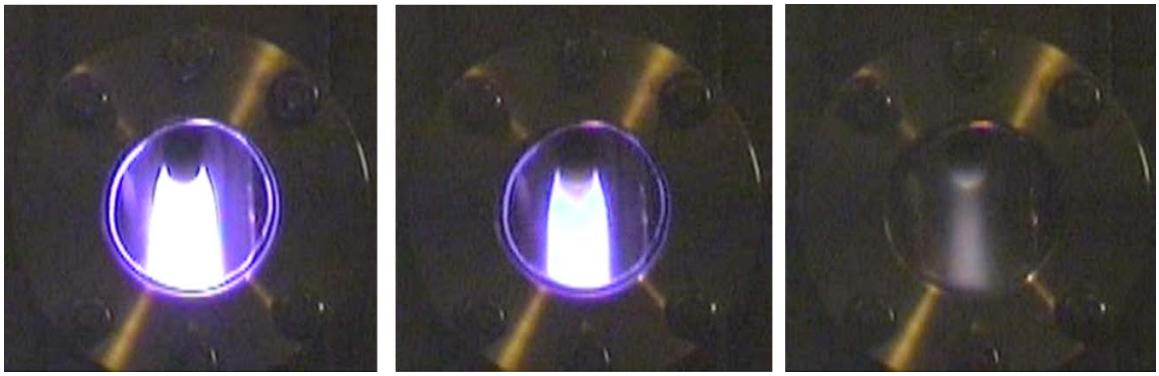

Figure 5-2: Blow off sequence for a natural gas flame with the 0.50 inch cylinder

Figure 5-3 shows the blow off sequence for the reverse step flameholder. The sequence is similar to that of the cylindrical flameholders in that, just before blow off, the flame becomes much less luminous and shrinks in size. However, unlike the flames anchored on cylinders, which tend to become narrower but do not shrink in the axial direction, the reverse step flames become shorter. The first image in Figure 5-3 shows that the flame extends fully across the test section and extends below the window. The second image in Figure 5-3 shows that just prior to blow off the flame recedes slightly from the walls of the test section and becomes considerably shorter. This is fundamentally an effect of the way that the reverse step is constructed; the step first recedes into the back wall of the test section, and then ascends back to the original height at a slope of fifteen degrees. This effectively confines the wake region to the depressed area immediately behind the step. Once again, as the flame becomes leaner, the point where

the reactants are ignited is pushed down stream. Once this point is beyond the depression behind the step, high temperature products are no longer transferred into the recirculation zone, stopping the ignition of reactants. The narrow flame band seen in the second image of Figure 5-3 is likely the small amount of hot products that remain after the ignition of new reactants has been halted.

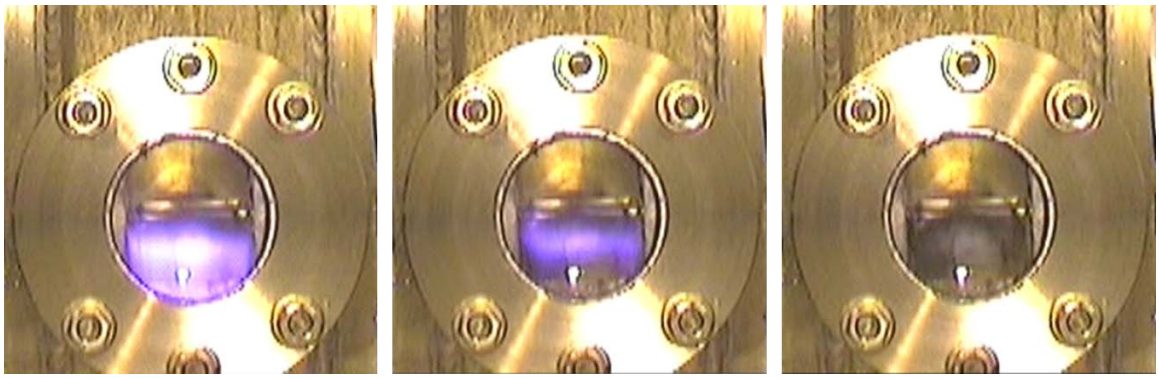

Figure 5-3: Blow off sequence for a natural gas flame with the reverse step

Figure 5-4 shows the sequence of blow off for the rotated airfoil. The blow off sequence is largely the same as that of the cylindrical flameholders. What is unique about this test feature is that because it is much longer in the direction of flow than either of the cylinders, when the flame is pushed downstream, one can see it travel down along the inside edge of the airfoil before finally being pushed off the trailing edge of the airfoil.

Figure 5-4: Blow off sequence for a natural gas flame with the rotated airfoil

The biggest difference between any of the tests in this experiment were found between hydrogen and natural gas flames. The hydrogen flames extinguished at much lower equivalence ratios than that or natural gas. Figure 5-5 shows a natural gas flame and a hydrogen flame stabilized on the 0.25 inch cylinder at 500° F (530 K) three atmospheres absolute pressure, and a bulk velocity of seventy meters per second. In both cases, the flame attaches at the points of flow separation on either side of the cylinder. In the case of the natural gas, the two flames expand into the wake region and form a single flame approximately one cylinder diameter downstream. Unlike the natural gas flame, the hydrogen flame is barely visible and the flames at either anchor point do not expand inward. This is not surprising because the lean hydrogen flame exhibits much lower expansion due to temperature rise than natural gas. While it would have been impossible to run hydrogen at flame temperatures as high as those of natural gas without triggering a flashback, if it were possible, the flame would likely be as wide as those fueled by natural gas.

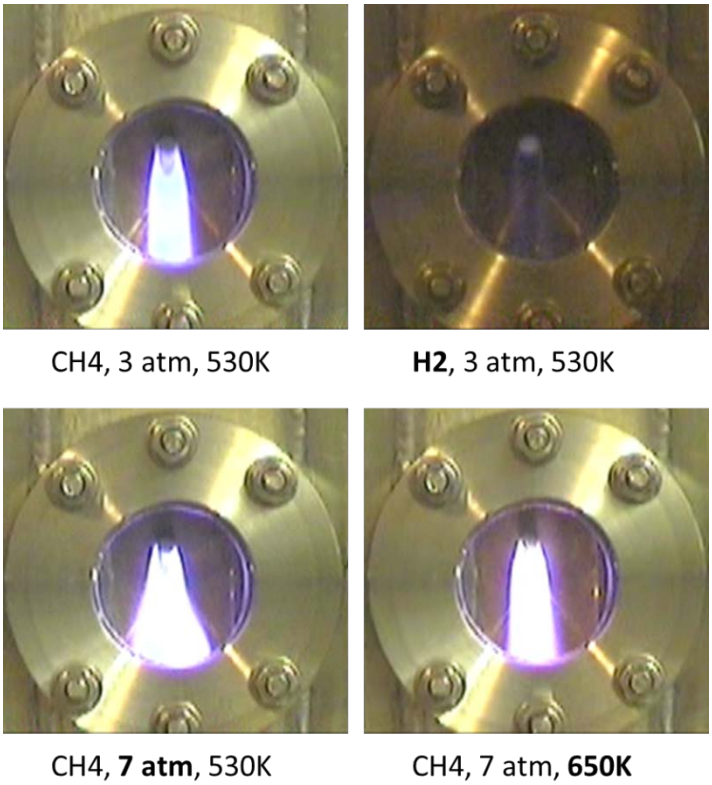

Figure 5-5: Effects of temperature, pressure and fuel type on the appearance of natural gas flames, stabilized with the 0.25 inch cylinder at 70 m/s bulk velocity

Figure 5-5 also shows the effects on the flame with increasing pressure and temperature. At seven atmospheres absolute pressure, the flame brush becomes much wider than at three atmospheres. However, the length of the recirculation zone appears to be unchanged. At 700° F (650 K) and seven atmospheres absolute pressure, the flame once again becomes narrow. However at higher temperatures the recirculation zone length appears to be shorter than either at 530 K. Note that in all of the natural gas images in Figure 5-5 the adiabatic flame temperature is approximately 2100 K. If the final temperature is constant and the pressure is increased, the density of the products increases. If the final temperature is constant and the inlet temperature increases, then the dilation ratio (the ratio of the temperatures of the products and reactants) is reduced, resulting in a more compact flame. These results are summarized in the table below.

Table 5-1: Effects of pressure and dilation ratio on flame thickness

Condition		Flame thickness
Pressure	Increases	Increases
	Decreases	Decreases
Dilation Ratio	Increases	Increases
	Decreases	Decreases

As blow off was approached, there were no obvious combustion instabilities observed for the center mounted test features, or for hydrogen flames. However, instabilities were observed when the reverse step flameholder was operated on natural gas (Figure 5-6). Combustion oscillations were not observed for hydrogen flames. Hydrogen flames blow off at much lower equivalence ratios, they emit much less light prior to blow off, making it very difficult to observe any small changes in the shape or location of the flame. Analysis of the combustion oscillations was performed on one second of recorded video of natural gas flames to determine their frequency of oscillations for the reverse step flameholder. The intensity of the combustion fluctuations were measured using the luminosity of the video images.

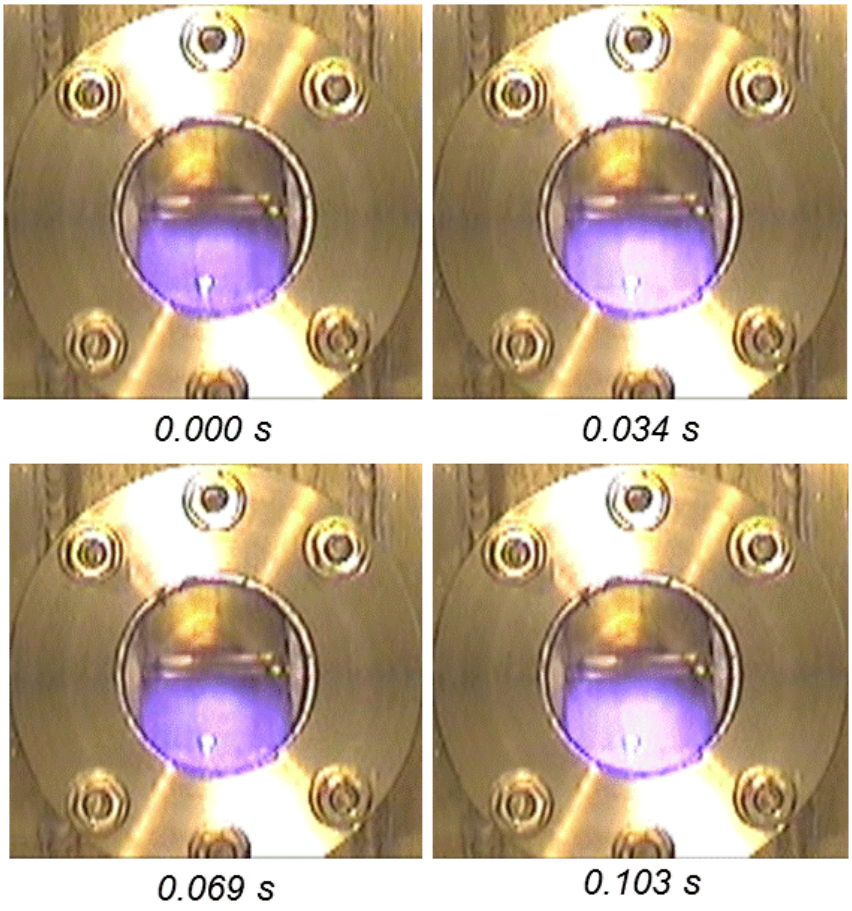

Figure 5-6: Combustion oscillations for a natural gas flame with reverse step flameholder

First, the color video was desaturated, resulting in a grayscale video. The individual frames were extracted and visually inspected to find a region of the flame whose intensity fluctuations could be measured. The luminosity of a single pixel in this region was measured for each frame and plotted as a function of time. However, the video was recorded at 29 frames per second, so considerable aliasing was present in the luminosity graphs. A least squares analysis was carried out to resolve the true frequency of oscillation. The frequency, amplitude, phase and offset of a sine function were systematically varied. With each adjustment, the square of the difference between measured intensity value and the value of the sine function at each point were totaled. The sum of the squared differences was used to measure the closeness of fit of the sine function to the measured value. Figure 5-7 and

Figure 5-8 show the results of this analysis for two experiments carried out at three atmospheres and 500° F (530K) inlet temperature, and 50 and 100 meters per second velocity.

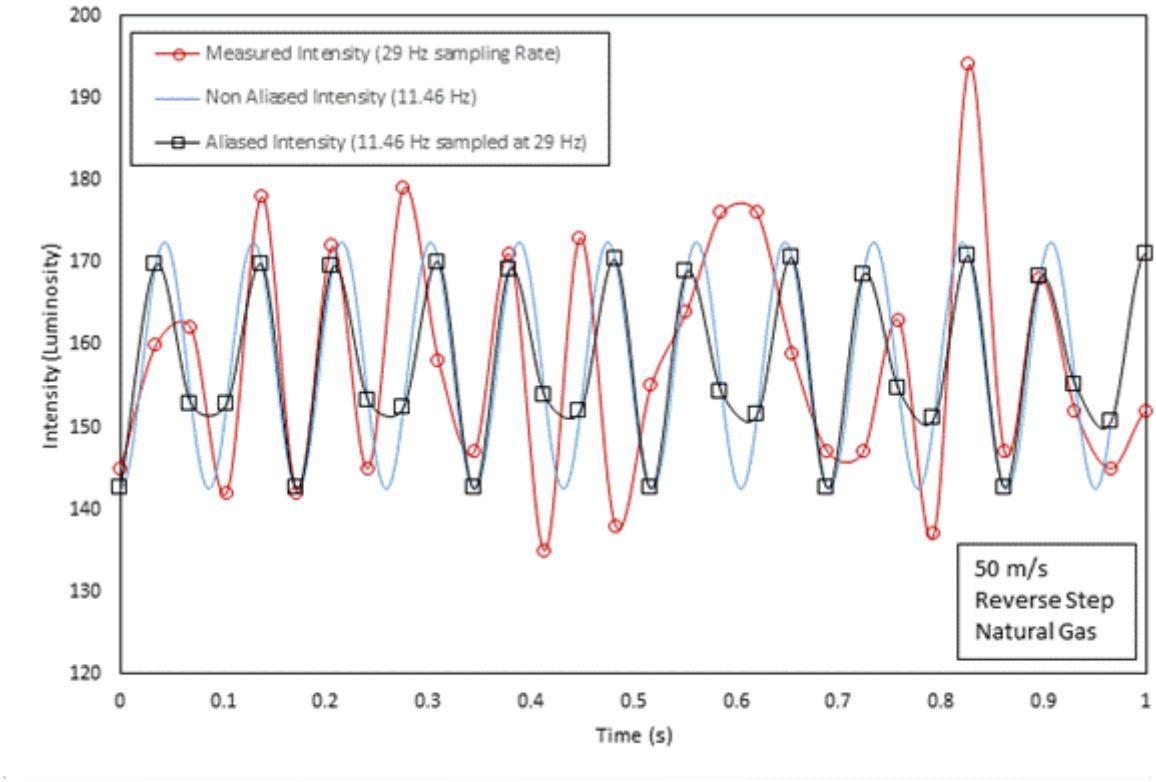

Figure 5-7: Flame luminosity as a function of time for the reverse step flameholder at 50 m/s

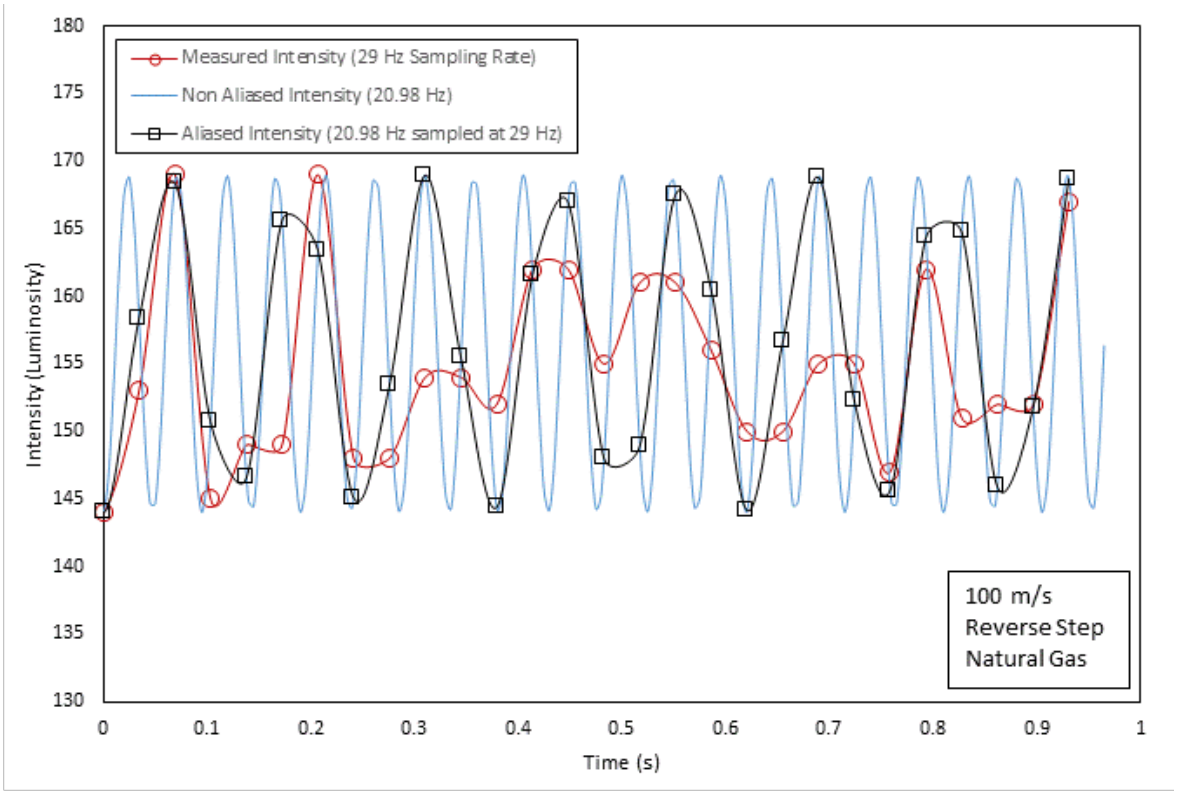

Figure 5-8: Flame luminosity as a function of time for the reverse step flameholder at 100 m/s

As can be seen in Figure 5-7 and Figure 5-8, the frequency of oscillation was found to be linearly proportional to the velocity of the reactants. The results of the least square analysis show that for conditions of Figure 5-7 and Figure 5-8, that at flame has oscillates at 11.46 Hz and 20.98 Hz, respectively.

5.1 Non Reacting Tests – LDV Results

One of the primary reasons for constructing a new test apparatus for this experiment was to guarantee fully developed flow at the test feature. As mentioned before, the previous test apparatus in the U.C. Irvine Combustion Laboratory for observing flameholding had poor flow development resulting in significant special variations in velocity. After construction of the new test apparatus, laser Doppler velocimetry was used to assess the velocity profile and turbulence levels of the flow field.

Because the test apparatus has a considerable amount of downstream equipment (e.g. back pressure valve, water drop out tank, quench pumps) whose functions could be impaired with the use of other seeding media such as alumina particles, water was used to seed the flow with particles. Because water can evaporate, LDV tests were performed at Reynolds numbers that were representative of the reacting tests but without preheating the air. The total range of Reynolds numbers of the reacting experiments was between 81,000 and 459,000. LDV experiments were carried out at Reynolds numbers of 146,000 and 295,000. Seventy percent of the reacting experiments were performed in this Reynolds number range. This is shown graphically in Figure 5-9.

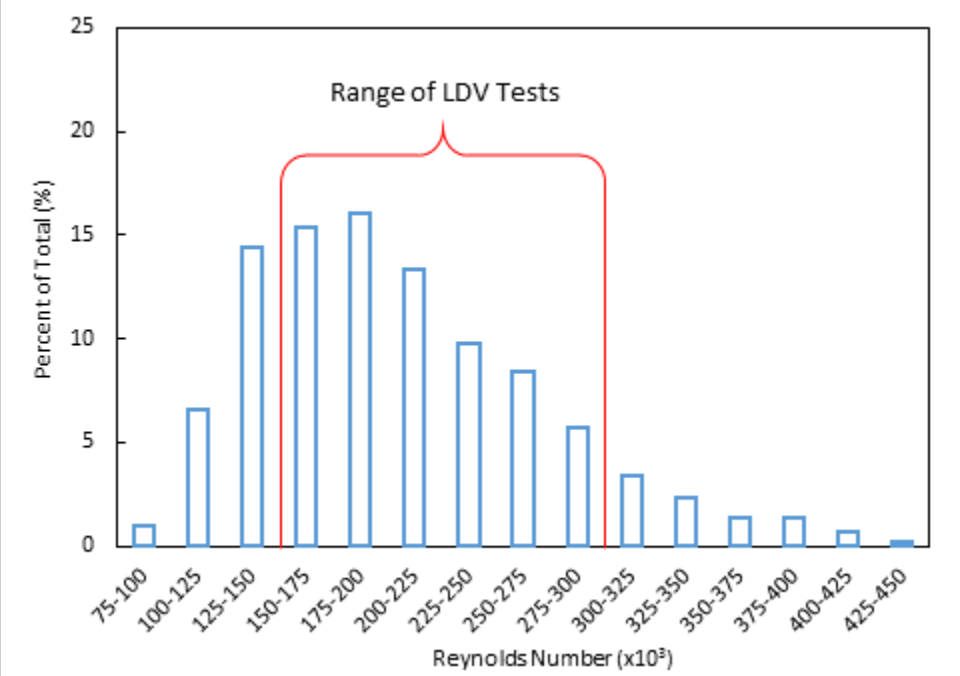

Figure 5-9: Reynolds number distribution of reacting tests

The first test (Reynolds number of 146,000) was carried out at a bulk velocity of 81 m/s, and 1.12 atmospheres. The second test (Reynolds number of 296,000) was carried out at a bulk velocity of 61 m/s and three atmospheres. Data was taken along center of the test section, at five millimeter intervals. The

first and last data points were taken at one millimeter from the edges of the test section. A schematic of the test points is shown in Figure 5-10.

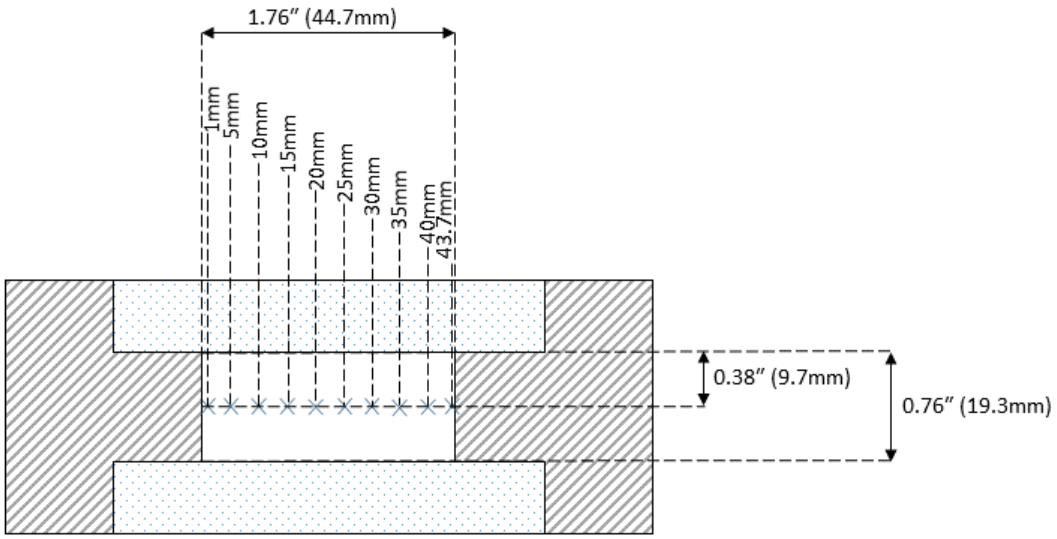

Figure 5-10: Schematic of laser Doppler velocimetry test points

Generally, the velocity at each Reynolds number was quite uniform. At a Reynolds number of 146,000, the spatial average velocity was 81.28 m/s with a standard deviation of 0.13 %. At a Reynolds number of 295,000, the special average velocity was 61.17 m/s with a standard deviation of 0.34%. The velocity profiles of these two tests are shown in Figure 5-11.

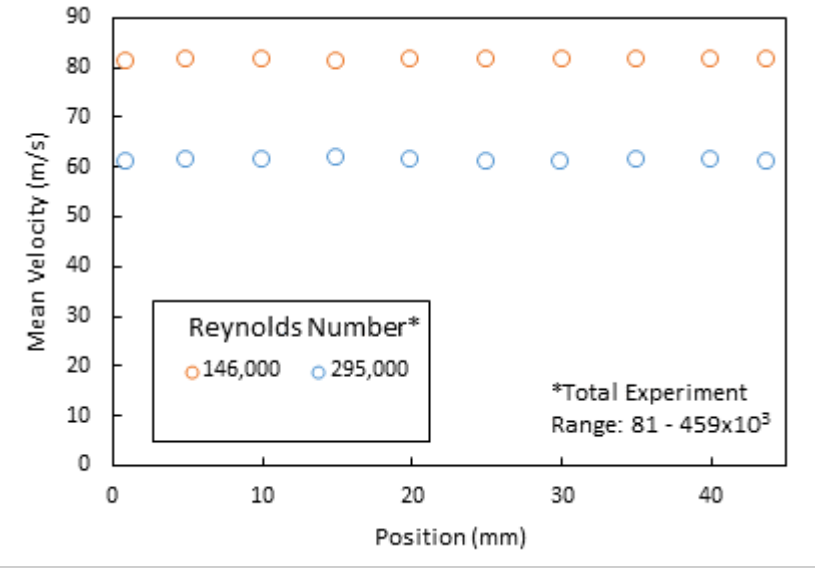

Figure 5-11: Velocity profiles measured with laser Doppler velocimetry

Measurements of the turbulence intensity were similarly uniform. At a Reynolds number of 146,000, the spatial average turbulence intensity was 4.31% of the bulk velocity, with a standard deviation of 2.27%. At a Reynolds number of 295,000, the spatial average turbulence intensity was 4.05% of the bulk velocity, with a standard deviation of 3.55%. The measured values of turbulence intensity are slightly higher than those predicted for fully developed pipe flow using the equation (Fluent 2006):

$$I = 0.16 \cdot {Re_{Dh}}^{-0.125}$$

Where *Dh* is the hydraulic diameter of the channel:

$$D_h = \frac{4(Area)}{Perimeter}$$

In this case the hydraulic diameter is equal to 1.06 inches (27 mm).

This correlation predicts turbulence intensities of 3.62% at a Reynolds number of 146,000, and 3.31% at a Reynolds number of 295,000. In both cases the measured value is approximately twenty percent higher than the predicted case. The turbulence intensity profiles are shown in Figure 5-12.

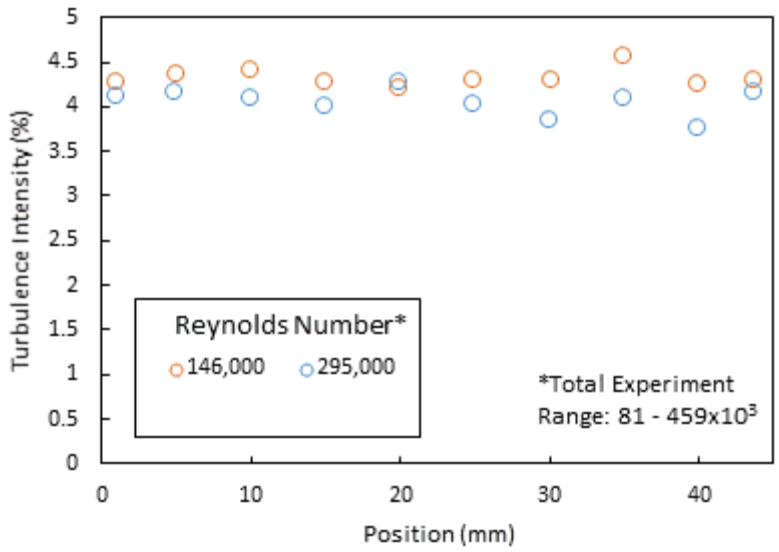

Figure 5-12: Turbulence Intensity profiles measured with laser Doppler velocimetry

It is not obvious whether or not this could be an artifact of the signal processing software, whose calculated turbulence levels are somewhat sensitive to input parameters. While every effort was made to ensure a perfectly smooth inner wall inside of the test apparatus, because it is constructed of several sections there are likely small gaps or other surface imperfections on the inner surface. Additionally, the pilot fuel injection points and spark igniter, while not protruding into the flow, could contribute to the measured turbulence levels being slightly higher than the predicted values. In any case, the important take away is that the turbulence levels follow the same trend as the correlation, albeit slightly higher, which predicts that they remain relatively constant over the range of experiments.

5.2 4.2 Reacting Tests

Initial reacting tests focused on the 0.25 inch cylinder and the reverse step. Both of these test features were operated on hydrogen and natural gas fuels and tested over a wide range to temperatures and pressures. It has been documented that with increasing inlet temperature that hydrogen has a diminishing stability envelope. That is, the region between equivalence ratio at flashback and that of

blow off decreases to the point where the flame either flashes back or blows off, with no stable region in between. This was observed when the 0.25 inch cylinder was operated on hydrogen. At 850° F (730K) nominal inlet temperature there was no range of equivalence ratio that stabilized the flame on the cylinder but did not also allow the flame to stabilize on walls of the test section. At 700° F (650K) a flame could still be stabilized at three and five atmospheres pressure, but not at any higher pressures. The symmetric airfoil was first tested in the neutral position. In this configuration a natural gas flame could not be stabilized under any conditions. With considerable difficulty, it was possible to stabilize a hydrogen flame under certain conditions. However, due to the lack of an appreciable recirculation zone in the wake of the airfoil, the flame stabilization method is different than for other typical bluff bodies. Hydrogen flames in this configuration were stabilized along the trailing edge of the airfoil, likely due to boundary layer growth decreasing the local flow velocity. Because the airfoil was all but immune to flameholding in the neutral position it was rotated in future tests. The airfoil was rotated until flow was observed to separate behind it. This was accomplished by igniting the center pilot fuel stream with a very low flow rate. This allowed the visualization of the flow. The airfoil could then be rotated until it was clear that the flow was not following along the inner surface of the airfoil. This is shown in Figure 5-13.

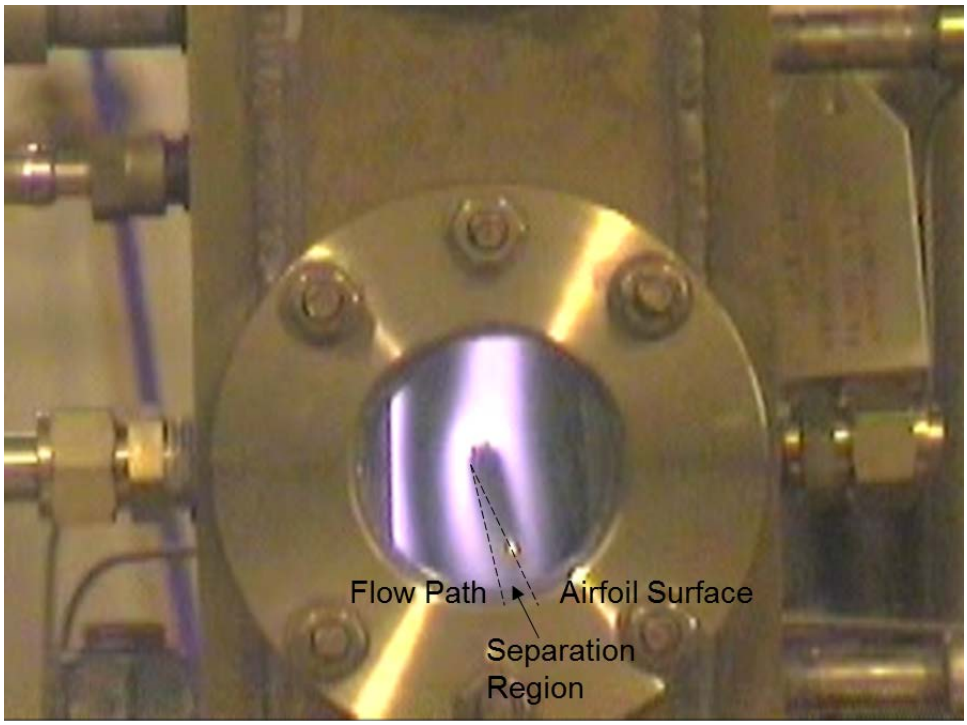

Figure 5-13: Separated flow in the wake of the rotated airfoil

Once flow was separated behind the airfoil, and not before, the airfoil began to readily hold a flame for both natural gas and hydrogen. Determining the appropriate physical dimension to characterize the rotated airfoil is more complicated than for the cylindrical or reverse step flameholders. While a case can be made for using either the chord length of the airfoil or thickness of the airfoil, neither of these dimensions were used. Instead the projected frontal width of the flame attachment points was used as the physical dimension for the rotated airfoil. The rotated airfoil projected a frontal width of 0.5 inches, which allows it to be compared to the 0.5 inch diameter cylinder. It was observed that in this configuration, that the airfoil had similar performance to the 0.5 inch cylinder (Figure 5-14).

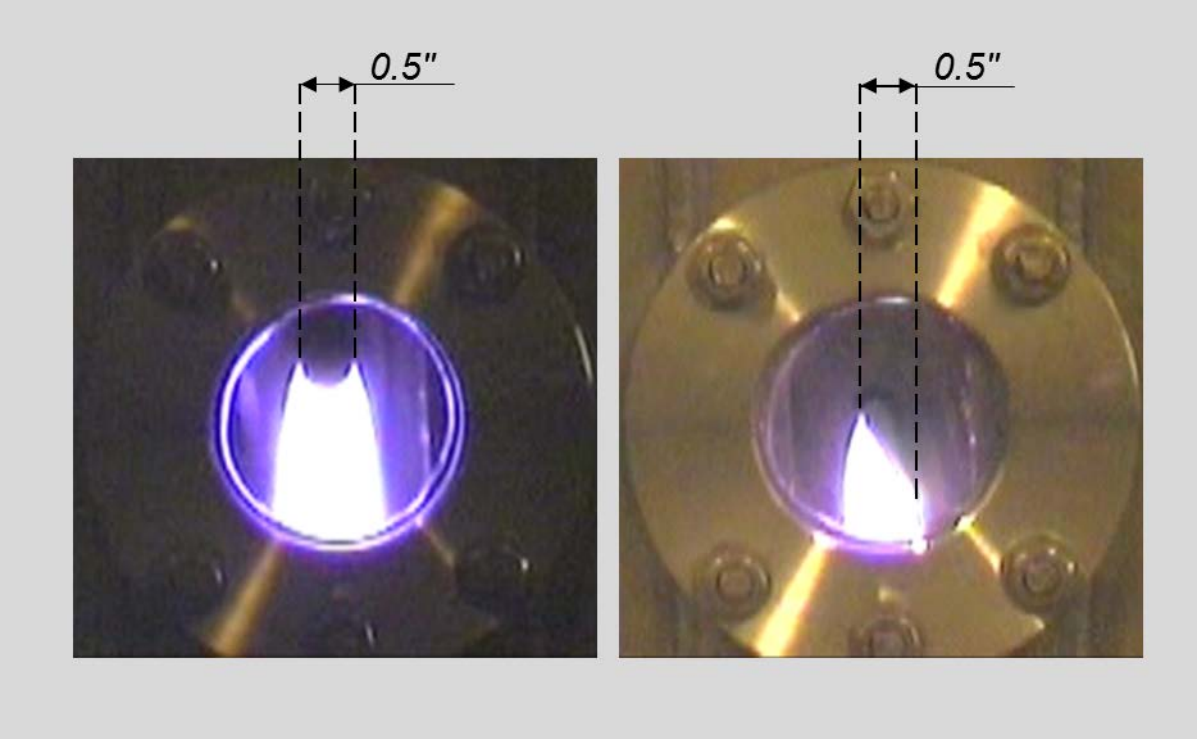

Figure 5-14: Rotated airfoil and 0.5 inch cylinder flame attachment width comparison

The goals of this study involve not only collecting data on flameholding for hydrogen and natural gas at elevated temperatures and pressures, but also developing correlations that predict when flameholding will occur, and determine what mechanisms are behind this phenomena. To this end, the flameholding data will be evaluated against current flameholding correlations to assess their validity. New flameholding correlations will also be discussed.

The results of this experiments are presented in Figure 5-15 and Figure 5-16. The equivalence ratio at blow off for different velocities is shown in Figure 5-15. The velocities shown in the following two figures are the velocities at the edge of the test feature calculated as:

$$U_{Edge} = U_{bulk}\left(\frac{A_{Channel}}{A_{Channel} - A_{Feature}}\right)$$

All velocities have also been corrected for the volume and temperature of the fuel present in the mixture. Two distinct groupings are seen representing natural gas and hydrogen. What is worth noting is that, for each test, (1) the equivalence ratio at blow off remains essentially unchanged as velocity increases and (2) the blow off equivalence ratio at which flames anchored behind the 0.25 inch cylinder and those anchored behind the step appear similar. Natural gas flames tend to extinguish between equivalence ratios of 0.6 and 0.9, while hydrogen flames are extinguished between 0.2 and 0.4. Figure 5-16 shows the adiabatic flame temperature at blow off for different velocities. It is clear that the groupings for each fuel type become more condensed; indicating the effect of inlet temperature can be represented by its change in flame temperature. Natural gas flames tended to be extinguished by 2100 K, while hydrogen flames tended to extinguish at 1400 K.

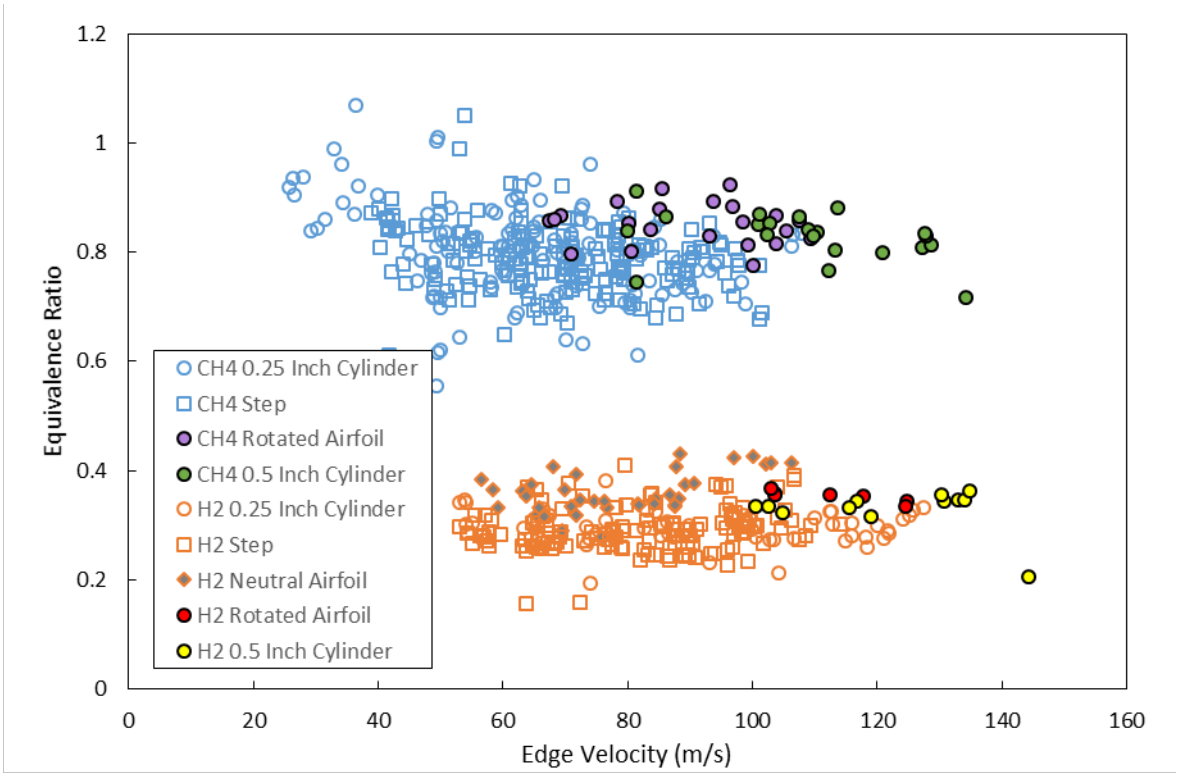

Figure 5-15: Equivalence Ratio at blow off as a function of velocity

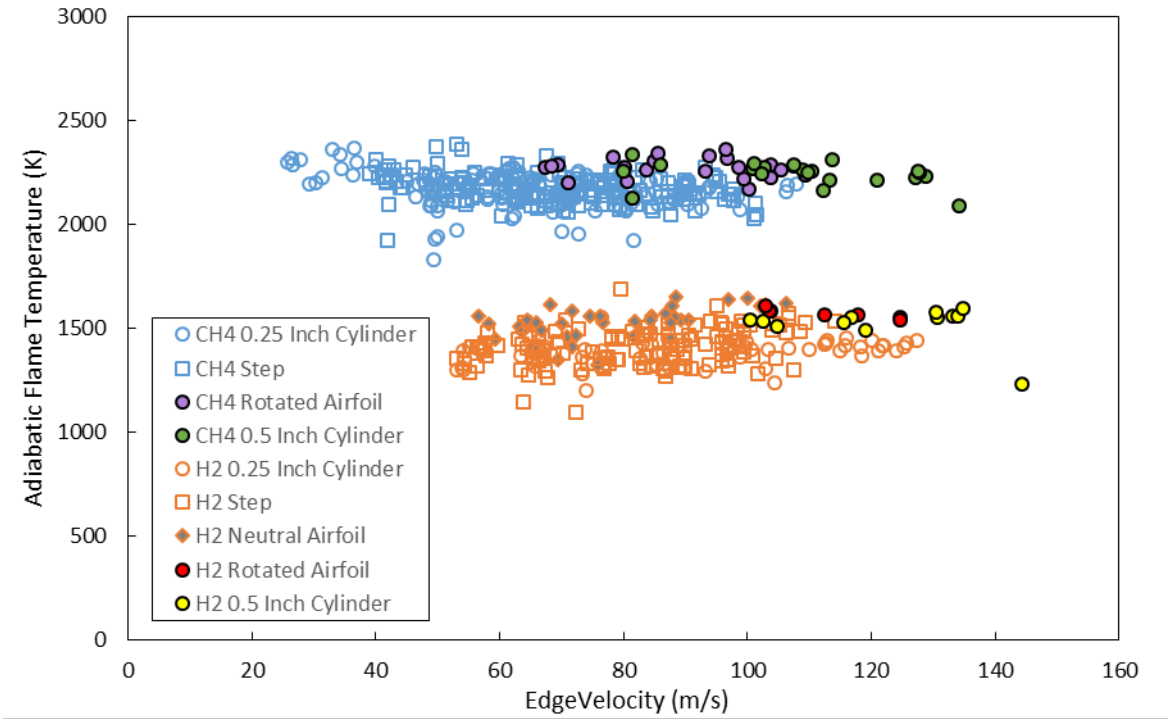

Figure 5-16: Adiabatic flame temperature at blow off as a function of velocity

Chapter 6 - Analysis

The goal for this study is to facilitate the adoption of hydrogen as a fuel for gas turbines by being able to predict when flameholding will occur for any fuel. The blow off data for both hydrogen and natural gas perform similarly, with the exception of the fact that hydrogen blows off at a much lower equivalence ratio/adiabatic flame temperature than natural gas. In order to use the data from this study, as well as other studies, a parameter common to both natural gas and hydrogen must be found that accurately predicts flameholding. A single expression must be found that predicts flameholding for both fuels.

6.1 Comparison with Previous Correlations

The fact that the point of blow off does not change substantially with increasing bluff body size seems to be at odds with much of the previous research that has been done on the subject of flameholding, but much of the previous research did not focus on the effects of blockage ratio. Blockage ratio, which is the ratio of the area of the flameholder to the area of the duct, increases with the size of the flameholder. The blockage ratio is not defined for open flames stabilized by bluff bodies, or rather, would approach a blockage ratio of zero. Ballal and Lefebvre's (1979) correlation for the blow off equivalence ratio indicates that for enclosed bluff bodies $\left(\text{Equivalence Ratio} \propto \left[U/\text{P}^{0.25}\text{Texp}\left(\frac{\text{T}}{150}\right)\text{D}(1-\text{B}) \right]^{0.16} \right)$, increasing the diameter tends to improve flame stability unless increasing bluff body size also increases blockage, which also increases the velocity at the edge of the flameholder, destabilizing the flame. Additionally, it is interesting that there is no observable effect of velocity. This is not an entirely unexpected behavior. Ballal and Lefebvre's correlation also predicts that at higher velocities (those above 40 m/s) that the effect of velocity is greatly reduced.

Generally, the correlation of Ballal and Lefebvre does an adequate job of describing the data obtained during this experiment. This can be seen in Figure 6-1 through Figure 6-3.

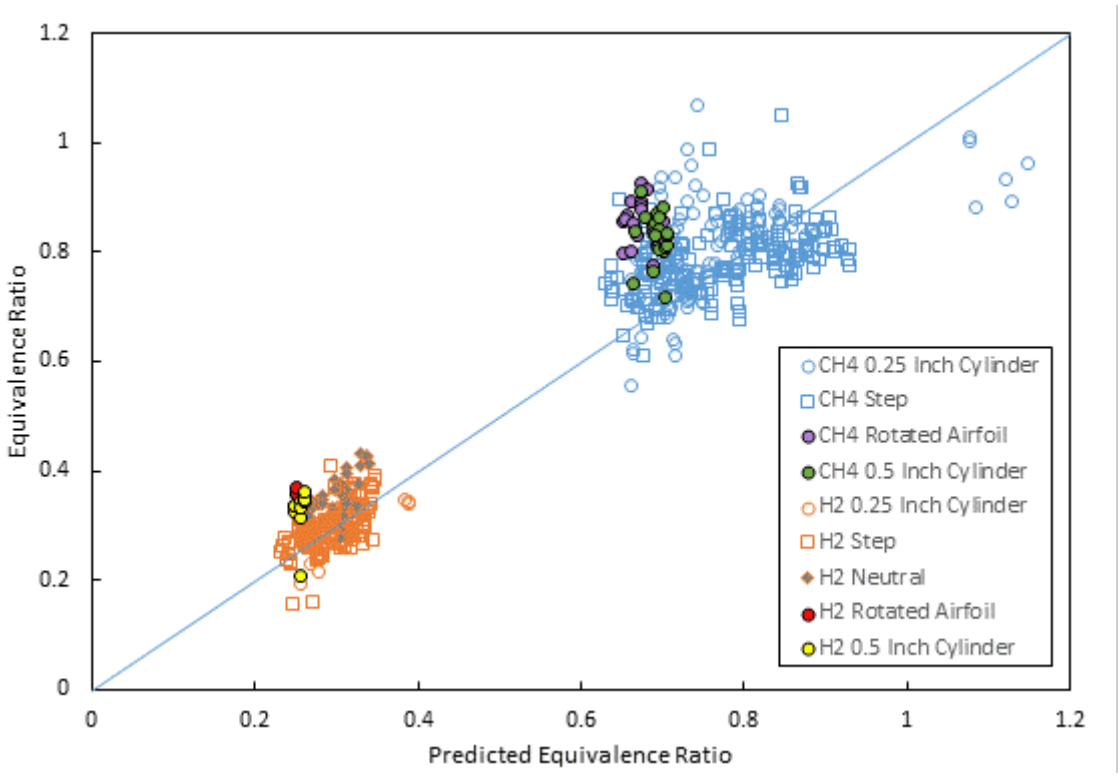

Figure 6-1: Comparison of data from the current study with correlation of Ballal and Lefebvre (1979)

Figure 6-1 shows the measured equivalence ratio at blow off for all of the experimental data compared to that predicted by this correlation. This correlation requires that a scaling coefficient be used. Unfortunately, though not unexpectedly, different scaling coefficients are used for natural gas and hydrogen. The predicted equivalence ratio for natural gas is scaled by 1.65, while hydrogen is scaled by 0.6.

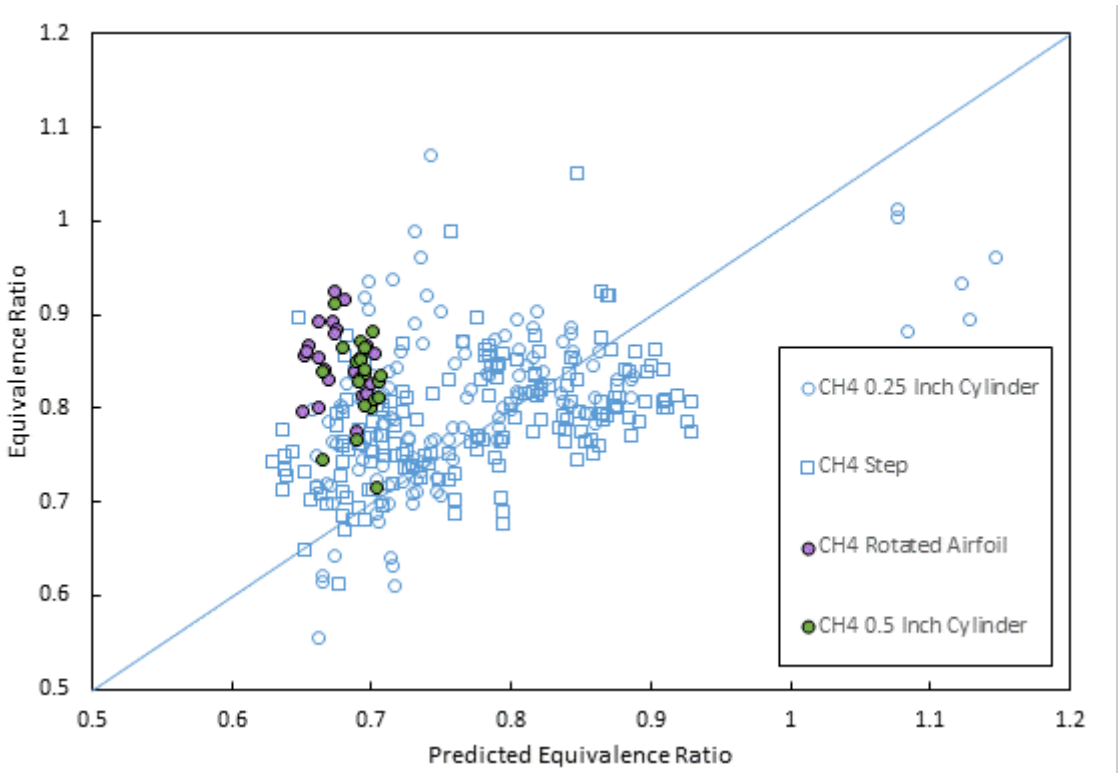

Figure 6-2: Comparison of natural gas data from the current study with correlation of Ballal and Lefebvre (1979)

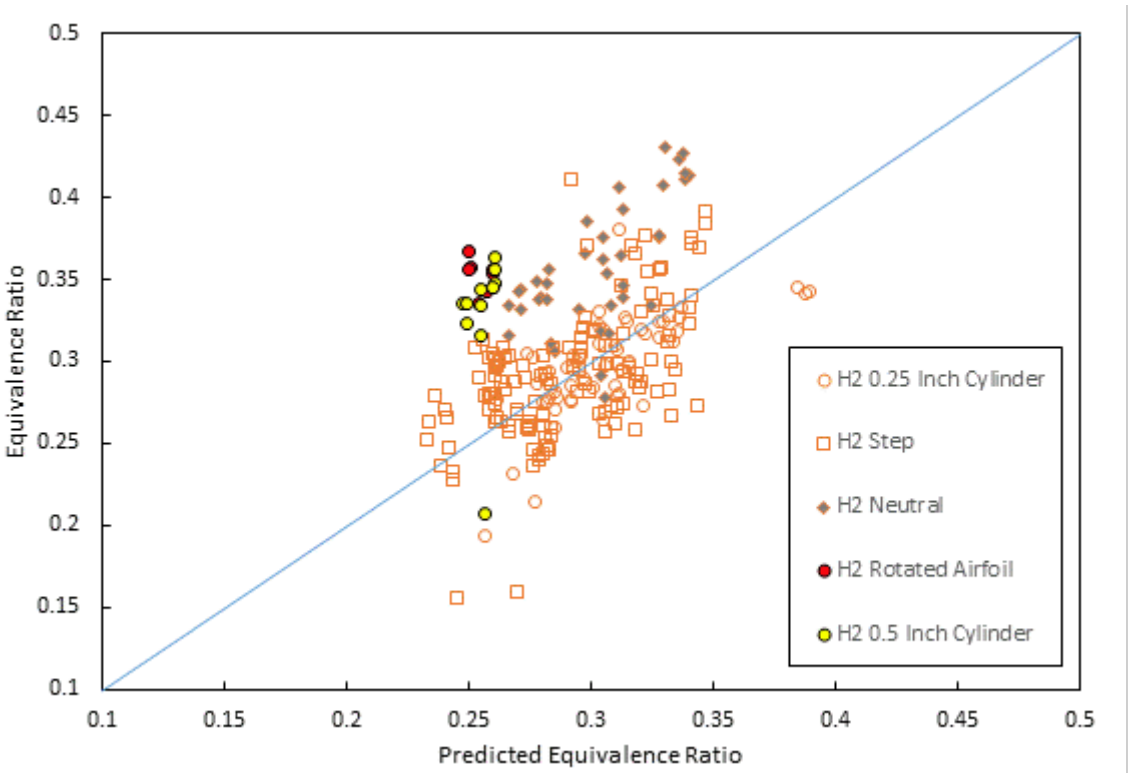

Figure 6-3: Comparison of hydrogen data from the current study with correlation of Ballal and Lefebvre (1979)

Figure 6-2 and Figure 6-3 show the measured equivalence ratio at blow off compared to predicted values for natural gas and hydrogen, respectively. By looking more closely at the data for each fuel, the correlation seems less able to accurately predict flame extinction Ballal and Lefebvre's equation correlates with the current data with an R^2 value of 0.122 for natural gas and 0.189 for hydrogen. While a general positive slope is clearly visible, the majority of the data do not fall on the one-to-one line. Additionally, the use of scaling coefficients makes this correlation of little use when predicting the behavior of new, untested fuels because a considerable amount of data is required before the scaling coefficient can be accurately predicting. Finally, while there may be some merit in the predictive abilities of this correlation, it provides little insight on the physical processes that are controlling the flame behavior.

6.1.1 Chemical Time Scales

Defining chemical times scales is necessary when determining Damköhler number. Typical definitions for chemical time scale include ignition delay time, flame sheet thickness divided by laminar flame speed, minimum perfectly stirred reactor time, and the inverse extinction strain rate. As part of the present work, analysis was carried out using ignition delay times, minimum perfectly stirred reactor times, and flame sheet thickness divided by laminar flame speed. For hydrogen, only ignition delay times and minimum perfectly stirred reactor times have been considered. The minimum perfectly stirred reactor time was used as a baseline for evaluating other methods of determining chemical time because it was used successfully by Shanbhogue (2009). The GRI 3.0 chemical kinetics mechanism was used for both natural gas and hydrogen. Methane was used to represent natural gas. CHEMKIN was used to calculate the reaction progress. The reactor temperature was set to the adiabatic flame temperature for the given inlet conditions in order to represent the reactants entering the flame zone and reacting. The minimum perfectly stirred reactor time was defined as the minimum residence time for which a temperature increase of at least 150K was observed. Ignition delay times were evaluated at the adiabatic flame temperature. Natural gas was evaluated using both low temperature ignition delay correlations (Beerer 2011) and high temperature ignition delay correlations (Burcat 1971). Only low temperature ignition delay correlations were used for hydrogen (Peschke and Spadaccini 1985). Additionally, Cantera was used to calculate ignition delay times for both hydrogen and natural gas. Cantera calculates ignition delay time by comparing reaction temperature as a function of time. The ignition delay time is defined as the temperature inflection point (where the temperature gradient is highest). Flame thickness divided by laminar flame speed was determined using CHEMKIN with the GRI 3.0 kinetic mechanism. Once again, natural gas was represented by methane. Flame thickness was taken as the flame temperature minus inlet temperature over the maximum temperature gradient. Results of these studies are shown in Figure 6-4 and Figure 6-5.

Figure 6-4 shows chemical time scale for all of the collected data as a function of velocity. It is not surprising to see that velocity has little to no effect on the chemical timescale at blow off because velocity had little effect on equivalence ratio and adiabatic flame temperature at blow off. Figure 6-5 shows the effect of adiabatic flame temperature on chemical timescale. Generally, increasing adiabatic flame temperature (moving toward a stoichiometric mixture) increases the reaction rate, resulting in smaller chemical times.

Both plots show a number of Cantera calculated ignition delay points for hydrogen at 0.001 seconds. This occurs when a temperature inflection point was not found, so the point of highest temperature gradient is found at the maximum calculation time. These were generally found at very lean hydrogen mixtures (adiabatic flame temperatures below 1400 K). This result makes the Cantera ignition delay times of questionable usefulness. However, those Cantera calculated ignition delay times that were successfully calculated seem to be of roughly the same values for methane and hydrogen. A similar trend was found with the perfectly stirred reactor times, which have similar values for both lean hydrogen and near stoichiometric methane flames. The low temperature ignition delay correlation times for methane were very close to the perfectly stirred reactor times for methane, but were significantly different than the low temperature ignition delay correlation times for hydrogen.

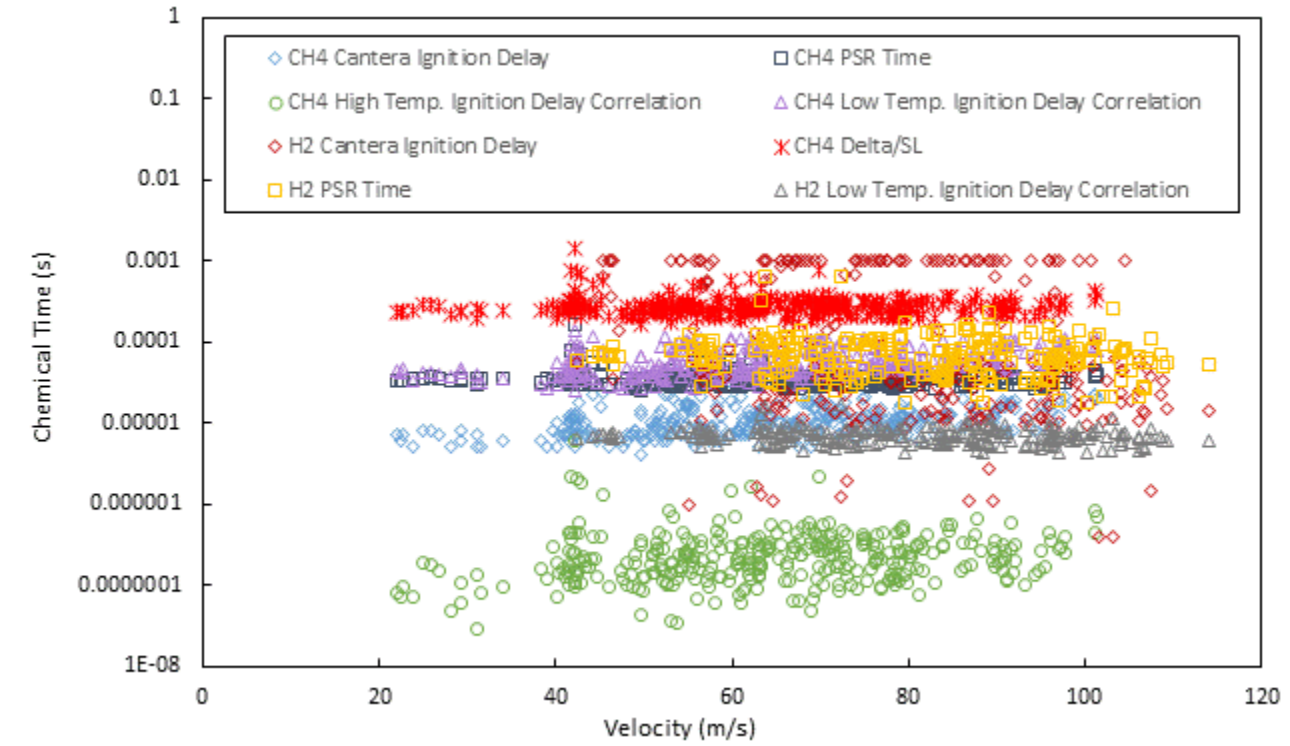

Figure 6-4: Chemical timescales evaluated with different methods plotted against edge velocity

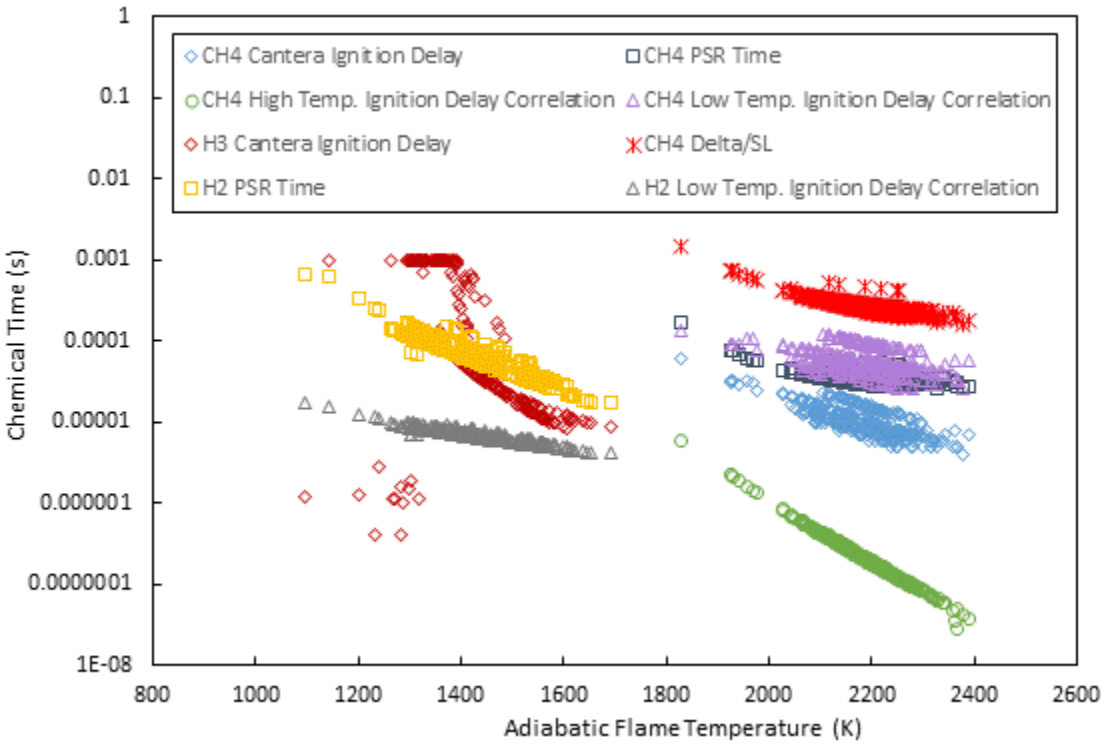

Figure 6-5: Chemical timescales evaluated with different methods plotted against adiabatic flame temperature

While empirical correlations such as those by Ballal and Lefebvre (1979) can produce acceptable flameholding predictions under some circumstances, they do not provide any insight into the mechanisms behind flameholding. Some of the earliest attempts to investigate the mechanisms behind flameholding attempted to correlate physical timescale with chemical timescale. The idea being that if the chemical time was appreciably longer than the physical timescale, then the flame would extinguish. If this were the case, one would expect to see chemical timescale increasing linearly with physical timescale. While this method was met with some success for atmospheric pressure experiments (Plee and Mellor 1979), there appears to be little correlation between physical timescales and chemical timescales of the data collected during this study. Figure 6-6 shows this. This is not surprising, as physical timescale is inversely proportional to velocity, and velocity was found to have little effect on adiabatic flame temperature, which correlates well with chemical timescale.

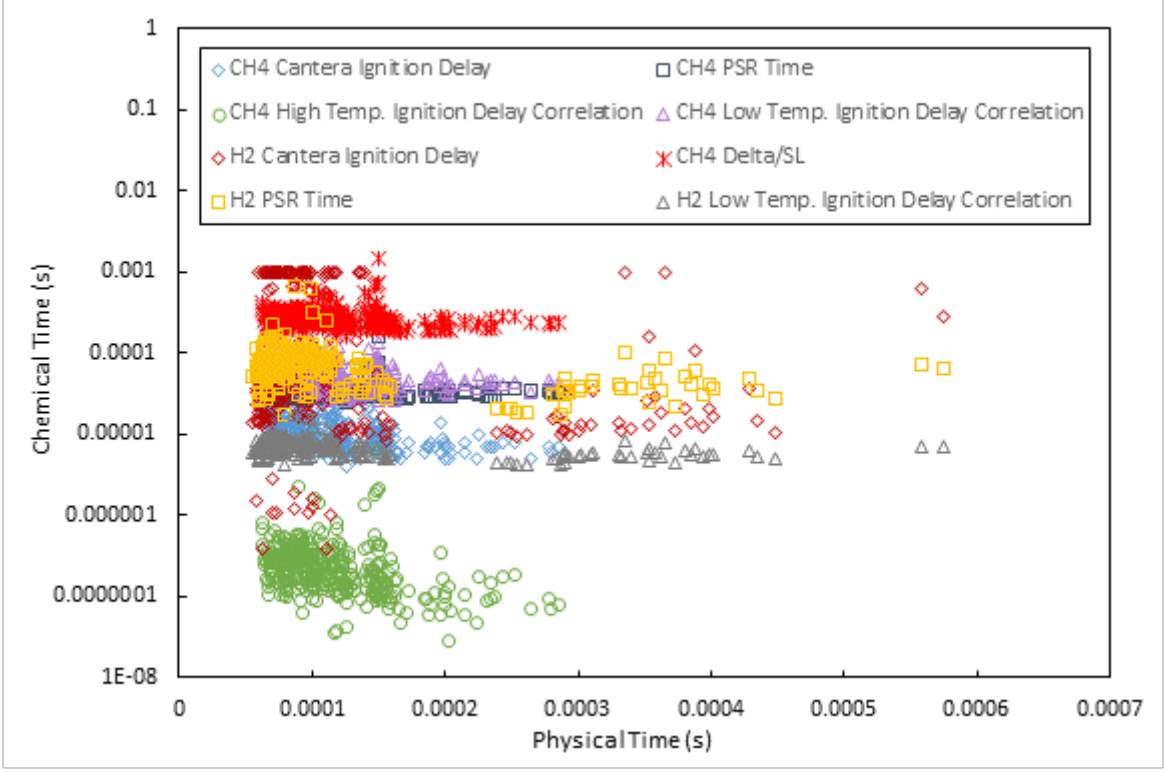

Figure 6-6: Chemical timescale calculated in a number of ways as a function of physical timescale

For clarity, Figure 6-7 shows just the chemical timescales that have good agreement between hydrogen and natural gas. Figure 6-7 shows the perfectly stirred reactor time for both hydrogen and natural gas as well as the low temperature ignition delay correlation for natural gas. The low temperature ignition delay correlation for hydrogen did not produce values on the same order of magnitude as low temperature correlation for natural gas, so it is not shown. It can be seen more clearly that the data from the current experiment shows no correlation between physical and chemical timescales calculated by any of these methods.

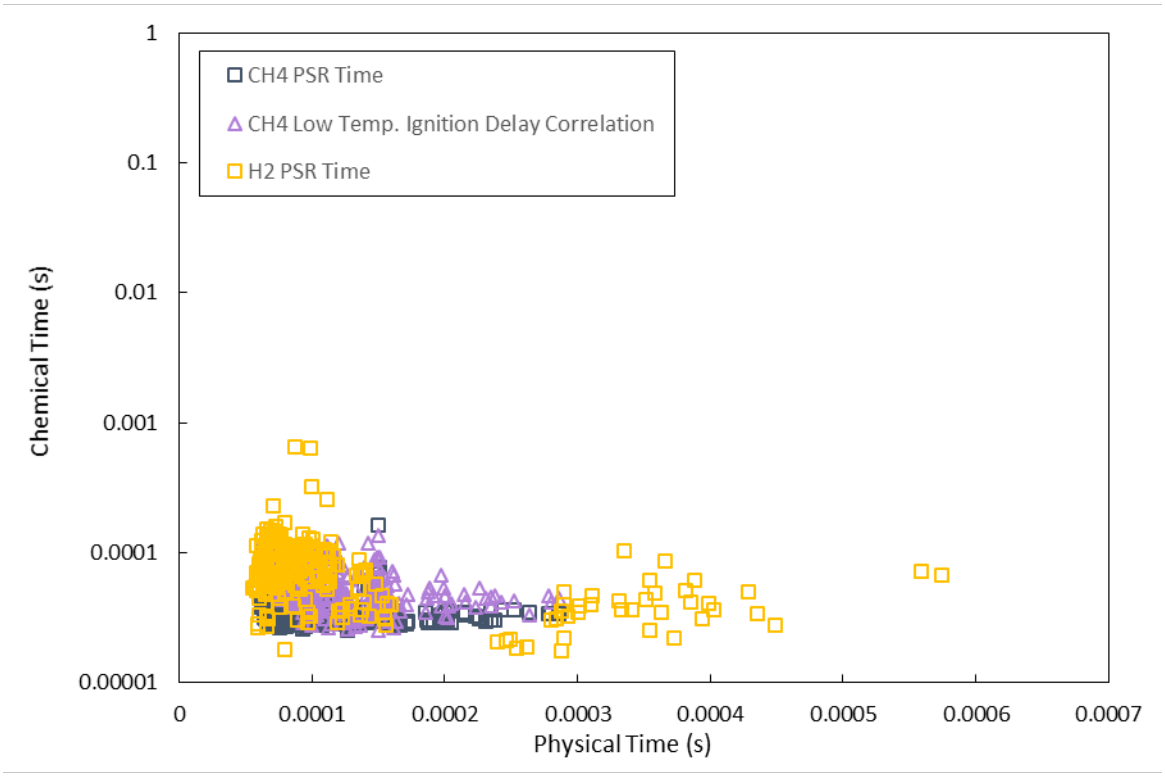

Figure 6-7: Chemical timescales calculated with the perfectly stirred reactor for hydrogen and natural gas, and the low temperature ignition delay correlation for natural gas as a function of physical timescale

Additionally, each of these chemical time scales was used to compare Damköhler number at blow off to Reynolds number with the goal of finding a single chemical time definition that would produce Damköhler numbers with low levels of scatter when correlated with Reynolds number for both hydrogen and natural gas. It was found that all chemical times produced Damköhler numbers with equivalent levels of scatter. The minimum perfectly stirred reactor time had low levels of scatter and produced correlations for both fuels that were of the same magnitude. For both fuels, low temperature ignition delay times also produced reasonably low levels of scatter but the hydrogen Damköhler values were roughly an order of magnitude larger than those for natural gas. Based on these results Damköhler number, based on minimum perfectly stirred reactor time, does the best job at accounting for fuel type and was used for analysis in this study. These results are shown in Figure 6-8.

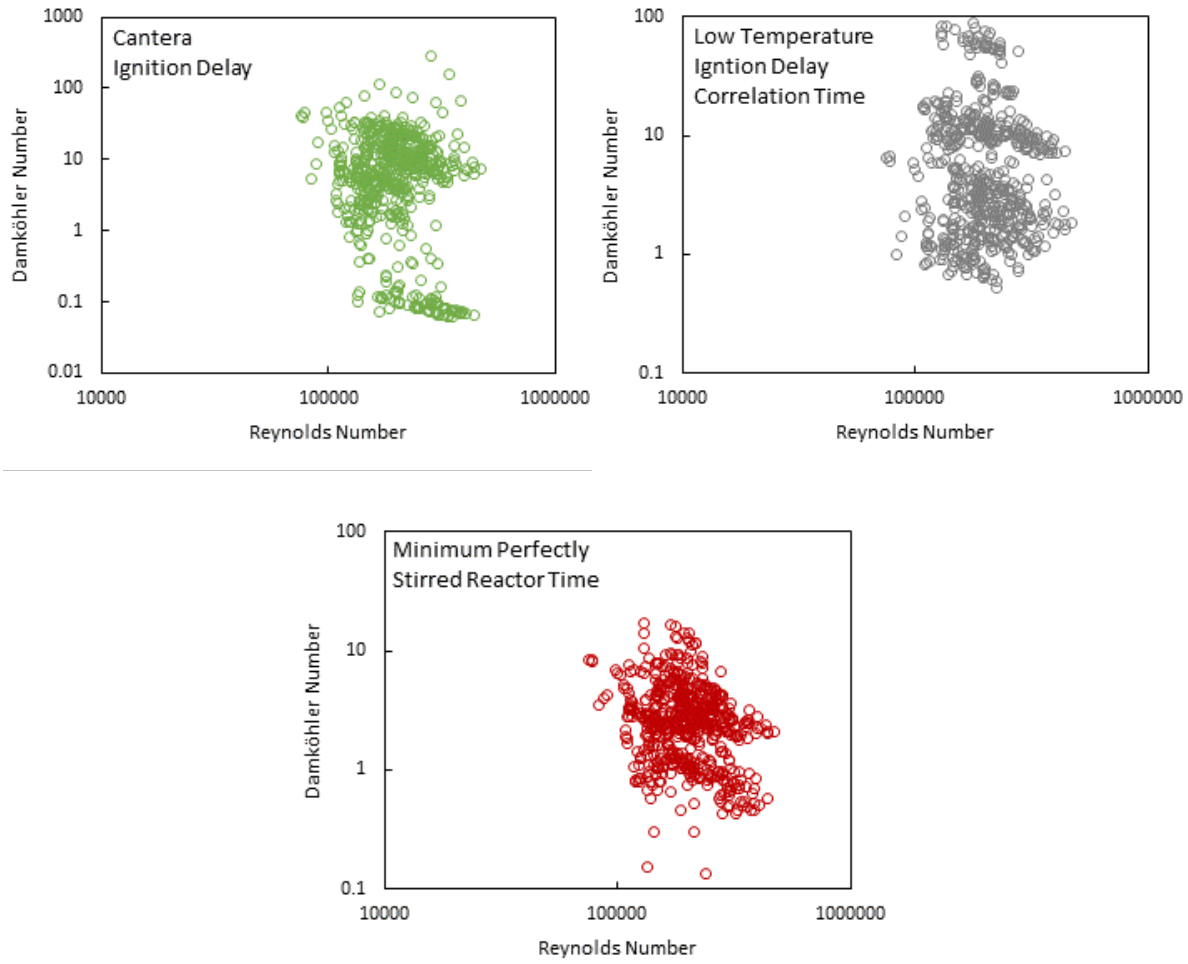

Figure 6-8: Several Damköhler numbers as function of duct Reynolds number

Results were also compiled in terms of Reynolds number and Damköhler number using the same methods employed by Shanbhogue et al (2009). Minimum perfectly stirred reactor time was used to define the chemical time scales, and physical time scale defined as boundary layer momentum thickness over the lip velocity. Boundary layer momentum thickness (δ) is proportional to frontal width of the feature and is defined as:

$$\delta = \frac{35 \cdot D}{\sqrt{Re_D}}$$

Reynolds number was calculated using the free stream velocity and frontal width of the feature in the case of cylinders and airfoils or step height. Results can be seen in Figure 6-9 - Figure 6-13.

Figure 6-9: Damköhler Number at blow off as a function of Reynolds Number for natural gas flames

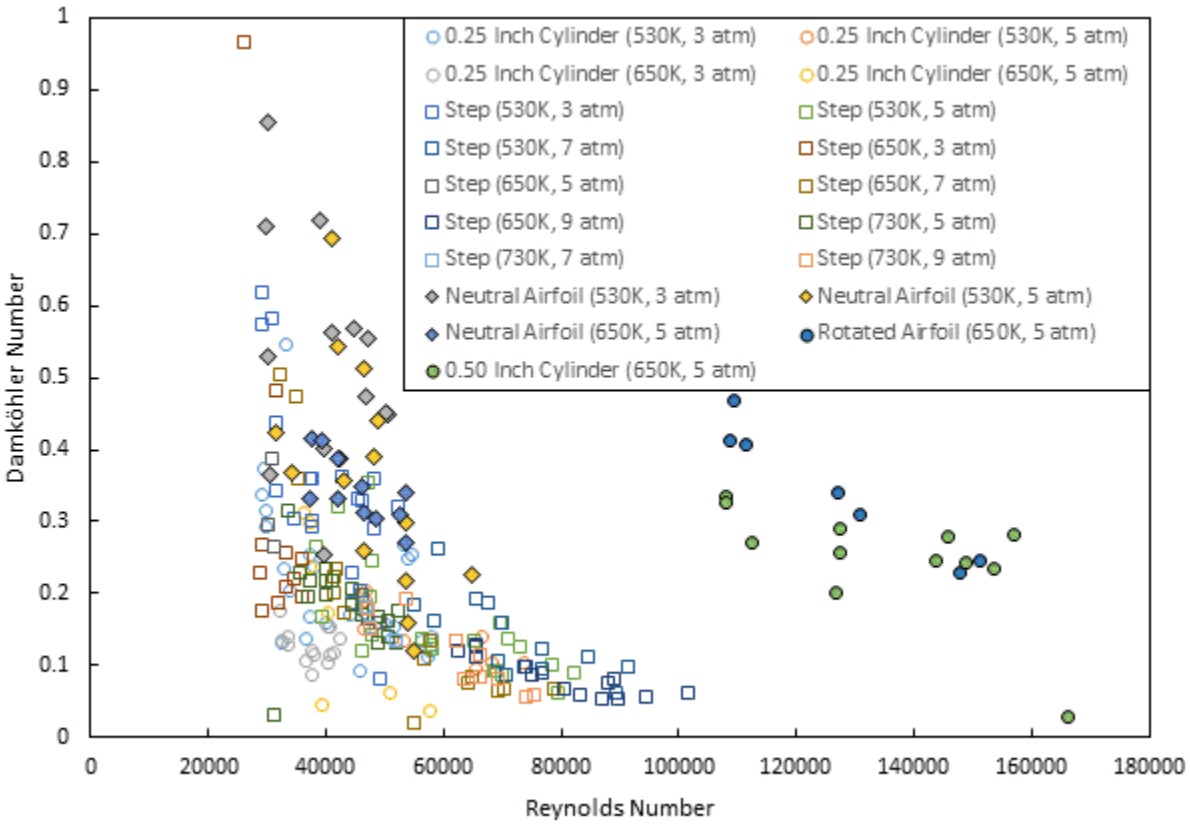

Figure 6-10: Damköhler Number at blow off as a function of Reynolds Number for hydrogen flames

Comparison of Figure 6-9 and Figure 6-10 show that, by expressing the data in this manner, hydrogen and natural gas appear to perform similarly, occupying a similar range of Damköhler number and Reynolds number. However, for both natural gas and hydrogen, the larger features (0.50 inch cylinder and rotated airfoil) appear to behave differently than the smaller features. This is a result of the higher Reynolds numbers associated with the wider features rather than a change in the Damköhler number. Recall that the adiabatic flame temperatures and values of Damköhler number at blow off were similar for both the larger and smaller features. Furthermore, pressure and inlet temperature also have a significant effect on these plots. This is most clearly seen for natural gas flames, as shown in Figure 6-11 and Figure 6-12.

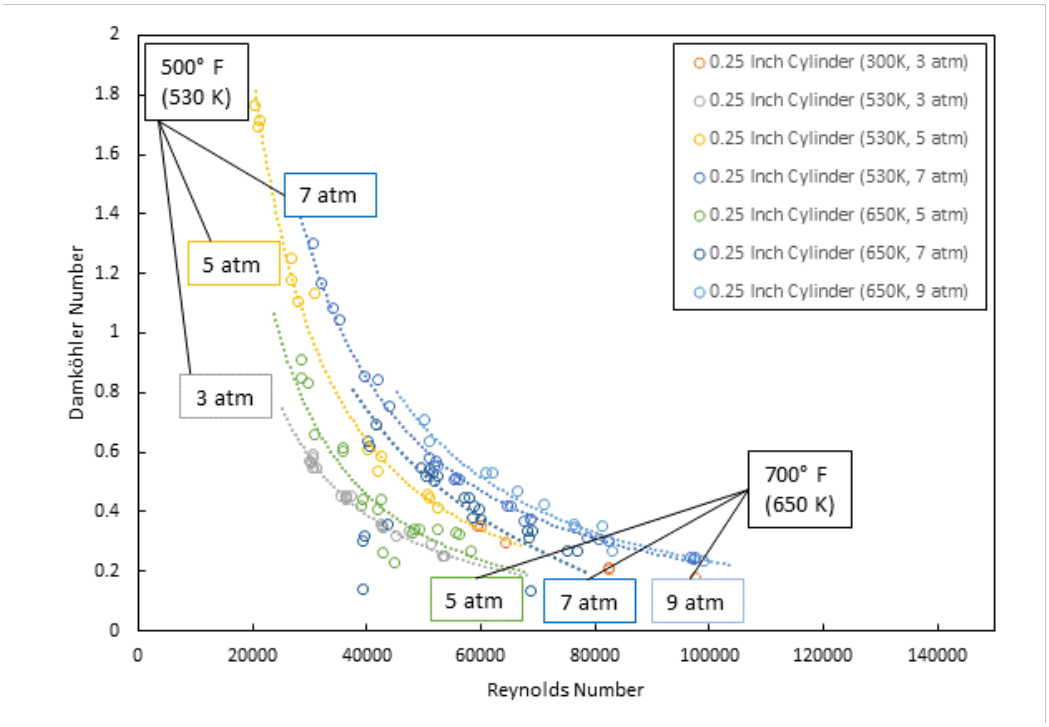

Figure 6-11: Effect of ressure and temperature on Reynolds-Damköhler plots for natural gas flames with 0.25 inch cylinder flameholder

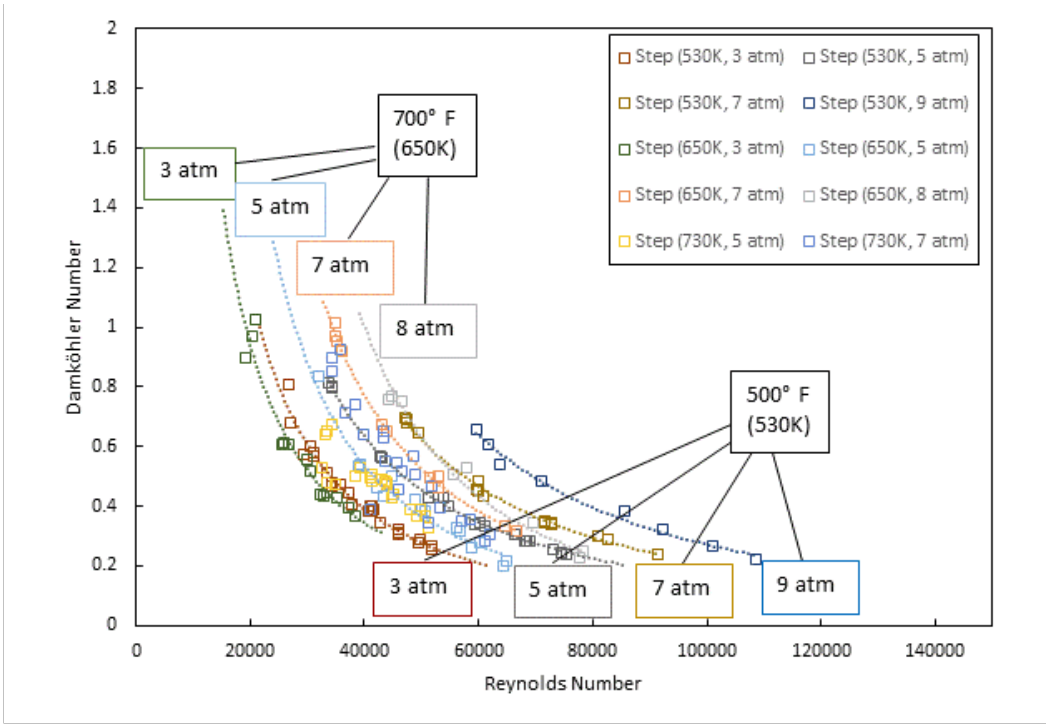

Figure 6-12: Effect of pressure and temperature on Reynolds-Damköhler plots for natural gas flames with 0.25 inch reverse step flameholder

Figure 6-11 and Figure 6-12 both show that increasing pressure tends to shift the curves of the Damköhler number – Reynolds number plots to the right, while increasing inlet temperature tends to shift these plots to the left. As was the case for the larger flameholders, the value of the Damköhler numbers are similar under all of these conditions; the effect of pressure and temperature is due to changes in the calculated value of Reynolds number. All cases exhibit similar behavior with respect velocity, inlet temperature, and pressure. In all cases each curve could be expressed in the form:

$$Da = aRe^{b}$$

The family of curves for natural gas flames typically takes the form:

$$Da = aRe^{-1.5}$$

Hydrogen flames produced less consistent exponential values, generally ranging from -1 to -2. These correlations are shown in Table 6-1.

Table 6-1: Comparison of Reynolds-Damköhler Correlations

Fuel	Feature	Nominal Inlet Temperature (K)	Nominal Pressure (atm)	Correlation Coefficients a	b
Natural Gas	Cylinder (0.25")	300	3	2.46E+06	-1.44
Natural Gas	Cylinder (0.25")	530	3	1.09E+06	-1.40
Natural Gas	Cylinder (0.25")	530	5	9.42E+06	-1.56
Natural Gas	Cylinder (0.25")	530	7	4.19E+06	-1.45
Natural Gas	Cylinder (0.25")	650	5	1.12E+07	-1.61
Natural Gas	Cylinder (0.25")	650	7	2.57E+02	-0.60
Natural Gas	Cylinder (0.25")	650	9	1.36E+07	-1.55
Hydrogen	Cylinder (0.25")	530	3	7.44E+03	-0.99
Hydrogen	Cylinder (0.25")	530	5	8.71E+04	-1.22
Hydrogen	Cylinder (0.25")	650	3	4.50E+01	-0.56
Hydrogen	Cylinder (0.25")	650	5	3.00E+17	-3.96
Natural Gas	Step	530	3	4.37E+06	-1.53
Natural Gas	Step	530	5	4.99E+06	-1.50
Natural Gas	Step	530	7	4.19E+06	-1.45
Natural Gas	Step	530	9	6.53E+07	-1.68
Natural Gas	Step	650	3	1.80E+06	-1.46
Natural Gas	Step	650	5	4.66E+07	-1.73
Natural Gas	Step	650	7	7.23E+07	-1.73
Natural Gas	Step	650	8	3.93E+09	-2.08
Natural Gas	Step	730	5	3.97E+04	-1.07
Natural Gas	Step	730	7	8.25E+07	-1.76
Hydrogen	Step	530	3	-1.28E-05	0.86
Hydrogen	Step	530	5	8.63E+05	-1.42
Hydrogen	Step	530	7	5.28E+08	-1.98
Hydrogen	Step	650	3	4.97E+11	-2.73
Hydrogen	Step	650	5	4.01E+05	-1.36
Hydrogen	Step	650	7	9.49E+10	-2.52
Hydrogen	Step	650	9	7.97E+07	-1.84
Hydrogen	Step	730	7	2.22E+10	-2.38
Hydrogen	Step	730	9	1.41E+10	-2.32
Hydrogen	Airfoil (Neutral)	530	5	5.69E+02	-0.69
Natural Gas	Airfoil (Rotated)	650	4	7.09E+06	-1.43
Natural Gas	Airfoil (Rotated)	650	5	5.08E+06	-1.39
Hydrogen	Airfoil (Rotated)	650	5	1.37E+09	-1.89
Natural Gas	Cylinder (0.50")	650	5	1.35E+07	-1.47

Figure 6-13 shows the data obtained from the current study plotted within the typical range of the data compiled by Shanbhogue (2009).The method employed by Shanbhogue (2009) to develop these correlations (minimum perfectly stirred reactor time and momentum thickness scaling) does capture the overall spread of the current data.

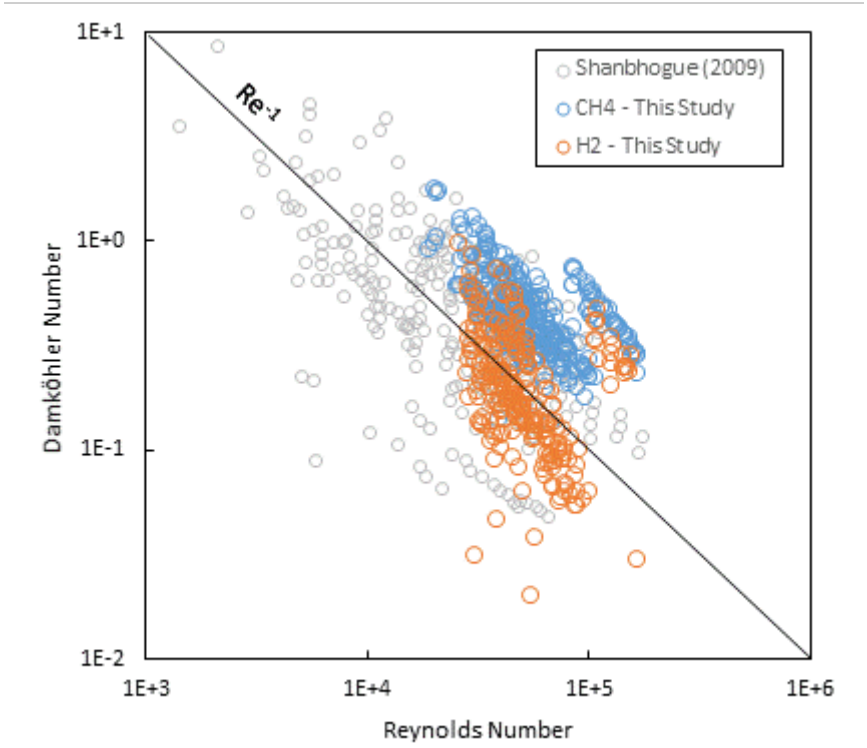

Figure 6-13: Comparison of data from the current study with data combined by Shanbhogue (2009)

While the data from the current study do fall within the range of data compiled by Shanbhogue (2009), several factors preclude the conclusion that the correlation of $Da=10^{5}Re^{-1}$ for two dimensional flameholders is capable of describing the new results. First, because of the of similarity of conditions between all of the studies compiled by Shanbhogue (2009) the scatter of the data was attributed to differences in flameholder geometries, fuel types and not making use of a term for blockage ratio. However in current study, changes in pressure and fuel type are what result in the spread of the data. Second, the slopes of the data obtained for the current study are generally much steeper than the

correlation previously developed. While Damköhler-Reynolds number scaling does provide some measure of coherence to the data, a single expression of the current form does not capture the effects of geometry, pressure, or fuel effects.

As mentioned before, the curves of the Damköhler-Reynolds number plots tend to be shifted to the right (higher Reynolds number) as pressure increases and to the left (lower Reynolds number) as reactant temperature increases. This suggests that rather that represent the data in the form:

$$Da = f(Re)$$

That a more appropriate way of correlating the data is with a function of the form:

$$Da = f\left(\frac{Re \cdot T}{P}\right)$$

However, Reynolds number is proportional to pressure and inversely proportional to temperature.

$$Re \propto \frac{P}{T}$$

Multiplying by temperature and dividing by pressure suggests that Damköhler number at blow off may simply be a function of velocity. Damköhler number at blow off is plotted as a function of velocity in Figure 6-15 and Figure 6-14. In Figure 6-15 Damköhler number was calculated using the same methods as Shanbhogue (2009) (perfectly stirred reactor time, and boundary layer momentum thickness), while in Figure 6-15 Damköhler number was calculated using perfectly stirred reactor time and the frontal width of the tests features.

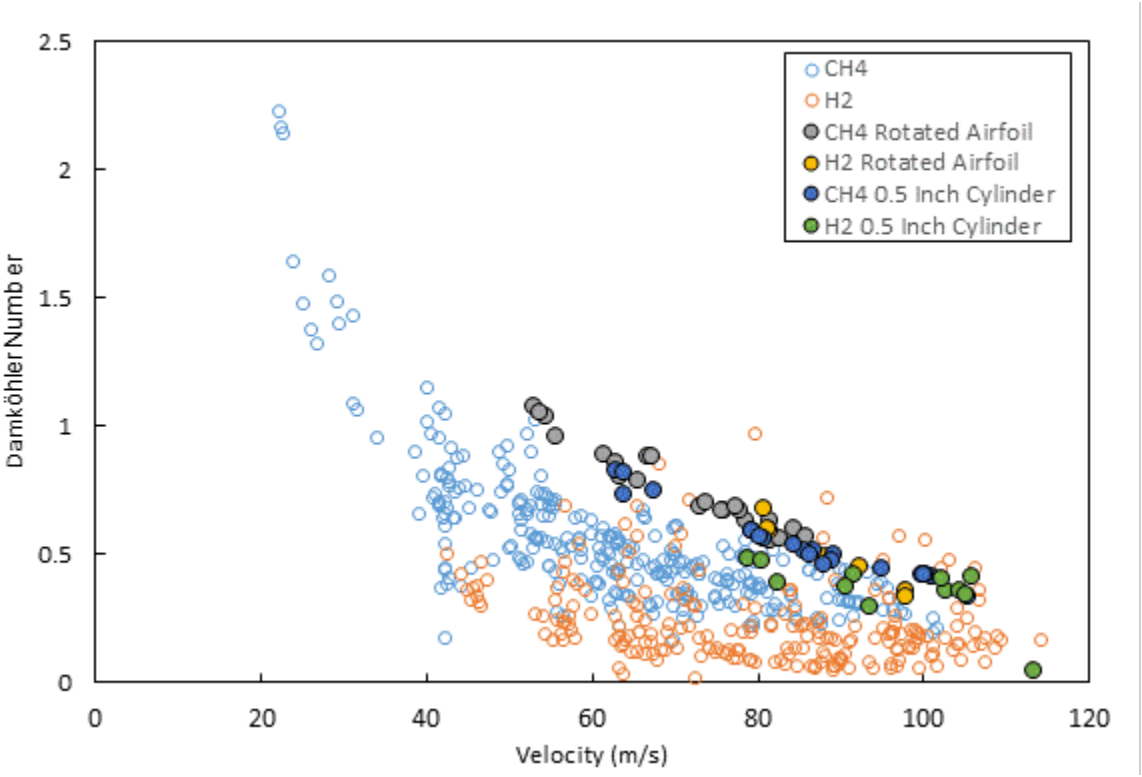

Figure 6-14: Damköhler Number using perfectly stirred reactor and boundary layer momentum thickness as a function of Velocity

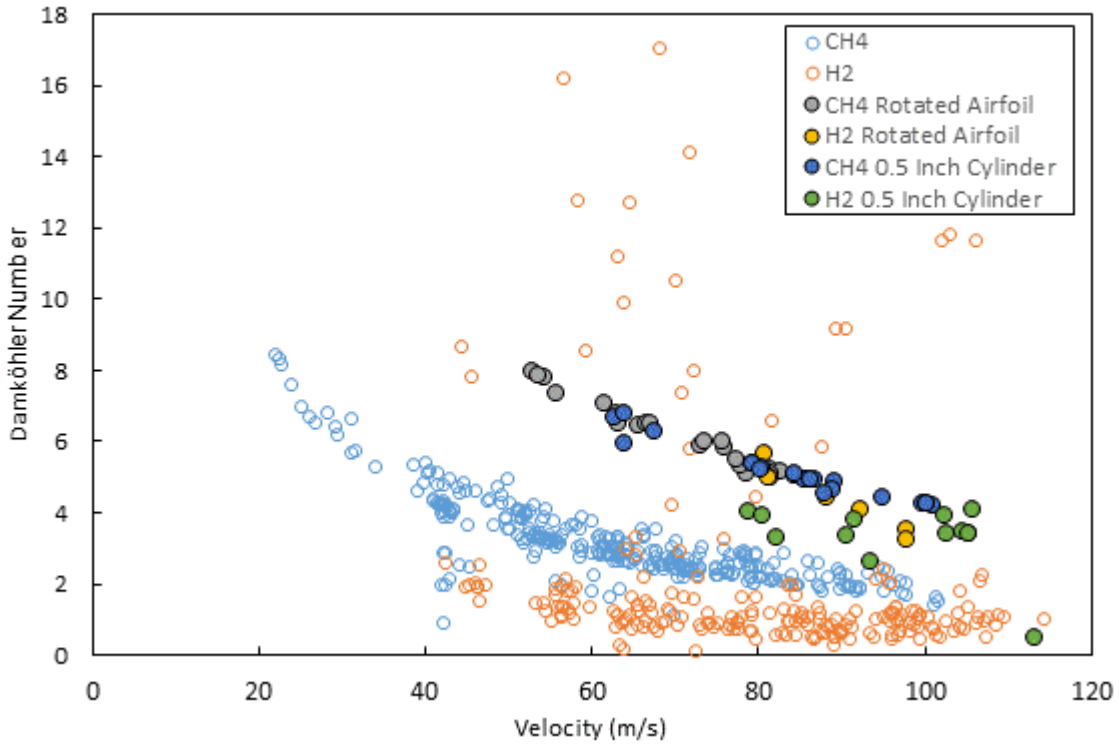

Figure 6-15: Damköhler Number using perfectly stirred reactor and feature width as a Function of Velocity

Clearly, using the boundary layer momentum thickness for the physical dimension does a more effective job of collapsing the experimental data than using the frontal width of the feature. Also, as shown in Figure 6-14, plotting Damköhler number as function of velocity does a reasonable job of collapsing hydrogen and natural gas data at multiple pressures and temperatures. However, this method does not capture the effect of bluff body size. The data for the 0.50 inch cylinder and the rotated airfoil fall on a separate curve from the rest of the data.

6.2 New Correlations

Based on the initial results of this experiment it is clear that velocity and pressure do not appear to contribute to the point of blow off. This is at odds with much of the work that has been done on flameholding. Typically, flameholding studies have found that an increase in velocity results in blow off occurring closer to a stoichiometric mixture of fuel and air. However, many of these experiments did not

measure turbulence levels and made use of calming screens and area-reducing nozzles in their test setups, both of which tend to reduce turbulence intensities. Those that did measure turbulence intensities (Ballal and Lefebvre, 1979), had measured turbulence intensities lower than those of this study. Additionally, the majority of these studies were performed at low pressures. Many studies (Hui et al. 2013, Far et al. 2010, Liu et al. 2014) have shown that as pressure increase, laminar flame speed is decreased significantly. This is the most likely reason for the lack of velocity influence. As velocity increases, the magnitude of the turbulent velocity fluctuation increases. Cheng (2008, 2008) and Beerer (2012) have found that turbulent local displacement flame speed increases linearly with turbulent fluctuation magnitude, usually of the form: $S_T = S_L + kU'$. The relative contribution of the laminar flame speed, which is constant for a given reactant mixture, decreases as turbulence level (i.e. velocity) increases. At very high velocities (i.e. very high turbulent flame speeds) or very lean mixtures the contribution of the laminar flame speed is essentially negligible compared to that of turbulence (Beerer 2012). This means that any changes in the velocity of the flow is compensated by an increase in turbulent flame speed, which allows the flame to stay stable. At low velocities (i.e. lower turbulent fluctuation magnitudes) and mixtures closer to stoichiometric this is not the case due to the much larger role of laminar flame speed. When velocity increases, the increase in turbulent flame speed solely due to turbulence is not enough to maintain stability, so laminar flame speed must increase in order to maintain a stable flame. This can only be achieved by shifting the reactant mixture closer to stoichiometric.

That being said, turbulent flame speeds do not, alone explain the discrepancy between the behavior or natural gas and that of hydrogen. Figure 6-16 and Figure 6-17 show the laminar and the local displacement turbulent flame speed as function of velocity for all of the data taken during this experiment. Turbulent flames speeds were calculated using the correlation from Cheng et al. (2009). The laminar flame speeds are generally much more disordered than the turbulent flame speeds. Even

though hydrogen flames could be stabilized at much lower equivalence ratios, reaching blow off at much lower laminar flame speeds, the turbulent flame speed at blow off is much higher than that of natural gas.

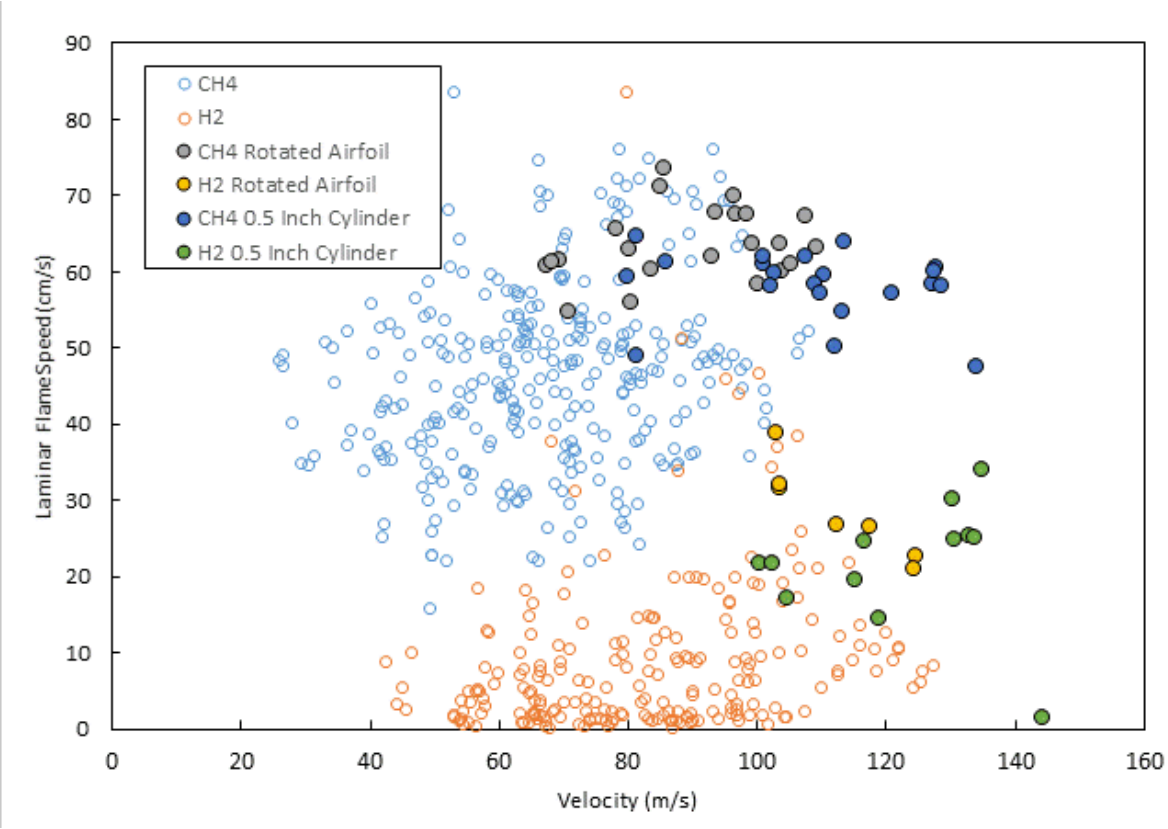

Figure 6-16: Laminar flame speed as a function of velocity

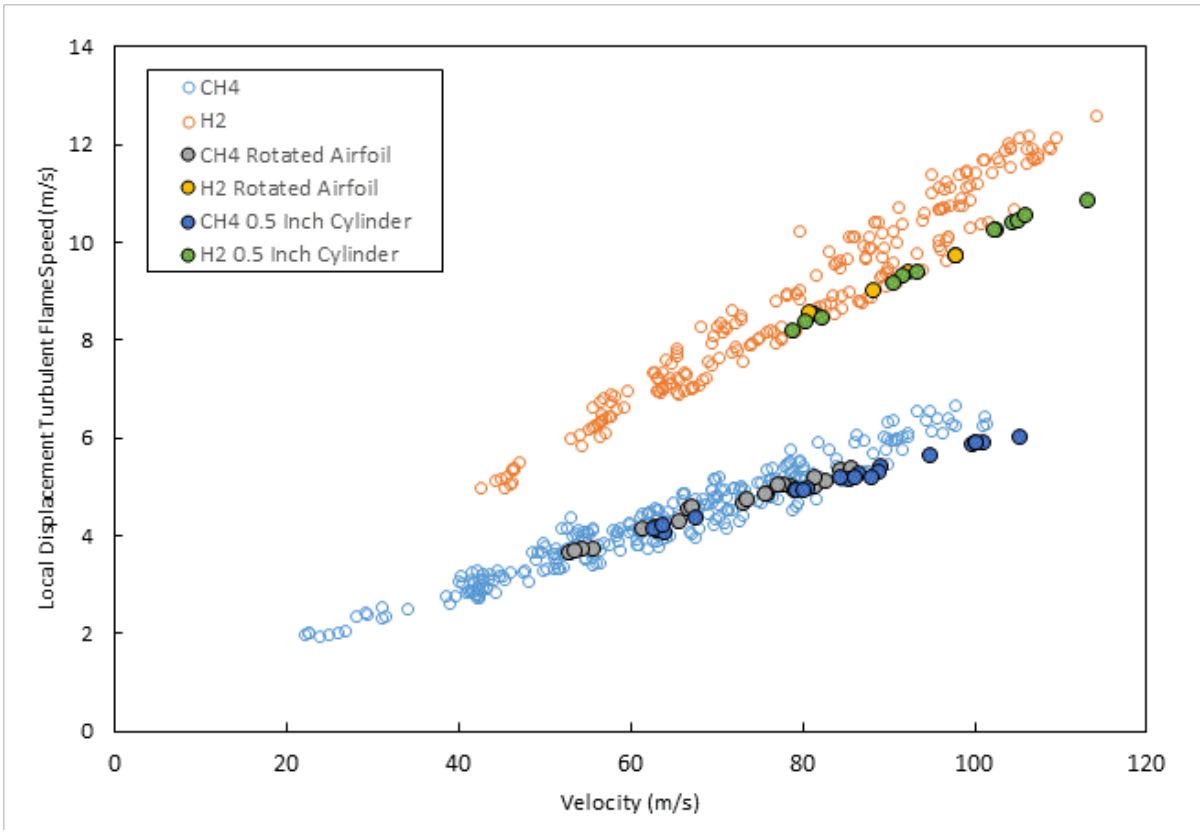

Figure 6-17: Local Displacement Flame Speed at blow off as a function of velocity.

Turbulent flame speeds explain why velocity has no observable effect on the equivalence ratio at blow off but does not collapse the existing data. However, the exclusive use of any flame propagation rate to explain the properties of a bluff body stabilized flame does not acknowledge the contribution of the wake region. The wake serves as a point where hot combustion products can be stored for a long enough period of time to and provide an ignition source for the incoming reactants. One can conclude that the heat transfer rate from the wake region to the fresh reactants must also be significant. The amount of heat transferred is proportional to the temperature in the wake and also to the amount of time that the reactants spend adjacent to the wake. Based on this, the following empirical function was developed:

$$U \propto S_T \left(\frac{T_{Burned}}{T_{Unburned}}\right)(1-B)$$

That is, at blow off the product of the turbulent flame speed the dilation ratio and one minus the blockage ratio is proportional to the free stream velocity. The data of the current study is represented in the manner below. The heat transfer rate from the wake to the free stream is captured by the dilation ratio. While *(1-B)* term captures the residence time effect. The product of the dilation ratio and *(1-B)* terms scales with the amount of heat transferred from the hot products in the wake region to the fresh reactants. Blockage ratio is typically calculated as the ratio of the frontal area of the flameholder and the area of the duct. This definition is fine for the cylindrical flameholders but does not readily apply for the reverse step flameholder because no part of it protrudes into the duct. Instead, blockage ratio for the reverse step was defined as the ratio of the step height and the sum of duct height and step height:

$$B = \frac{H_{Step}}{H_{Duct} + H_{Step}}$$

The blockage ratios for each of the flameholders are shown in the table below:

Table 6-2: Test feature blockage ratios

Feature	*Feature Dimension (in.)*	*Blockage Ratio - B*	*(1-B)*
0.25 Inch Cylinder	0.25	0.142	0.858
0.50 Inch Cylinder	0.50	0.284	0.716
Reverse Step	0.25	0.248	0.752
Rotated Airfoil	0.50	0.284	0.716

The product of turbulent flame speed, dilation ratio and *(1-B)*, indicate that the stability of the flame is controlled by the turbulent transfer of radicals and heat from products to reactants as facilitated by the turbulence of the mixture, temperature gradients and residence time. The data from this experiment is expressed using the developed blow off correlation in Figure 6-18. This blow off correlation appears to do an excellent job of organizing the experimental data.

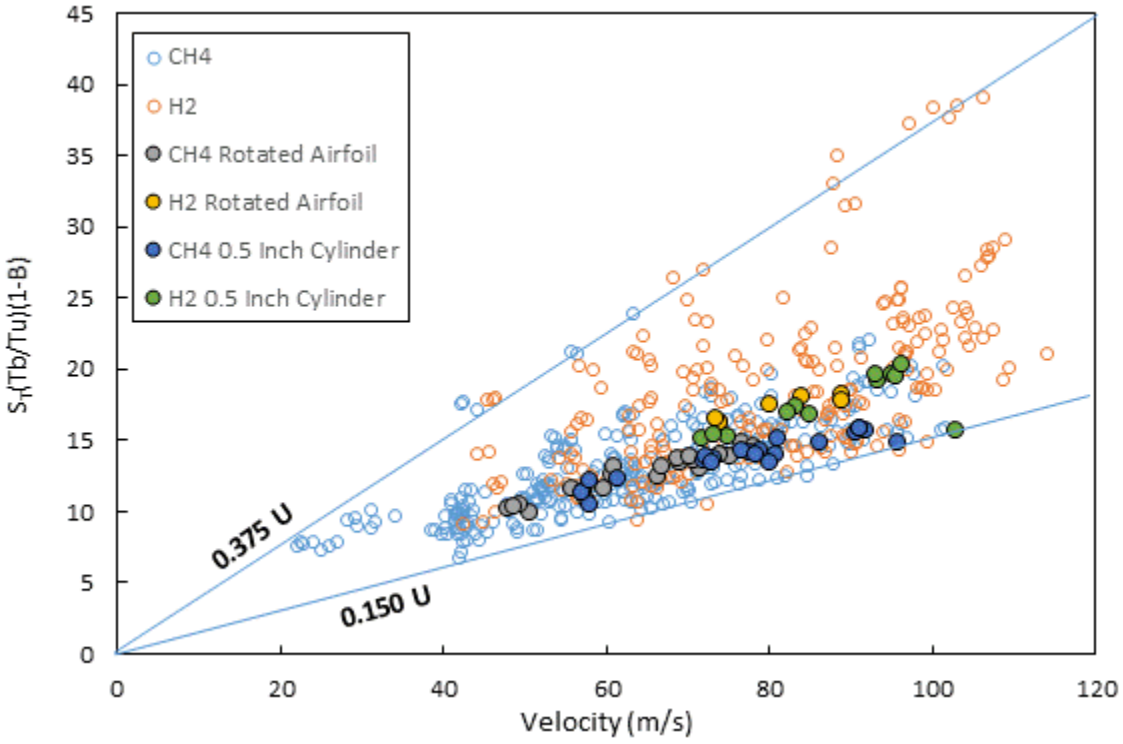

Figure 6-18: Empirical blow off correlation as a function of free stream velocity

Turbulent flame extinction is a stochastic event. Figure 6-18 shows two correlation lines. The lower line represents the ultimate point of blow off; below this line no flames are stable. This lower line has a slope of 0.150:

$$0.150\ U = S_T \left(\frac{T_{Burned}}{T_{Unburned}}\right)(1 - B)$$

The upper line represents the onset of blow off events, where flames may begin to extinguish. This line has a slope of 0.375:

$$0.375\ U = S_T \left(\frac{T_{Burned}}{T_{Unburned}}\right)(1 - B)$$

Between these two lines represents the probable range of blow off. The range shown in Figure 6-18 captures the stochastic nature of blow off by representing it not as a fixed point but a range over which

flame extinction becomes more probable. Blow off should be characterized as stochastic because of the many factors, which are outside of what can be predicted without uncertainty, that ultimately lead to blow off. The time scale over which the blow off condition is approached is also significant and can contribute to the uncertainty of blow off. Changes in the time scale over which blow off is approached it affects the amount of heat which is transferred either to or from the flameholder, which can significantly contribute to whether or not a flame is stable. Additionally, longer time scales increase the likelihood that combustion oscillation will upset the stability of the flame.

Figure 6-19 shows a probability of a flame blowing off along any slope between 0.150 and 0.375.

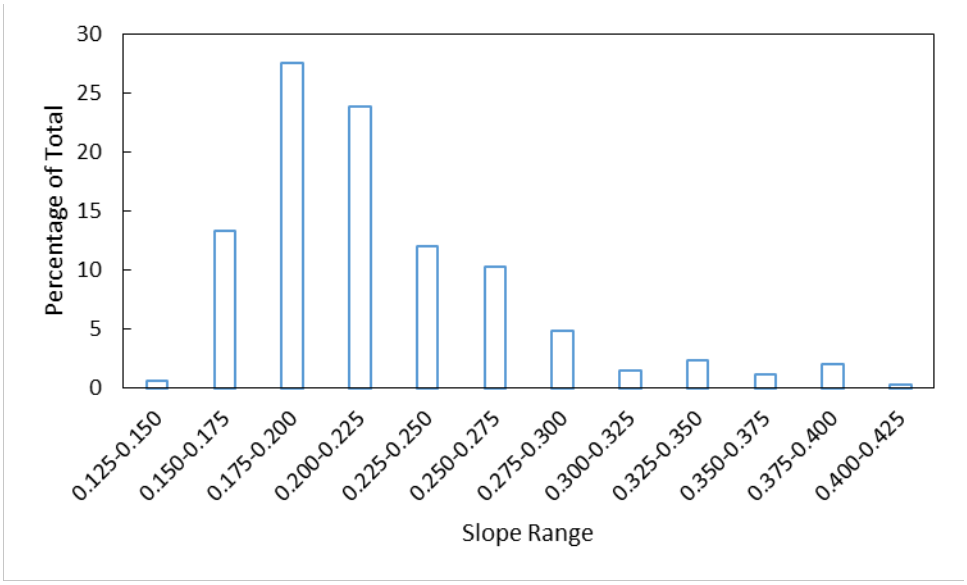

Figure 6-19: Probability of blow off as a function of slope

It is apparent that the data follows a Rayleigh distribution. The probability density function that best describes the data is:

$$P(s) \propto (s - 0.15) exp\left(\frac{-(s - 0.15)^2}{650}\right)$$

Where the term *s* is the slope of the blow off correlation function. The term 0.15 that occurs in the first and second term is a shifting term. This represents the value below which, the probability is zero. This corresponds to the lower slope of 0.150 of the correlation function.

Figure 6-20 Average slope values for blow off points of non-random data groups plots the average slope values for several non-random groups (e.g. Hydrogen data vs. natural gas data and reverse step vs. cylinder). It shows that no single group behaves differently than the set of data as a whole.

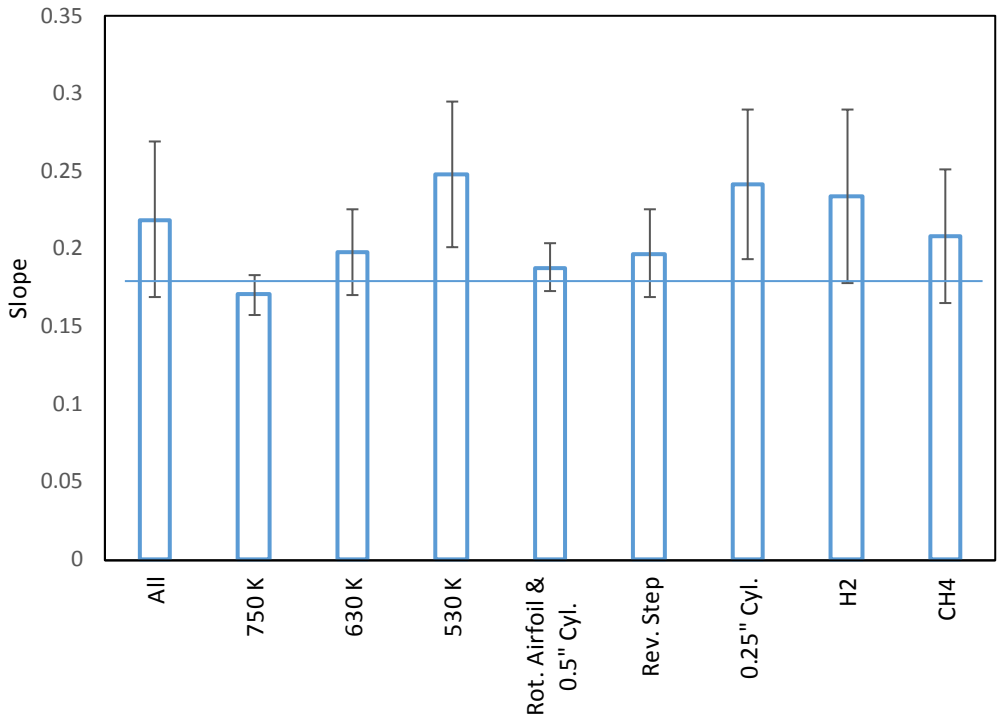

Figure 6-20 Average slope values for blow off points of non-random data groups

An equivalent way to think about this correlation is to rewrite it in terms of the bluff body edge velocity:

$$U_{Edge} = \frac{U}{(1-B)} \propto S_T \left(\frac{T_{Burned}}{T_{Unburned}} \right)$$

However, if one is designing a premixer, the geometry of the duct and bluff body are not known and must be determined. This result is somewhat remarkable because it implies that increasing the width of

a bluff body has the effect of destabilizing the flame. One would expect to see in increase in flameholding propensity as the width of the flameholder increases due to an increase in the size of the recirculation zone.

Increasing size likely does make a difference, but only when blockage is very small. This behavior was also observed by Ballal and Lefebvre (1979). Premixers are narrow, so even very small features result in fairly large blockage ratios. Increasing the size of bluff body does increase the volume of the recirculation zone, but the potential improvement in stability is more than offset by the destabilizing effect of increasing edge velocity. It is likely that if even smaller features than those used in this study were investigated, improvements due to increasing bluff body width would be observed.

As an example, suppose a gas turbine premixer is being designed. The premixer design has a blockage ratio of 0.7. The flow is composed of air and hydrogen at 600 K and an equivalence ratio of 0.3. It is desired to determine the minimum average velocity through the premixer that will avoid flameholding. Furthermore, the turbulent velocity fluctuation magnitude inside the premixer is has been measured to be five percent of the bulk velocity. Based on the reactant mixture properties, the adiabatic flame temperature of the mixture is 1467 K, and the laminar flame speed is nine cm/s. The dilation ratio is calculated as:

$$\frac{T_{Burned}}{T_{Unburned}} = \frac{1467\ K}{600\ K} = 2.445$$

The turbulent flame speed can be calculated as:

$$S_T = S_L + 3.73U' = 0.09\frac{m}{s} + 3.73(0.05)(U)$$

Using the correlation developed here:

$$\left(0.09\frac{m}{s}+0.1865U\right)(2.445)(1-0.7)=0.15U$$

$$\left(0.0660\frac{m}{s}+0.1368U\right)=0.15U$$

$$.1320\frac{m}{s}=0.0132U$$

$$10\frac{m}{s}=U$$

Based on this correlation, any velocity below 10 m/s will allow the flame to anchor in the premixer. This limit could be further reduced by lowering the dilation ratio (going to a leaner equivalence ratio), or increasing the blockage ratio (making the duct narrower), or lowering the turbulent flame speed (decreasing turbulence in the duct). In a realistic premixer, however, equivalence ratio is likely to have some spatial non-uniformity. This would result in the premixing being more prone to flameholding due to the presence of near-stoichiometric packets of reactants, which act as a pilot for the reaction as a whole. Furthermore, this non-uniformity would be greater near the points of fuel injection. In order to apply this correlation under these circumstances, one would need to have knowledge of the spatial distribution of equivalence ratios at the geometric feature in question. Using the value of equivalence ratio that is closest to stoichiometric at the geometric feature to calculate laminar flame speed and T_{Burned} would be a conservative means of applying this correlation.

Additional examples demonstrating the use of this correlation can be found in Appendix C.

In order to validate this expression it was compared with data obtained from previous studies. Perhaps the most similar work was done by Potter and Wong (1958), which used cylindrical flameholders in a rectangular duct. However, Potter and Wong's experiment was done at low pressure, without preheat and at a fixed equivalence ratio of one. Also compared was the data from Ballal and Lefebvre (1979), which was obtained at near atmospheric pressure with varying levels of preheat. However, Ballal and

Lefebvre's study was done with reverse cone flameholders in a circular duct As noted by Shanbhogue (2009), axisymmetric flameholders do not necessarily behave the same as two dimensional flameholders (like those of this study). Nevertheless, Ballal and lefebvre's data is included here because turbulence intensity was varied as a parameter of the study. Propane was used as the fuel for both experiments, which should behave similarly to natural gas, in terms of flame speeds. Both Potter and Wong's and Ballal and Lefebvre's data are plotted alongside the data of the current study in Figure 6-21.

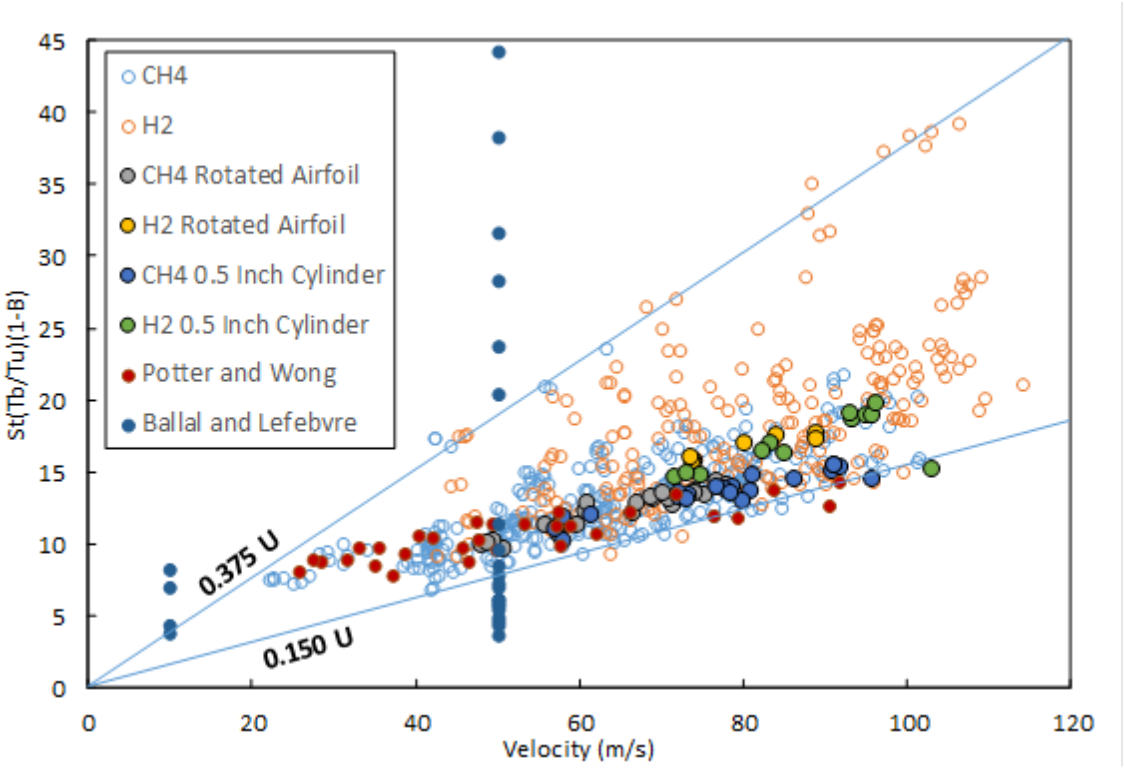

Figure 6-21: Empirical blow off correlation of current study and that of Potter and Wong (1958) and Ballal and Lefebvre (1979) as a function of free stream velocity

One can see that Potter and Wong's data does follow the same trend as the data from the current study. Potter and Wong did not measure turbulence levels, but did use several calming grids and a converging nozzle prior upstream of their test section. It has been assumed that the turbulent fluctuation

magnitudes are those of fully developed pipe flow upstream of a contraction nozzle with an area reduction ratio of 3:1. Correspondingly, there is some measure of uncertainty in this data.

The data of Ballal and Lefebvre, however, does not fit well with the correlation. However, Ballal and Lefebvre found that increasing turbulence decreases stability, which is the opposite of what was found here. Figure 6-22 Turbulent combustion regime diagram showing data from the current study, Potter and Wong (1958), and Ballal and Lefebvre (1979) shows the data from the current study along with that of Potter and Wong, and Ballal and Lefebvre plotted on a turbulent combustion regime diagram. One can see that all data sets tend to fall in different regimes. The data obtained by Ballal and Lefebvre is almost entirely within the corrugated flame regime, which is characterized flames whose internal structure is not affected by the turbulent fluctuations. This partially explains why Ballal and Lefebvre did not observe flame stability enhancements with increasing turbulence levels. Furthermore it is worth noting that, like much of data from the current experiment, gas turbine combustion occurs within the thin reaction zones regime (where turbulent eddies are small enough to enter the flame zone and alter/enhance mixing of reactants and products) (Griebel et al. 2005), so the data of Ballal and Lefebvre is not especially pertinent. That data obtained by Potter and Wong appears to be at the nexus of several different regimes also making it of questionable applicability to gas turbines.

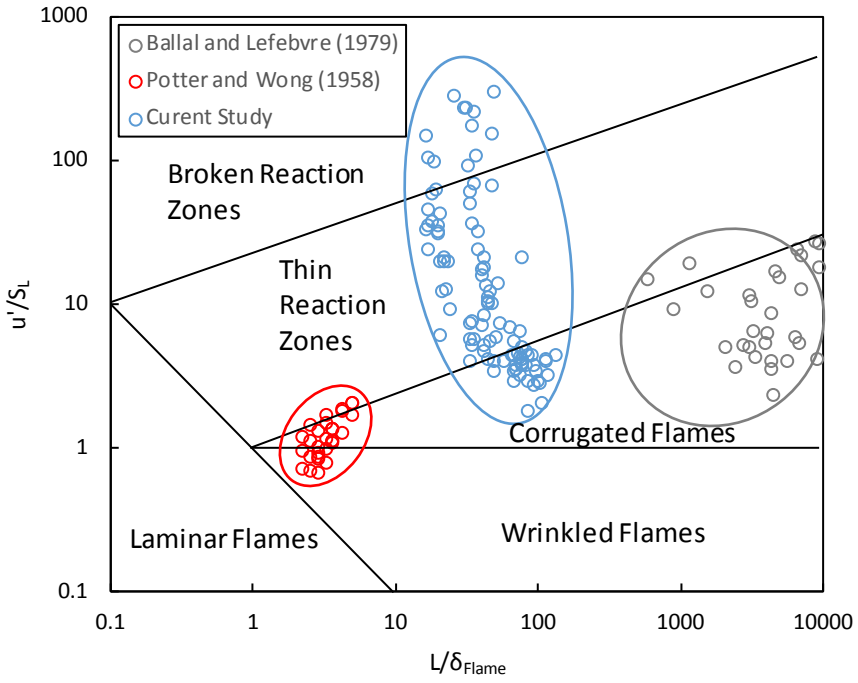

Figure 6-22 Turbulent combustion regime diagram showing data from the current study, Potter and Wong (1958), and Ballal and Lefebvre (1979)

There is much better agreement between the data of the current study and that of Potter and Wong (1958) than either of these studies with that of Ballal and Lefebvre (1979). What may be more significant than the flame regime, is simply the role of turbulent length scale. The data obtained by Ballal and Lefebvre (1979) had much larger turbulent length scales (on the order of 1 cm) than either the data from this study or that of Potter and Wong (1958) (both on the order of 0.1 cm). Therefore, rather than the transition between corrugated flames and thin reaction zones denoting where the correlation does or does not apply, perhaps a more appropriate measure would be where turbulent length scales are appreciably below one centimeter.

Analyzing the turbulent combustion regime diagram drives home the larger point that many studies on bluff body flameholding do not fall within the thin reaction zones regime or have turbulent length scales on the order of one centimeter. Many studies make use of converging nozzles upstream of the test section and were done at low pressures and within large ducts (on the order of 10 cm). Converging

nozzles lower turbulence intensities and lower pressure tend to increase laminar flame speeds; these two experimental features result in much lower values of u'/S_L. Additionally, large diameter ducts, which are not representative of gas turbine premixers, result in large turbulent length scales. Because the flames in these studies do not fall within the same flame regime as those within a gas turbine and have fairly large turbulent length scales, conclusions drawn from them may not be directly applicable to gas turbine combustion.

Chapter 7 - Summary and Conclusions

7.1 Summary

A new test apparatus was constructed in order to study flameholding of natural gas and hydrogen flames at conditions representative of gas turbine premixer passageways. The new test apparatus includes the ability to rotate and swap the test features, as well as have optical access both at the feature, and upstream of it. The cross section of the test section was designed to mimic a premixer passageway and also to achieve velocities at high as 100 meters per second at pressures up to ten atmospheres. The test rig was designed to operate safely up to ten atmospheres and 800 K inlet temperature, simultaneously. Laser Doppler velocimetry was used to measure the velocity profile at the entrance to the test section and verify that the flow was fully developed. Also, turbulence levels were quantified and compared to empirical correlations.

A survey of current advanced premixer hardware was carried out and several classes of features were identified. Four examples of these features were constructed for testing: a 0.25 inch diameter cylinder, a 0.5 inch diameter cylinder, a 0.25 inch reverse facing step, and a symmetric airfoil with 0.25 inch thickness and a chord length of one inch. All reacting experiments focused on identifying the equivalence ratio at blow off for each test feature and each fuel. These tests were done at pressures, temperatures and velocities that are relevant to gas turbine premixers. Tests were carried out at temperatures between 80°F (300 K) and 900°F (755 K), though the majority were performed between 500°F (533 K) and 800°F (700K). Experiments were between three and nine atmospheres. For each temperature-pressure combination, tests were typically conducted with free stream velocities between 40 and 100 m/s. The effect of airfoil's angle of rotation was also investigated.

The results of the reacting experiments were compared against existing blow off correlations. All of correlations that were investigated were found to be inadequate in one way or another. The most

prominent discrepancy was the inability of any one correlation to accurately predict the behavior of both natural gas and hydrogen flames. Based on the poor agreement between the data of this experiment and existing correlations a new correlation was developed based on turbulent flame propagation rates that accurately describes the current experimental data and captures the stochastic nature of blow off.

7.2 Conclusions

Adiabatic flame temperature should be used as the characteristic temperature to describe blow off. Changes in inlet temperature will affect the equivalence ratio at blow off. Increasing inlet temperature results in lower equivalence ratios at blow off. Decreasing inlet temperature has the opposite effect. However, in this experiment, for a given flame holder and fuel type, the point of blow off occurs at a specific adiabatic flame temperature, regardless of combination of inlet temperature and equivalence ratio used to achieve that particular flame temperature.

Velocity doesn't affect equivalence ratio at blow off when pressure or turbulence magnitudes are high. Turbulent flame speeds correlations are generally composed of a laminar flame speed term and a turbulence magnitude term, typically taking the form: $S_T = S_L + kU'$. As pressure increases, laminar flame speeds decrease along with the contribution of laminar flame speed towards turbulent flame speed. As velocity increases, the magnitude of the turbulent velocity fluctuation increases along with the contribution of the turbulent component of turbulent flame speed. When turbulent flame speeds are high, any changes in the velocity of the flow is compensated by an increase in turbulent flame speed, which allows the flame to stay stable. When turbulent flame speeds are low, and at lower pressures this is not the case due to the much larger role of laminar flame speed. When velocity increases, the increase in turbulent flame speed solely due to turbulence is not enough to maintain stability, so laminar flame

speed must increase in order to maintain a stable flame. This can only be achieved by shifting the reactant mixture closer to stoichiometric.

Hydrogen flames can anchor in boundary layer of streamlined bodies. This is a fundamentally different mechanism than for bluff bodies with recirculation zones. Despite the lack of an appreciable recirculation zone, streamlined bodies can still have flame anchoring. If the length is long enough the boundary layer can grow larger than the quenching distance. When there are regions outside of the quenching distance with velocities lower than the flame propagation rate, a flame can be stabilized. Hydrogen flames are especially capable of this due to hydrogen's much higher flame propagation rates and narrower quenching distances Flameholding can be prevented on streamlined bodies by keeping the length as short as possible to minimize boundary layer growth.

Product of ST, dilation ratio, and (1-B) correlates well with bulk velocity at blow off.

$$U \propto S_T \left(\frac{T_{Burned}}{T_{Unburned}}\right)(1-B)$$

An equivalent way to write this is in terms of the velocity at the edge of the bluff body:

$$U_{Edge} = \frac{U}{(1-B)} \propto S_T \left(\frac{T_{Burned}}{T_{Unburned}}\right)$$

The wake serves as a point where hot combustion products can be stored for a long enough period of time to and provide an ignition source for the incoming reactants. The amount of heat transferred is proportional to the temperature in the wake and also to the amount of time that the reactants spend adjacent to the wake. The heat transfer rate from the wake to the free stream is captured by the dilation ratio. While *(1-B)* term captures the residence time effect.

Flame extinction is stochastic event. While the majority of work on the subject of flame holding and blow off seem to characterize blow off as an exact, repeatable point. The results of this study show that

the exact point of blow off cannot usually be predicted exactly due to the interaction of the many variables that influence the behavior of the flame. Rather, blow off can be analyzed statistically with a probability density function:

$$P(s) \propto (s - 0.15) exp\left(\frac{-(s - 0.15)^2}{650}\right)$$

In this experiment the onset of blow was found to occur when the product of turbulent flame speed, dilation ratio, and one minus the blockage ratio is less than 0.375 times the bulk reactant velocity. Blow off becomes increasingly more likely as that product approaches 0.150 times the bulk velocity.

Turbulent flame regime has a significant effect on how flames respond to turbulence. In order for flame holding correlations to accurately predict the behavior of flames within a gas turbine, they must be based on flames within the same turbulent flame regime. Unlike data from most other studies on flameholding, the data obtained during this study was from the thin-reaction-zones regime, which is representative of gas turbine flames, and thus can be used to predict flame behavior within a gas turbine.

7.3 Recommendations

The use of the turbulent flame regime diagram, as well as investigations into turbulent length scales, provide some insight into the apparent discrepancies between the current study and the results of others. However, additional work is needed to fully explain these differences. New flameholding studies that directly measure turbulent length scales may provide further insight. Additionally, it is recommended that this study be repeated, but with a test apparatus with a larger cross section. This would be helpful in bridging the gap between the results of this study and those of earlier studies conducted within larger diameter test sections.

Chapter 8 - References

Alstom Gas Turbines, Gas Turbine Products, http://www.alstom.com/products-services/product-catalogue/power-generation/gas-power/gas-turbines/

Ballal, D.R., Lefebvre, 1979, Weak Extinction Limits of Turbulent Flowing Mixtures, ASME Journal of Engineering for Power, pp. 343-348

Barrère, M., Mestre, A., 1954, Stabilisation des Flammes par des Obstacles, Selected Combustion Problems: Fundamentals and Aeronautical Applications, 426-446

Beerer, D., McDonell, V., Samuelsen, S., 2011, An Experimental Ignition Delay Study of Alkane Mixtures in Turbulent Flows at Elevated Pressures and intermediate Temperatures, Journal of Engineering of Gas Turbines and Power, 011502-7

Beerer, D., McDonell, V., Therkelsen, P., Cheng, R.K., 2012, Flashback, Blow Out, Emissions, and Turbulent Displacement Flame Speed Measurements in a Hydrogen and methane Fired Low-Swirl Injector at Elevated Pressures and Temperatures, Proceedings of ASME Turbo Expo 2012, GT2012-68216, 1-12

Beerer, D., McDonell, V., Therkelsen, P., Cheng, R.K., 2014 Flashback and Turbulent Flame Speed Measurements in Hydrogen/Methane Flames Stabilized by a Low-Swirl Injector at Elevated Pressures and Temperatures, Journal of Engineering for Gas Turbines and Power, 031502-1 – 031502-9

Borghi, R., 1985, On the Structure and Morphology of Premixed Flames, Recent Advances in the Aerospace Sciences, Plenum Press, New York

Burcat, A., Scheller, K., Lifshitx, A., 1971, Shock-Tube Investigation of Comparative Ignition delay Times for C1-C5 Alkanes, Combustion and Flame, 29-33

Cheng, R.K., Littlejohn, D., 2008, Laboratory Studies of the Flow Field Characteristics of Low-Swirl Injectors for Adaptation to Fuel-Flexible Turbines, Journal of Engineering for Gas Turbines and Power, 031503-1 – 031503-9

Cheng, R.K., Littlejohn, D., Nazeer, W.A., Smith, K.O., 2008, Laboratory Study of Premixed H2-Air and H2-N2-Air Flames in a Low-Swirl Injector for Ultralow Emissions Gas Turbines, Journal of Engineering for Gas Turbines and Power, 021501-1 – 021501-10

Cheng, R.K., Littlejohn, D., Strakey, P., Sidwell, T., 2009, Laboratory investigations of low-swirl injectors with H2 and CH4 at Gas Turbine Conditions, Proceedings of the Combustion Institute, 32, 3001-3009

Choudhury, P.R., Camble, A.B., 1962, Flame Stabilization by Wall Recesses, Proceedings of the Symposium (international) on Combustion, 963-970

Driscoll, J.F., 2008, Turbulent Premixed Combustion: Flamelet Structure and its Effect on Turbulent Burning Velocities, Progress in Energy and Combustion Science, 91-134

Egolfopoulos, F.N., Zhang, H., Zhang, Z., 1997, Wall Effects on the Propagation and Extinction of Steady, Strained, Laminar Premixed Flames, Combustion and Flame, 237-242

Far, K.E., Parsinejad, F., Metghalchi, H., 2010, Flame Structure and Laminar Burning Speeds of JP-8/Air Premixed Mixtures at High Temperatures and Pressures, Fuel, 89, pp. 1041-1049

Fetting, F., Choudhury, P.R., Wilhelm, R.H., 1958, Turbulent Flame Blow-Off Stability. Effect of Auxiliary Gas Addition into Separation Zone, Proceedings of the Symposium (international) on Combustion, 621-632

Filippi, F., Fabbrovich-Mazza, L., 1960, Control of Bluff-Body Flameholder Stability Limits, Proceedings of the Symposium (international) on Combustion, 956-963

Fluent Inc., 2006, “Determining Turbulence Parameters”, Fluent 6.3 User’s Guide, pp. 7-14 – 7-17

GE Energy, Heavy Duty Gas Turbine Products Brochure, http://www.ge-energy.com/content/multimedia/_files/downloads/GEH12985H.pdf

Griebel, P. Bombach, R., Inauen, A., Schären, R., Schenker, S., Siewert, P., 2005, Flame Characteristics and Turbulent Flame Speeds of Turbulent, High-Pressure, Lean Premixed Methane/Air Flames, ASME Turbo Expo GT2005-68565

Hui, X., Sung, C.J., 2013, Laminar Flame Speeds of Transportation-Relevant Hydrocarbons and Jet Fuels at Elevated Temperatures and Pressures, Fuel, 109, pp. 191-200

Ju, Y., Guo, H., Maruta, K., Liu, F., 1997, On the Extinction Limit and Flammability Limit of Non-Adiabatic Stretched Methane-Air Premixed Flames, Journal of Fluid Mechanics, 315-334

Koseki, H., Sato, M., 2002, Experimental Investigation of Flashback During Start-up in Practical Premixed Combustion, Applied Energy, 237-259

Lefebvre, A.H., Ballal, D.R., 1976, Flame Quenching in Turbulent Flowing Gaseous Mixtures, Proceedings of the Symposium (international) on Combustion, 1689-1698

Lieuwen, T., Yang, V., Yetter, R., 2010, Synthesis Gas Combustion, CRC Press, Boca Raton

Liu, K., Fu, J., Deng, B., Yang, J., Tang, Q., Liu, J., 2014, The Influence of Pressure and Temperature on Laminar Flame Propagation of n-butanol, Iso-Octane and Their Blends, Energy, 73, pp. 703-715

Longwell, J.P., 1953, Flame Stabilization by Bluff Bodies and Turbulent Flames in Ducts, Proceedings of the Symposium (international) on Combustion, 90-97

Marzelli, S., 2010, Flameholding Studies for Lean Premixed Fuel Injectors for Application in Gas Turbine Engines, MS thesis, Department of Mechanical Engineering, Pennsylvania State University

Peschke, W.T., Spadaccini, L.J., 1985, Determination of Autoignition and Flame Speed Characteristics of Coal Gases having Medium Heating Values, Electric Power Research Institute Project Number 2357-1, Report No. A4291

Peters, N., 1999, The Turbulent Burning Velocity for Large-Scale and Small Scale Turbulence, Journal of Fluid Mechanics, 384, 107-132

Plee, S.L., Mellor, A.M., 1979, Characteristic Time Correlation for Lean Blowoff of Bluff-Body-Stabilized Flames, Combustion and Flame, Vol. 35, pp. 61-90

Potter, A., Wong, E., 1958 Effect of Pressure and Duct Geometry on Bluff-Body Flame Stabilization, NACA TN 4381, National Advisory Committee for Aeronautics

Rizk, N.K., Lefebvre, A.H., 1983, Influence of Laminar Flame Speed on the Blowoff Velocity of Bluff-Body Stabilized Flames, Proceedings of the 19th Joint Propulsion Conference

Rizk, N.K., Lefebvre, A.H., 1986, Relationship between flame stability and drag of bluff-body flameholders, Journal of Propulsion and Power, 361

Roberds, D. W., McGregor, W.K., Hartsfield, B.W., Schulz, R.J., Schulz, Rhodes, R.P., 1989, Measurements of Residence Time, Air Entrainment Rate and Base Pressure in the Near Wake of a Cylindrical Body in Supersonic Flow, AIAA Journal, 1524-1529

Roffe, G., Venkataramani, K.S., 1978, Experimental Study of the Effects of Flameholder Geometry on Emissions and Performance of Lean Premixed Combustors, NASA report CR-135424

Samuelsen, G.S., McDonell, V.G., Couch, P.M., 2004, Characterization of Flameholding Tendencies in Premixer Passages for Gas Turbine Application, Proceedings of the Joint Propulsion Conference and Exhibit, 1-30

Shanbhogue, S.J., Husain, S., Lieuwen, T., 2009, Lean Blowoff of Bluff Body Stabilized Flames: Scaling and Dynamics, Progress in Energy and Combustion Science, 98-120

Siemens Gas Turbines, Industrial Gas Turbines Performance Data, http://www.energy.siemens.com/hq/en/fossil-power-generation/gas-turbines/

Solar Turbines, Turbine Performance Data, https://mysolar.cat.com/cda/layout?m=41100&x= 7

Stwalley, R.M., Lefebvre, A.H., 1987, Flame Stabilization Using Large Flameholders of Irregular Shape, Proceedings of the 25th Joint Propulsion Conference, 1-9

Venkateswaran, P., Marshall, A., Hyuk Shin, D., Noble, D., Seitzman, J., Lieuwen, T., 2011, Measurements and Analysis of Turbulent Consumption Speeds of H2/CO Mixtures, Combustion and Flame, 1602-1614

Venkateswaran, P., Marshall, A., Seitzman, J., Lieuwen, T., 2014, Turbulent Consumption Speeds of High Hydrogen Content Fuels from 1-20 atm, Journal of Engineering for Gas Turbines and Power, 011504-1-7

Williams, G.C., Woo, P.T., Shipman, C.W., 1957, Boundary Layer Effects on Stability Characteristics of Bluff-Body Flameholders, Proceedings of the Symposium (international) on Combustion, 427-438

Wright, F.H., 1959, Bluff-body stabilization: Blockage effects, Combustion and Flame, 319-337

Yamaguchi, S., Ohiwa, N., Hasegawa, T., 1985, Structure and Blow-Off Mechanism of Rod-Stabilized Premixed Flame, Combustion and Flame, Vol. 62, pp. 31-41

Appendix A – Quartz Window Pressure Capabilities

Maximum Pressure on an Unclamped Quartz Window

Equation:

$$P = \frac{.84 S_{max} t^2}{r_0^2}$$

P=Pressure differential

S_{max}=Maximum stress

t=Thickness of window

r_0=Unsupported radius of disc

Given:

t=.5in

S_{max}=$7x10^6 Pa$ (with 7:1 factor of safety)

r_0=1.125in

Conversion:

$$\frac{7x10^6 Pa}{1}\frac{1atm}{101325Pa} = 69atm$$

Calculation:

$$P = \frac{(.84)(69atm)(.5in)^2}{(1.125in)^2} = \mathbf{11.44atm}$$

Appendix B – Entrance Length Calculations

Entrance Length for Fully Developed Flow

$$L_E = 4.4DRe^{1/6}$$

$$Re = \frac{\rho VD}{\mu} = \frac{\dot{m}D}{\mu A}$$

For rectangular pipes use hydraulic diameter:

$$D_H = \frac{4A}{P}$$

Where P is the perimeter: 2(L+W). Reynolds number is then:

$$Re = \frac{4\dot{m}}{\mu P}$$

Entrance length is:

$$L_E = 4.4 \cdot \frac{4A}{P} \cdot \left(\frac{4\dot{m}}{\mu P}\right)^{1/6} = 4.4\left(\frac{4LW}{2(L+W)}\right)\left(\frac{4\dot{m}}{\mu P}\right)^{1/6} = 8.8\frac{LW}{L+W}\left(\frac{2\dot{m}}{\mu(L+W)}\right)^{1/6}$$

Substituting in dimensions:

L= 1.76" = .0447m

W= 0.76"=0.0193m

The required entrance length is greatest when the mass flow rate is highest – 1.3 lb/s

$\dot{m}$=1.3 lb/s=0.59 kg/s

μ (500F)=2.8x10^{-5} Ns/m^2

$$L_E = 8.8\frac{(.0447)(.0193)}{.0447+.0193}\left(\frac{2(0.59)}{2.8\cdot 10^{-5}(.0447+.0193)}\right)^{1/6} = (0.1186)(6.58\cdot 10^{-5})^{1/6}$$

$$\boldsymbol{L_E} = 1.11m = \mathbf{44}"$$

Appendix C – Example Problems

Example Problem 1:

A gas turbine is operating at 700K and 8 atm absolute pressure. The premixer has a blockage ratio of 0.65. The bulk velocity through the premixer is 70 m/s, and the turbulence intensity has been measured (or predicted with CFD) at 4%. The reactant mixture has an adiabatic flame temperature of 1600 K. The engine is typically operated on natural gas. Is it possible to operate at the same conditions using hydrogen as the fuel without risking flameholding in the premixer?

Solution:

Flame holding will not occur if the following conditions is met:

$$0.150\ U > \ S_T \left(\frac{T_{Burned}}{T_{Unburned}}\right)(1 - B)$$

$$0.150\ (70\frac{m}{s}) > \ S_T \left(\frac{1600\ K}{700\ K}\right)(1 - 0.65)$$

$$10.5\ m/s > \ 0.8 \cdot S_T$$
$$13.5\ m/s > S_T$$

An adiabatic flame temperature of 1600 K, with an inlet temperature of 700K corresponds to equivalence ratios of:

$$\Phi_{CH4} = 0.395$$
$$\Phi_{H2} = 0.328$$

And laminar flame speeds of:

$$\mathrm{S}_{L,CH4} = 0.09\ m/s$$

$$\mathrm{S}_{L,H2} = 0.22\ m/s$$

Now, turbulent flame speeds can be calculated

$$u' = 70\frac{m}{s} \cdot 0.004 = 2.8\frac{m}{s}$$

$$\mathrm{S}_{T,CH4} = 0.09\frac{m}{s} + 1.73\left(2.8\frac{m}{s}\right) = 4.93\ m/s$$

$$\mathrm{S}_{T,H2} = 0.22\frac{m}{s} + 3.15\left(2.8\frac{m}{s}\right) = 9.04\ m/s$$

$$\boxed{13.5\frac{m}{s} > 9.04\frac{m}{s}}$$

This engine can be run on hydrogen without danger of flameholding

Example Problem 2:

Given the operating conditions of Example 1, determine the minimum blockage ratio that will not risk flameholding when operating on hydrogen.

Solution:

Flame holding will not occur if the following conditions is met:

$$0.150\,U > S_T\left(\frac{T_{Burned}}{T_{Unburned}}\right)(1-B)$$

$$\frac{0.150\,U}{S_T}\left(\frac{T_{Unurned}}{T_{Burned}}\right) > (1-B)$$

Substituting in the conditions from Example 1:

$$\frac{0.150\ \cdot 70\,m/s}{9.04\,m/s}\left(\frac{700\,K}{1600\,K}\right) > (1-B)$$

$$0.508 > (1-B)$$

$$\boxed{B > (1-0.508) = 0.492}$$

Flameholding will not occur when blockage is maintained above 0.492

Example Problem 3:

A gas turbine is operating at 700K and 8 atm absolute pressure. The premixer has a blockage ratio of 0.65. The bulk velocity through the premixer is 70 m/s, and the turbulence intensity has been measured at 4%. The engine will be operated on hydrogen.Determine the maximum firing temperature that will not risk flameholding within the premixer.

Solution:

Flame holding will not occur if the following conditions is met:

$$0.150\,U > S_T\left(\frac{T_{Burned}}{T_{Unburned}}\right)(1-B)$$

$$\left(\frac{0.150\,U}{1-B}\right)(T_{Unburned}) > S_T \cdot T_{Burned}$$

Plugging in values:

$$\left(\frac{0.150\ \cdot 70m/s}{1-0.65}\right)(700) = 21000\ \frac{m\cdot K}{s} > S_T \cdot T_{Burned}$$

$$21000\ \frac{m\cdot K}{s} > (S_L + 3.15\cdot 0.04\cdot 70\ m/s)\cdot T_{Burned} = (S_L + 8.82m/s)\cdot T_{Burned}$$

Iterative analysis yields that at an equivalence ratio of $\Phi = 0.514$ yeilds:

$$T_{Burned} = 1952\ K$$

$$S_L = 1.93\ m/s$$

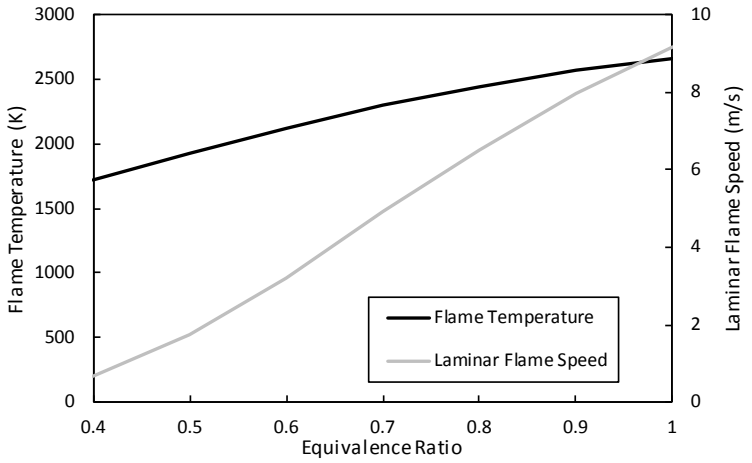

$$21000\ \frac{m\cdot K}{s} > \left(1.93\frac{m}{s} + \frac{8.82m}{s}\right)\cdot 1952K = 20984\ \frac{m\cdot K}{s}$$

The maximum firing temperature without risking flameholding within the premixer is around 1950K.

Appendix D – Tabulated Blow Off Data

Natural Gas – 0.25 Inch Cylinder

Fuel	Feature	Absolute Pressure (atm)	Mix. Vel. (m/s)	Edge Velocity (m/s)	Mix. Temp. (K)	Fuel Flow (g/s)	Air Flow (kg/s)	Equivalence Ratio	Adiabatic Flame Temp. (K)
CH4	0.25" Cyl.	3.11	53	53	508	4.75	0.090	0.90	2275
CH4	0.25" Cyl.	2.99	56	56	510	4.43	0.091	0.84	2197
CH4	0.25" Cyl.	3.03	55	55	510	4.33	0.091	0.82	2167
CH4	0.25" Cyl.	3.13	54	54	511	4.70	0.091	0.89	2258
CH4	0.25" Cyl.	3.07	56	56	520	4.51	0.092	0.85	2213
CH4	0.25" Cyl.	3.14	55	55	523	4.32	0.091	0.81	2170
CH4	0.25" Cyl.	3.12	55	55	523	4.36	0.092	0.82	2176
CH4	0.25" Cyl.	7.40	68	68	494	14.34	0.283	0.87	2238
CH4	0.25" Cyl.	7.44	67	67	494	13.39	0.282	0.82	2161
CH4	0.25" Cyl.	7.34	67	67	489	13.16	0.281	0.80	2139
CH4	0.25" Cyl.	3.12	54	54	506	4.45	0.093	0.83	2177
CH4	0.25" Cyl.	3.18	60	60	504	4.95	0.106	0.81	2149
CH4	0.25" Cyl.	3.13	62	62	504	5.54	0.107	0.89	2254
CH4	0.25" Cyl.	3.19	62	62	503	5.59	0.109	0.88	2246
CH4	0.25" Cyl.	3.12	62	62	503	5.36	0.107	0.86	2220
CH4	0.25" Cyl.	3.07	63	63	504	5.32	0.107	0.85	2212
CH4	0.25" Cyl.	3.27	75	75	510	6.16	0.135	0.78	2119
CH4	0.25" Cyl.	3.17	73	73	507	6.01	0.127	0.81	2160
CH4	0.25" Cyl.	3.30	70	70	507	5.90	0.128	0.79	2134
CH4	0.25" Cyl.	3.18	72	72	507	6.21	0.126	0.85	2206
CH4	0.25" Cyl.	3.45	73	73	502	6.97	0.139	0.86	2221
CH4	0.25" Cyl.	3.40	80	80	504	7.30	0.151	0.83	2183
CH4	0.25" Cyl.	3.22	91	91	511	7.72	0.160	0.83	2188
CH4	0.25" Cyl.	3.22	91	91	511	7.55	0.160	0.81	2160
CH4	0.25" Cyl.	3.17	92	92	512	7.73	0.159	0.83	2193
CH4	0.25" Cyl.	6.91	43	43	503	7.91	0.166	0.82	2173
CH4	0.25" Cyl.	7.01	42	42	503	7.78	0.165	0.81	2161
CH4	0.25" Cyl.	7.06	42	42	504	7.46	0.164	0.78	2114
CH4	0.25" Cyl.	6.99	52	52	506	8.95	0.201	0.77	2094

CH4	0.25" Cyl.	7.01	52	52	503	9.49	0.204	0.80	2145
CH4	0.25" Cyl.	7.11	51	51	504	9.36	0.204	0.79	2130
CH4	0.25" Cyl.	7.36	61	61	510	11.66	0.245	0.82	2174
CH4	0.25" Cyl.	7.28	59	59	510	10.91	0.235	0.80	2147
CH4	0.25" Cyl.	7.23	61	61	509	11.66	0.240	0.84	2199
CH4	0.25" Cyl.	5.18	42	42	610	4.47	0.100	0.76	2165
CH4	0.25" Cyl.	5.22	40	40	608	4.42	0.097	0.79	2193
CH4	0.25" Cyl.	5.34	43	43	612	4.29	0.105	0.70	2067
CH4	0.25" Cyl.	5.02	41	41	606	4.28	0.096	0.76	2158
CH4	0.25" Cyl.	5.27	50	50	610	5.18	0.121	0.74	2122
CH4	0.25" Cyl.	5.24	50	50	605	5.24	0.121	0.75	2134
CH4	0.25" Cyl.	5.31	53	53	604	5.31	0.133	0.69	2044
CH4	0.25" Cyl.	5.26	53	53	600	5.19	0.131	0.68	2026
CH4	0.25" Cyl.	8.59	63	63	596	11.66	0.255	0.79	2191
CH4	0.25" Cyl.	7.79	71	71	601	11.33	0.261	0.75	2135
CH4	0.25" Cyl.	9.10	42	42	605	7.37	0.177	0.72	2091
CH4	0.25" Cyl.	9.26	38	38	597	7.75	0.167	0.80	2207
CH4	0.25" Cyl.	9.16	40	40	598	7.43	0.171	0.75	2136
CH4	0.25" Cyl.	9.13	51	51	596	10.38	0.220	0.81	2226
CH4	0.25" Cyl.	9.19	47	47	601	9.49	0.203	0.80	2217
CH4	0.25" Cyl.	9.18	48	48	596	9.87	0.205	0.83	2248
CH4	0.25" Cyl.	9.06	61	61	603	11.48	0.256	0.77	2174
CH4	0.25" Cyl.	9.21	55	55	602	11.17	0.237	0.81	2228
CH4	0.25" Cyl.	9.24	63	63	602	12.86	0.271	0.82	2237
CH4	0.25" Cyl.	9.35	64	64	606	11.47	0.281	0.70	2067
CH4	0.25" Cyl.	9.75	73	73	603	14.02	0.333	0.72	2099
CH4	0.25" Cyl.	5.31	62	62	610	5.66	0.154	0.63	1958
CH4	0.25" Cyl.	5.21	59	59	607	5.77	0.142	0.70	2060
CH4	0.25" Cyl.	5.20	60	60	608	5.43	0.146	0.64	1969
CH4	0.25" Cyl.	5.28	58	58	605	5.99	0.144	0.72	2089
CH4	0.25" Cyl.	5.12	69	69	608	6.64	0.163	0.70	2064
CH4	0.25" Cyl.	5.46	69	69	605	7.44	0.177	0.72	2101
CH4	0.25" Cyl.	5.16	68	68	606	6.74	0.163	0.71	2078
CH4	0.25" Cyl.	5.19	69	69	604	6.90	0.167	0.71	2081
CH4	0.25" Cyl.	5.30	76	76	606	8.33	0.187	0.76	2161

CH4	0.25" Cyl.	5.34	79	79	606	8.13	0.197	0.71	2080
CH4	0.25" Cyl.	5.24	78	78	606	8.42	0.189	0.77	2165
CH4	0.25" Cyl.	5.66	84	84	601	9.67	0.223	0.75	2131
CH4	0.25" Cyl.	5.73	80	80	596	9.58	0.215	0.77	2157
CH4	0.25" Cyl.	5.81	80	80	594	9.98	0.220	0.78	2175
CH4	0.25" Cyl.	6.76	44	44	598	6.44	0.138	0.80	2210
CH4	0.25" Cyl.	6.85	43	43	605	5.69	0.136	0.72	2091
CH4	0.25" Cyl.	6.84	42	42	611	4.84	0.135	0.62	1930
CH4	0.25" Cyl.	6.98	52	52	596	8.26	0.170	0.83	2255
CH4	0.25" Cyl.	7.10	52	52	595	8.21	0.174	0.81	2222
CH4	0.25" Cyl.	7.22	51	51	601	7.69	0.174	0.76	2153
CH4	0.25" Cyl.	6.90	51	51	599	7.76	0.164	0.81	2226
CH4	0.25" Cyl.	7.04	61	61	606	9.05	0.198	0.78	2193
CH4	0.25" Cyl.	7.11	61	61	606	8.69	0.202	0.74	2124
CH4	0.25" Cyl.	7.24	59	59	605	8.34	0.198	0.72	2102
CH4	0.25" Cyl.	7.27	70	70	613	8.39	0.236	0.61	1924
CH4	0.25" Cyl.	3.02	42	42	298	6.92	0.118	1.01	2252
CH4	0.25" Cyl.	3.12	44	44	297	6.61	0.129	0.88	2118
CH4	0.25" Cyl.	3.04	42	42	297	6.94	0.119	1.00	2249
CH4	0.25" Cyl.	3.18	56	56	298	8.93	0.164	0.93	2187
CH4	0.25" Cyl.	3.11	56	56	296	8.55	0.164	0.89	2135
CH4	0.25" Cyl.	3.27	63	63	296	10.80	0.193	0.96	2217
CH4	0.25" Cyl.	6.84	43	43	613	4.92	0.136	0.62	1942
CH4	0.25" Cyl.	6.90	42	42	612	4.40	0.136	0.56	1829
CH4	0.25" Cyl.	7.04	45	45	608	5.59	0.149	0.64	1975
CH4	0.25" Cyl.	6.96	42	42	605	5.68	0.136	0.72	2094
CH4	0.25" Cyl.	7.01	53	53	604	8.32	0.170	0.84	2270
CH4	0.25" Cyl.	7.13	51	51	605	7.55	0.169	0.77	2165
CH4	0.25" Cyl.	6.96	62	62	601	9.20	0.200	0.79	2198
CH4	0.25" Cyl.	7.02	58	58	596	9.20	0.192	0.82	2240
CH4	0.25" Cyl.	7.13	57	57	597	8.68	0.190	0.78	2186
CH4	0.25" Cyl.	7.18	68	68	599	10.15	0.228	0.77	2162
CH4	0.25" Cyl.	7.25	68	68	598	10.30	0.231	0.77	2164
CH4	0.25" Cyl.	7.09	69	69	601	9.89	0.229	0.74	2125
CH4	0.25" Cyl.	7.25	76	76	601	11.15	0.258	0.74	2129

CH4	0.25" Cyl.	7.21	75	75	602	10.74	0.252	0.73	2111
CH4	0.25" Cyl.	7.54	84	84	600	12.31	0.300	0.71	2070
CH4	0.25" Cyl.	7.82	77	77	592	12.13	0.287	0.73	2095
CH4	0.25" Cyl.	5.04	22	22	509	3.23	0.060	0.92	2302
CH4	0.25" Cyl.	5.03	23	23	510	3.25	0.062	0.90	2286
CH4	0.25" Cyl.	5.09	23	23	508	3.39	0.062	0.94	2319
CH4	0.25" Cyl.	5.10	29	29	506	4.27	0.082	0.89	2267
CH4	0.25" Cyl.	4.88	29	29	502	4.37	0.078	0.96	2338
CH4	0.25" Cyl.	5.23	31	31	501	5.51	0.089	1.07	2368
CH4	0.25" Cyl.	5.03	28	28	502	4.46	0.078	0.99	2360
CH4	0.25" Cyl.	5.19	43	43	502	6.09	0.125	0.84	2193
CH4	0.25" Cyl.	4.93	43	43	500	5.72	0.118	0.84	2190
CH4	0.25" Cyl.	4.88	45	45	500	5.60	0.123	0.78	2110
CH4	0.25" Cyl.	5.15	53	53	504	7.77	0.149	0.90	2272
CH4	0.25" Cyl.	5.13	53	53	504	7.54	0.150	0.86	2230
CH4	0.25" Cyl.	4.95	56	56	503	7.67	0.154	0.85	2218
CH4	0.25" Cyl.	6.70	25	25	499	4.57	0.094	0.84	2196
CH4	0.25" Cyl.	6.82	27	27	497	5.13	0.102	0.86	2224
CH4	0.25" Cyl.	6.81	26	26	496	4.87	0.099	0.84	2201
CH4	0.25" Cyl.	6.52	24	24	490	4.78	0.088	0.94	2315
CH4	0.25" Cyl.	6.75	34	34	497	6.74	0.128	0.90	2281
CH4	0.25" Cyl.	6.94	32	32	497	6.53	0.122	0.92	2301
CH4	0.25" Cyl.	6.71	31	31	499	5.88	0.116	0.87	2239
CH4	0.25" Cyl.	6.88	41	41	507	7.62	0.154	0.85	2216
CH4	0.25" Cyl.	6.63	41	41	504	7.58	0.150	0.87	2243
CH4	0.25" Cyl.	6.59	42	42	506	7.64	0.153	0.86	2227
CH4	0.25" Cyl.	6.89	50	50	505	9.68	0.191	0.87	2246
CH4	0.25" Cyl.	6.84	50	50	498	9.70	0.190	0.88	2247

Natural Gas – Reverse Step

Fuel	Feature	Absolute Pressure (atm)	Mix. Vel. (m/s)	Edge Velocity (m/s)	Mix. Temp. (K)	Fuel Flow (g/s)	Air Flow (kg/s)	Equivalence Ratio	Adiabatic Flame Temp. (K)
CH4	Step	3.04	63	63	500	5.65	0.106	0.92	2289
CH4	Step	3.06	61	61	500	5.60	0.104	0.93	2295
CH4	Step	3.09	63	63	504	5.47	0.107	0.88	2241
CH4	Step	3.13	68	68	504	5.61	0.119	0.81	2155
CH4	Step	3.07	71	71	508	5.74	0.120	0.82	2177
CH4	Step	3.21	71	71	509	6.22	0.124	0.86	2229
CH4	Step	3.07	69	69	510	6.19	0.116	0.92	2295
CH4	Step	5.05	54	54	509	7.44	0.149	0.86	2229
CH4	Step	5.15	53	53	510	7.27	0.150	0.83	2195
CH4	Step	5.13	53	53	510	7.29	0.150	0.84	2199
CH4	Step	5.27	65	65	506	9.17	0.190	0.83	2187
CH4	Step	5.36	63	63	506	9.23	0.186	0.85	2219
CH4	Step	5.33	62	62	507	8.92	0.183	0.84	2197
CH4	Step	5.12	63	63	507	8.36	0.178	0.81	2156
CH4	Step	5.14	71	71	502	9.47	0.205	0.79	2133
CH4	Step	5.24	71	71	502	9.76	0.207	0.81	2153
CH4	Step	5.29	72	72	503	9.79	0.212	0.79	2135
CH4	Step	5.50	75	75	503	10.60	0.230	0.79	2131
CH4	Step	5.24	83	83	509	11.26	0.238	0.81	2163
CH4	Step	5.29	81	81	507	11.02	0.237	0.80	2146
CH4	Step	5.35	82	82	509	11.24	0.240	0.80	2151
CH4	Step	5.29	87	87	508	11.69	0.254	0.79	2131
CH4	Step	5.37	87	87	508	11.66	0.260	0.77	2104
CH4	Step	5.28	90	90	507	11.99	0.262	0.78	2123
CH4	Step	3.30	77	77	497	6.94	0.142	0.84	2189
CH4	Step	3.38	76	76	506	6.93	0.142	0.84	2196
CH4	Step	3.43	76	76	508	7.04	0.144	0.84	2202
CH4	Step	3.17	72	72	498	6.37	0.127	0.86	2218
CH4	Step	3.09	75	75	497	6.10	0.130	0.81	2144
CH4	Step	3.21	79	79	499	6.96	0.141	0.85	2201
CH4	Step	3.13	84	84	499	6.92	0.147	0.81	2148
CH4	Step	3.12	80	80	499	7.01	0.140	0.86	2222
CH4	Step	3.22	90	90	508	7.81	0.159	0.84	2200
CH4	Step	3.18	92	92	509	7.53	0.160	0.81	2155
CH4	Step	3.14	92	92	508	7.43	0.160	0.80	2144
CH4	Step	3.19	91	91	508	7.43	0.160	0.80	2143
CH4	Step	3.28	95	95	505	8.17	0.172	0.81	2161
CH4	Step	3.28	98	98	503	8.17	0.179	0.79	2118

CH4	Step	3.19	101	101	505	8.10	0.180	0.78	2105
CH4	Step	3.14	97	97	501	8.01	0.171	0.81	2147
CH4	Step	3.06	54	54	501	5.50	0.090	1.05	2361
CH4	Step	3.05	61	61	508	4.74	0.102	0.80	2136
CH4	Step	3.12	55	55	508	4.53	0.094	0.82	2177
CH4	Step	5.06	42	42	505	5.90	0.118	0.86	2224
CH4	Step	5.14	42	42	505	5.79	0.118	0.84	2205
CH4	Step	5.05	42	42	506	5.73	0.116	0.85	2210
CH4	Step	7.00	42	42	504	8.25	0.164	0.87	2238
CH4	Step	7.11	42	42	504	8.14	0.163	0.86	2226
CH4	Step	7.11	41	41	504	8.16	0.162	0.86	2233
CH4	Step	7.14	43	43	505	8.38	0.170	0.84	2210
CH4	Step	7.25	79	79	507	14.13	0.319	0.76	2088
CH4	Step	7.83	81	81	505	16.21	0.354	0.79	2126
CH4	Step	8.13	79	79	507	15.62	0.358	0.75	2072
CH4	Step	8.61	79	79	505	16.82	0.377	0.77	2096
CH4	Step	9.12	42	42	504	11.04	0.212	0.90	2280
CH4	Step	9.53	39	39	504	10.40	0.205	0.87	2248
CH4	Step	9.48	42	42	506	9.86	0.222	0.76	2094
CH4	Step	9.26	48	48	506	11.89	0.245	0.83	2194
CH4	Step	9.20	62	62	501	15.24	0.317	0.83	2180
CH4	Step	9.25	67	67	502	15.54	0.349	0.76	2091
CH4	Step	9.35	56	56	498	14.87	0.291	0.88	2251
CH4	Step	6.74	55	55	502	9.81	0.205	0.82	2172
CH4	Step	6.80	56	56	503	9.65	0.210	0.79	2127
CH4	Step	6.81	55	55	504	9.80	0.207	0.81	2164
CH4	Step	7.27	51	51	502	9.84	0.207	0.82	2168
CH4	Step	7.04	64	64	503	11.56	0.252	0.79	2127
CH4	Step	7.12	63	63	504	11.27	0.248	0.78	2115
CH4	Step	7.04	63	63	502	11.21	0.248	0.78	2110
CH4	Step	7.09	64	64	504	11.60	0.251	0.79	2133
CH4	Step	7.26	71	71	505	12.94	0.287	0.78	2108
CH4	Step	7.22	70	70	503	12.99	0.280	0.80	2140
CH4	Step	8.31	71	71	504	14.31	0.330	0.75	2061
CH4	Step	7.95	73	73	503	14.36	0.323	0.76	2091
CH4	Step	3.03	52	52	595	3.25	0.075	0.74	2117
CH4	Step	3.18	52	52	589	3.72	0.078	0.82	2218
CH4	Step	3.13	53	53	580	4.51	0.079	0.99	2388
CH4	Step	3.14	70	70	595	4.65	0.104	0.77	2162
CH4	Step	3.04	70	70	596	4.40	0.100	0.76	2140
CH4	Step	3.06	70	70	597	4.53	0.101	0.77	2160
CH4	Step	5.38	101	101	605	10.05	0.255	0.68	2027
CH4	Step	5.41	101	101	605	10.30	0.256	0.69	2048

CH4	Step	5.26	96	96	602	10.17	0.237	0.74	2122
CH4	Step	3.20	79	79	601	5.80	0.116	0.86	2277
CH4	Step	3.18	82	82	605	5.68	0.120	0.81	2226
CH4	Step	3.19	86	86	607	5.55	0.127	0.75	2136
CH4	Step	3.19	93	93	602	6.82	0.138	0.85	2274
CH4	Step	3.13	90	90	601	6.13	0.131	0.81	2213
CH4	Step	3.05	90	90	600	5.93	0.129	0.79	2192
CH4	Step	3.24	98	98	597	6.73	0.149	0.78	2170
CH4	Step	3.23	95	95	593	6.87	0.144	0.82	2225
CH4	Step	5.06	55	55	597	5.62	0.131	0.74	2116
CH4	Step	5.25	50	50	592	6.24	0.123	0.87	2295
CH4	Step	5.10	64	64	603	6.68	0.153	0.75	2139
CH4	Step	5.24	63	63	604	6.71	0.154	0.75	2137
CH4	Step	4.94	73	73	606	7.28	0.166	0.75	2144
CH4	Step	5.36	70	70	598	8.42	0.174	0.83	2249
CH4	Step	5.06	71	71	598	7.21	0.170	0.73	2105
CH4	Step	5.07	79	79	591	9.07	0.188	0.83	2244
CH4	Step	5.20	79	79	594	8.73	0.195	0.77	2163
CH4	Step	5.21	79	79	591	8.72	0.196	0.77	2154
CH4	Step	5.20	90	90	593	9.81	0.221	0.76	2152
CH4	Step	5.16	88	88	590	9.71	0.217	0.77	2158
CH4	Step	5.30	92	92	595	9.44	0.230	0.70	2064
CH4	Step	5.06	66	66	666	5.62	0.142	0.68	2078
CH4	Step	4.96	66	66	663	6.18	0.139	0.76	2198
CH4	Step	4.90	65	65	659	5.51	0.137	0.69	2094
CH4	Step	4.92	76	76	660	7.00	0.160	0.75	2178
CH4	Step	5.22	78	78	663	8.02	0.173	0.80	2249
CH4	Step	5.19	79	79	664	7.73	0.172	0.77	2213
CH4	Step	5.31	89	89	663	8.83	0.202	0.75	2185
CH4	Step	5.34	90	90	658	8.79	0.205	0.74	2158
CH4	Step	5.18	78	78	643	8.29	0.175	0.81	2255
CH4	Step	5.22	80	80	649	8.52	0.179	0.82	2266
CH4	Step	5.26	80	80	649	8.39	0.181	0.80	2238
CH4	Step	7.07	63	63	658	8.24	0.191	0.74	2170
CH4	Step	7.03	60	60	657	8.17	0.180	0.78	2223
CH4	Step	7.14	59	59	654	8.29	0.179	0.79	2240
CH4	Step	7.02	70	70	671	9.09	0.206	0.76	2202
CH4	Step	7.12	68	68	665	10.05	0.202	0.86	2329
CH4	Step	7.13	73	73	672	9.62	0.219	0.76	2199
CH4	Step	7.54	73	73	652	10.27	0.237	0.74	2167
CH4	Step	7.26	40	40	599	6.90	0.135	0.88	2315
CH4	Step	7.22	40	40	600	6.40	0.136	0.81	2225
CH4	Step	6.99	42	42	596	6.66	0.136	0.84	2267

CH4	Step	7.03	43	43	601	6.83	0.140	0.84	2265
CH4	Step	6.98	42	42	612	4.84	0.136	0.61	1925
CH4	Step	5.30	86	86	673	8.54	0.190	0.77	2219
CH4	Step	5.35	83	83	672	8.65	0.185	0.80	2263
CH4	Step	5.24	87	87	675	8.40	0.190	0.76	2203
CH4	Step	5.42	97	97	679	9.14	0.218	0.72	2148
CH4	Step	5.35	94	94	675	9.55	0.210	0.78	2236
CH4	Step	5.40	96	96	676	9.51	0.215	0.76	2207
CH4	Step	5.30	78	78	670	7.63	0.174	0.75	2192
CH4	Step	5.25	76	76	672	7.44	0.166	0.77	2215
CH4	Step	5.17	69	69	680	5.96	0.149	0.69	2097
CH4	Step	5.25	66	66	673	6.69	0.144	0.80	2254
CH4	Step	5.14	66	66	673	6.31	0.142	0.76	2209
CH4	Step	7.40	51	51	682	6.54	0.158	0.71	2143
CH4	Step	7.18	49	49	675	6.57	0.145	0.78	2232
CH4	Step	7.12	49	49	675	6.35	0.146	0.75	2192
CH4	Step	7.15	50	50	666	7.73	0.148	0.90	2378
CH4	Step	7.27	54	54	680	7.16	0.163	0.75	2202
CH4	Step	7.08	58	58	679	7.24	0.170	0.73	2168
CH4	Step	7.07	60	60	684	6.68	0.177	0.65	2043
CH4	Step	6.99	68	68	679	7.99	0.197	0.70	2117
CH4	Step	7.29	70	70	668	8.47	0.217	0.67	2064
CH4	Step	7.13	64	64	661	8.25	0.195	0.73	2149
CH4	Step	7.22	76	76	681	9.46	0.229	0.71	2139
CH4	Step	7.33	81	81	684	10.06	0.245	0.70	2131
CH4	Step	7.36	82	82	657	10.51	0.260	0.70	2097
CH4	Step	7.33	79	79	663	10.19	0.246	0.71	2127
CH4	Step	7.34	85	85	675	10.31	0.260	0.68	2086
CH4	Step	8.28	51	51	674	7.50	0.177	0.73	2160
CH4	Step	8.32	49	49	670	7.33	0.172	0.73	2165
CH4	Step	8.25	44	44	669	6.68	0.154	0.74	2178
CH4	Step	7.02	54	54	617	7.26	0.175	0.71	2094
CH4	Step	6.98	54	54	609	8.11	0.174	0.80	2221
CH4	Step	7.12	52	52	611	7.77	0.170	0.78	2197
CH4	Step	8.44	64	64	676	9.42	0.227	0.71	2141
CH4	Step	8.19	67	67	679	9.44	0.229	0.71	2135
CH4	Step	7.97	65	65	685	8.81	0.215	0.70	2129
CH4	Step	7.23	62	62	607	8.97	0.209	0.74	2124
CH4	Step	7.10	62	62	599	9.45	0.206	0.79	2193
CH4	Step	7.14	61	61	604	8.91	0.203	0.76	2150
CH4	Step	7.29	76	76	599	11.02	0.262	0.72	2097
CH4	Step	7.32	75	75	604	10.74	0.255	0.72	2100
CH4	Step	7.62	88	88	611	12.37	0.309	0.69	2049

CH4	Step	7.82	85	85	606	12.64	0.309	0.70	2068
CH4	Step	8.37	46	46	597	8.88	0.180	0.85	2277
CH4	Step	8.34	44	44	597	7.80	0.172	0.78	2178
CH4	Step	8.21	45	45	592	8.29	0.173	0.82	2238
CH4	Step	8.22	56	56	599	9.50	0.218	0.75	2138
CH4	Step	8.48	57	57	603	10.61	0.226	0.81	2223
CH4	Step	8.41	70	70	606	11.62	0.275	0.73	2107

Natural Gas – Rotated Airfoil and 0.50 Inch cylinder

Fuel	Feature	Absolute Pressure (atm)	Mix. Vel. (m/s)	Edge Velocity (m/s)	Mix. Temp. (K)	Fuel Flow (g/s)	Air Flow (kg/s)	Equivalence Ratio	Adiabatic Flame Temp. (K)
CH4	Rtd. Airfoil	5.28	51	51	594	5.86	0.126	0.80	2201
CH4	Rtd. Airfoil	5.13	50	50	587	6.07	0.120	0.87	2288
CH4	Rtd. Airfoil	5.12	48	48	588	5.82	0.117	0.86	2276
CH4	Rtd. Airfoil	5.13	49	49	588	5.94	0.118	0.86	2282
CH4	Rtd. Airfoil	5.27	58	58	597	6.63	0.142	0.80	2208
CH4	Rtd. Airfoil	5.28	60	60	597	7.21	0.148	0.84	2262
CH4	Rtd. Airfoil	5.19	56	56	594	7.06	0.136	0.89	2324
CH4	Rtd. Airfoil	5.09	57	57	597	6.76	0.136	0.85	2278
CH4	Rtd. Airfoil	5.22	67	67	606	7.73	0.160	0.83	2255
CH4	Rtd. Airfoil	5.24	67	67	603	8.38	0.161	0.89	2330
CH4	Rtd. Airfoil	5.22	69	69	605	8.53	0.166	0.88	2321
CH4	Rtd. Airfoil	5.45	69	69	605	9.23	0.171	0.92	2365
CH4	Rtd. Airfoil	5.46	74	74	588	9.65	0.191	0.87	2290
CH4	Rtd. Airfoil	5.30	75	75	601	9.03	0.185	0.84	2262
CH4	Rtd. Airfoil	4.17	61	61	597	6.03	0.118	0.88	2307
CH4	Rtd. Airfoil	4.09	61	61	591	6.24	0.117	0.92	2342
CH4	Rtd. Airfoil	4.30	72	72	599	6.50	0.144	0.77	2171
CH4	Rtd. Airfoil	4.09	71	71	595	6.44	0.136	0.81	2221
CH4	Rtd. Airfoil	4.16	74	74	596	6.87	0.145	0.82	2225
CH4	Rtd. Airfoil	4.19	70	70	594	6.88	0.138	0.85	2275
CH4	Rtd. Airfoil	4.29	77	77	594	7.70	0.154	0.86	2279
CH4	Rtd. Airfoil	4.48	78	78	597	7.87	0.164	0.83	2241
CH4	0.50" Cyl.	5.21	58	58	596	6.20	0.143	0.74	2125
CH4	0.50" Cyl.	5.26	57	57	592	6.91	0.141	0.84	2258
CH4	0.50" Cyl.	5.15	61	61	587	7.55	0.150	0.86	2286
CH4	0.50" Cyl.	5.26	58	58	585	7.68	0.145	0.91	2340
CH4	0.50" Cyl.	5.25	72	72	594	8.79	0.178	0.85	2273
CH4	0.50" Cyl.	5.43	73	73	592	9.30	0.188	0.85	2274
CH4	0.50" Cyl.	5.26	72	72	590	9.08	0.179	0.87	2295
CH4	0.50" Cyl.	5.34	73	73	592	8.90	0.184	0.83	2247
CH4	0.50" Cyl.	5.41	79	79	598	9.69	0.199	0.84	2258
CH4	0.50" Cyl.	5.34	81	81	595	10.40	0.203	0.88	2312
CH4	0.50" Cyl.	5.60	78	78	595	10.01	0.204	0.84	2261
CH4	0.50" Cyl.	5.35	77	77	594	9.68	0.192	0.86	2290
CH4	0.50" Cyl.	5.34	86	86	604	9.96	0.214	0.80	2212
CH4	0.50" Cyl.	5.69	81	81	599	10.06	0.215	0.80	2214
CH4	0.50" Cyl.	5.85	80	80	603	9.73	0.218	0.77	2162
CH4	0.50" Cyl.	5.80	78	78	600	10.22	0.212	0.83	2249

CH4	0.50" Cyl.	5.41	91	91	607	10.68	0.227	0.81	2226
CH4	0.50" Cyl.	5.47	92	92	605	10.98	0.232	0.81	2230
CH4	0.50" Cyl.	5.39	91	91	605	10.96	0.227	0.83	2252
CH4	0.50" Cyl.	5.47	91	91	602	11.22	0.231	0.83	2257
CH4	0.50" Cyl.	5.35	96	96	612	9.87	0.237	0.72	2094

Hydrogen – 0.25 Inch Cylinder

Fuel	Feature	Absolute Pressure (atm)	Mix. Vel. (m/s)	Edge Velocity (m/s)	Mix. Temp. (K)	Fuel Flow (g/s)	Air Flow (kg/s)	Equivalence Ratio	Adiabatic Flame Temp. (K)
H2	0.25" Cyl.	3.03	57	57	502	0.88	0.091	0.33	1439
H2	0.25" Cyl.	3.03	56	56	502	0.85	0.091	0.32	1419
H2	0.25" Cyl.	3.10	56	56	500	0.84	0.093	0.31	1390
H2	0.25" Cyl.	3.01	58	58	501	0.86	0.093	0.32	1411
H2	0.25" Cyl.	3.06	63	63	509	0.79	0.103	0.26	1282
H2	0.25" Cyl.	3.11	71	71	506	1.00	0.117	0.29	1357
H2	0.25" Cyl.	3.00	65	65	499	1.14	0.103	0.38	1553
H2	0.25" Cyl.	3.18	63	63	506	0.92	0.106	0.30	1361
H2	0.25" Cyl.	2.95	65	65	503	0.93	0.103	0.31	1390
H2	0.25" Cyl.	2.99	73	73	512	0.94	0.116	0.28	1327
H2	0.25" Cyl.	3.08	77	77	507	1.10	0.126	0.30	1370
H2	0.25" Cyl.	3.09	72	72	503	1.12	0.119	0.32	1425
H2	0.25" Cyl.	3.09	71	71	503	1.11	0.116	0.33	1432
H2	0.25" Cyl.	3.06	85	85	505	1.28	0.138	0.32	1409
H2	0.25" Cyl.	3.26	84	84	505	1.35	0.146	0.32	1414
H2	0.25" Cyl.	3.10	88	88	511	1.16	0.145	0.27	1308
H2	0.25" Cyl.	3.11	96	96	506	1.49	0.158	0.32	1428
H2	0.25" Cyl.	3.15	96	96	503	1.52	0.161	0.32	1426
H2	0.25" Cyl.	3.21	94	94	503	1.47	0.161	0.31	1400
H2	0.25" Cyl.	3.15	107	107	502	1.67	0.180	0.32	1410
H2	0.25" Cyl.	3.18	106	106	504	1.63	0.180	0.31	1395
H2	0.25" Cyl.	3.13	109	109	501	1.75	0.181	0.33	1443
H2	0.25" Cyl.	3.07	107	107	501	1.67	0.175	0.33	1430
H2	0.25" Cyl.	5.06	47	47	541	1.05	0.119	0.30	1410
H2	0.25" Cyl.	5.14	46	46	530	1.06	0.121	0.30	1394
H2	0.25" Cyl.	5.06	46	46	529	1.00	0.121	0.29	1354
H2	0.25" Cyl.	5.03	56	56	511	1.27	0.148	0.29	1360
H2	0.25" Cyl.	5.20	54	54	513	1.28	0.148	0.30	1366
H2	0.25" Cyl.	4.99	56	56	515	1.19	0.148	0.28	1320
H2	0.25" Cyl.	4.90	64	64	507	1.38	0.168	0.28	1330
H2	0.25" Cyl.	5.23	74	74	500	1.85	0.207	0.31	1381
H2	0.25" Cyl.	5.33	74	74	501	1.77	0.213	0.29	1329
H2	0.25" Cyl.	5.06	75	75	502	1.66	0.205	0.28	1315
H2	0.25" Cyl.	5.12	84	84	504	2.01	0.231	0.30	1365
H2	0.25" Cyl.	3.11	46	46	317	1.20	0.120	0.35	1315
H2	0.25" Cyl.	3.07	45	45	308	1.20	0.120	0.34	1301
H2	0.25" Cyl.	3.06	46	46	313	1.19	0.120	0.34	1301
H2	0.25" Cyl.	2.97	85	85	601	0.97	0.114	0.29	1436
H2	0.25" Cyl.	3.06	86	86	603	0.96	0.118	0.28	1402
H2	0.25" Cyl.	3.17	103	103	593	1.29	0.148	0.30	1443
H2	0.25" Cyl.	3.05	103	103	602	1.14	0.142	0.28	1394
H2	0.25" Cyl.	3.08	104	104	602	1.20	0.145	0.29	1418

H2	0.25" Cyl.	5.02	63	63	624	0.80	0.143	0.19	1201
H2	0.25" Cyl.	5.09	63	63	609	1.15	0.143	0.28	1402
H2	0.25" Cyl.	5.14	80	80	618	1.23	0.183	0.23	1295
H2	0.25" Cyl.	5.03	89	89	606	1.28	0.206	0.21	1240
H2	0.25" Cyl.	2.97	88	88	613	0.93	0.116	0.28	1401
H2	0.25" Cyl.	2.97	91	91	613	0.96	0.120	0.28	1403
H2	0.25" Cyl.	3.08	99	99	613	1.10	0.135	0.28	1416
H2	0.25" Cyl.	3.00	98	98	613	1.03	0.131	0.27	1391
H2	0.25" Cyl.	3.04	101	101	614	1.10	0.136	0.28	1409
H2	0.25" Cyl.	3.03	101	101	616	1.03	0.136	0.26	1367
H2	0.25" Cyl.	3.13	99	99	593	1.24	0.141	0.30	1453
H2	0.25" Cyl.	3.13	96	96	581	1.23	0.140	0.30	1441
H2	0.25" Cyl.	3.02	104	104	589	1.22	0.144	0.29	1416

Hydrogen – Reverse Step

Fuel	Feature	Absolute Pressure (atm)	Mix. Vel. (m/s)	Edge Velocity (m/s)	Mix. Temp. (K)	Fuel Flow (g/s)	Air Flow (kg/s)	Equivalence Ratio	Adiabatic Flame Temp. (K)
H2	Step	3.15	80	80	492	1.33	0.136	0.34	1447
H2	Step	3.12	84	84	503	1.43	0.137	0.36	1503
H2	Step	4.84	53	53	497	1.21	0.139	0.30	1356
H2	Step	4.79	55	55	502	1.12	0.144	0.27	1286
H2	Step	5.23	56	56	505	1.43	0.154	0.32	1413
H2	Step	4.91	66	66	500	1.74	0.172	0.35	1475
H2	Step	4.93	66	66	502	1.51	0.174	0.30	1362
H2	Step	5.14	63	63	504	1.40	0.176	0.27	1301
H2	Step	4.88	66	66	499	1.60	0.174	0.32	1404
H2	Step	4.83	65	65	503	1.29	0.170	0.26	1273
H2	Step	5.03	78	78	499	1.77	0.212	0.29	1333
H2	Step	5.07	77	77	499	1.74	0.211	0.28	1322
H2	Step	5.11	74	74	499	1.72	0.206	0.29	1333
H2	Step	5.14	90	90	501	2.06	0.251	0.28	1319
H2	Step	5.17	90	90	500	2.06	0.252	0.28	1318
H2	Step	5.16	85	85	500	2.08	0.237	0.30	1367
H2	Step	4.97	97	97	500	2.38	0.258	0.32	1403
H2	Step	5.14	97	97	500	2.42	0.267	0.31	1392
H2	Step	4.95	96	96	500	2.42	0.253	0.33	1430
H2	Step	4.86	97	97	500	2.10	0.255	0.28	1321
H2	Step	5.33	105	105	501	2.58	0.300	0.30	1353
H2	Step	5.26	102	102	502	2.25	0.291	0.27	1283
H2	Step	5.29	101	101	502	2.50	0.286	0.30	1366
H2	Step	7.03	56	56	503	1.75	0.214	0.28	1319
H2	Step	6.87	54	54	503	1.67	0.201	0.29	1331
H2	Step	7.01	57	57	499	1.99	0.215	0.32	1409
H2	Step	3.12	84	84	506	1.41	0.136	0.36	1501
H2	Step	3.20	84	84	513	1.38	0.140	0.34	1473
H2	Step	7.06	67	67	508	2.00	0.255	0.27	1296
H2	Step	6.89	67	67	502	2.23	0.247	0.31	1390
H2	Step	7.15	67	67	504	2.23	0.256	0.30	1365
H2	Step	7.12	68	68	507	1.95	0.261	0.26	1265
H2	Step	6.90	66	66	505	2.17	0.241	0.31	1391
H2	Step	6.81	78	78	506	2.41	0.282	0.29	1354
H2	Step	6.89	73	73	506	2.14	0.271	0.27	1300
H2	Step	6.85	77	77	507	2.26	0.283	0.27	1307
H2	Step	7.04	84	84	510	2.69	0.312	0.30	1363
H2	Step	7.17	88	88	507	2.87	0.336	0.29	1353

H2	Step	7.05	87	87	508	2.49	0.330	0.26	1268
H2	Step	3.08	96	96	493	1.58	0.160	0.34	1453
H2	Step	3.19	96	96	492	1.76	0.163	0.37	1526
H2	Step	3.09	97	97	496	1.52	0.161	0.32	1418
H2	Step	3.16	98	98	498	1.61	0.167	0.33	1441
H2	Step	3.07	94	94	492	1.68	0.154	0.38	1535
H2	Step	3.24	96	96	491	1.79	0.166	0.37	1525
H2	Step	3.09	107	107	494	1.98	0.174	0.39	1572
H2	Step	3.15	104	104	496	1.87	0.174	0.37	1523
H2	Step	3.30	107	107	491	2.10	0.187	0.38	1554
H2	Step	3.09	107	107	502	1.43	0.180	0.27	1299
H2	Step	3.07	78	78	504	1.23	0.126	0.33	1448
H2	Step	3.03	71	71	499	1.23	0.112	0.38	1542
H2	Step	2.98	73	73	502	1.18	0.114	0.35	1495
H2	Step	3.15	64	64	500	1.14	0.106	0.37	1529
H2	Step	3.08	65	65	499	1.13	0.106	0.37	1518
H2	Step	3.11	70	70	501	1.11	0.115	0.33	1439
H2	Step	2.99	80	80	586	1.26	0.105	0.41	1691
H2	Step	2.96	89	89	594	0.98	0.120	0.28	1402
H2	Step	3.02	86	86	594	1.02	0.117	0.30	1440
H2	Step	3.16	83	83	592	1.07	0.119	0.31	1464
H2	Step	3.18	95	95	598	1.21	0.136	0.30	1459
H2	Step	3.04	95	95	591	1.38	0.128	0.37	1607
H2	Step	3.05	96	96	600	1.13	0.131	0.29	1438
H2	Step	3.15	97	97	596	1.27	0.136	0.32	1498
H2	Step	3.17	105	105	603	1.41	0.148	0.33	1518
H2	Step	3.11	104	104	607	1.31	0.143	0.31	1491
H2	Step	3.20	106	106	608	1.35	0.150	0.31	1478
H2	Step	4.90	60	60	609	1.07	0.130	0.28	1418
H2	Step	4.98	58	58	608	1.15	0.128	0.31	1479
H2	Step	4.93	58	58	610	1.06	0.126	0.29	1429
H2	Step	4.92	69	69	616	1.25	0.150	0.29	1434
H2	Step	4.93	65	65	614	1.24	0.140	0.30	1472
H2	Step	4.94	79	79	622	1.47	0.170	0.30	1463
H2	Step	4.92	79	79	622	1.43	0.169	0.29	1446
H2	Step	5.03	87	87	614	1.64	0.193	0.29	1444
H2	Step	5.13	91	91	613	1.76	0.206	0.29	1446
H2	Step	5.04	87	87	612	1.71	0.193	0.30	1470
H2	Step	4.99	89	89	612	1.68	0.197	0.29	1444
H2	Step	5.06	99	99	619	1.82	0.219	0.29	1434
H2	Step	4.99	98	98	621	1.79	0.213	0.29	1442
H2	Step	5.05	99	99	616	1.96	0.219	0.31	1486
H2	Step	6.87	46	46	594	1.31	0.144	0.31	1479

H2	Step	6.89	42	42	595	1.19	0.132	0.31	1467
H2	Step	7.11	45	45	596	1.22	0.145	0.29	1425
H2	Step	8.99	66	66	600	2.03	0.272	0.26	1346
H2	Step	8.62	65	65	599	1.95	0.257	0.26	1353
H2	Step	8.59	69	69	596	2.12	0.270	0.27	1375
H2	Step	8.63	68	68	596	2.10	0.270	0.27	1368
H2	Step	8.60	79	79	600	2.33	0.311	0.26	1348
H2	Step	8.84	79	79	601	2.40	0.318	0.26	1352
H2	Step	8.61	78	78	598	2.34	0.305	0.26	1360
H2	Step	9.14	87	87	605	2.48	0.362	0.24	1297
H2	Step	8.66	86	86	598	2.43	0.344	0.24	1307
H2	Step	8.66	85	85	602	2.40	0.334	0.25	1320
H2	Step	9.00	91	91	605	2.61	0.373	0.24	1307
H2	Step	8.87	90	90	598	2.76	0.364	0.26	1353
H2	Step	9.05	94	94	599	2.83	0.390	0.25	1324
H2	Step	9.11	88	88	595	2.84	0.366	0.27	1365
H2	Step	9.44	97	97	596	3.16	0.419	0.26	1347
H2	Step	6.92	58	58	607	1.38	0.180	0.26	1367
H2	Step	6.90	57	57	611	1.42	0.174	0.28	1414
H2	Step	6.81	57	57	613	1.37	0.174	0.27	1391
H2	Step	6.85	57	57	613	1.40	0.173	0.28	1408
H2	Step	6.96	56	56	612	1.42	0.174	0.28	1413
H2	Step	6.90	66	66	621	1.56	0.201	0.27	1386
H2	Step	7.15	70	70	622	1.69	0.220	0.26	1380
H2	Step	6.97	65	65	620	1.58	0.197	0.27	1406
H2	Step	6.77	76	76	602	1.78	0.235	0.26	1356
H2	Step	6.89	75	75	593	1.90	0.237	0.28	1386
H2	Step	6.84	72	72	609	1.08	0.231	0.16	1097
H2	Step	6.94	83	83	593	1.96	0.265	0.25	1331
H2	Step	6.79	83	83	591	1.89	0.263	0.25	1310
H2	Step	7.10	89	89	600	2.07	0.290	0.25	1316
H2	Step	7.48	96	96	602	2.43	0.327	0.26	1343
H2	Step	7.10	89	89	605	2.04	0.288	0.24	1315
H2	Step	5.20	64	64	674	0.63	0.140	0.16	1144
H2	Step	4.91	81	81	660	1.39	0.164	0.29	1483
H2	Step	5.11	78	78	664	1.33	0.163	0.28	1458
H2	Step	5.00	92	92	674	1.60	0.183	0.30	1519
H2	Step	5.13	87	87	674	1.57	0.179	0.30	1522
H2	Step	5.05	99	99	680	1.72	0.199	0.30	1516
H2	Step	5.24	100	100	684	1.79	0.207	0.30	1517
H2	Step	5.13	99	99	683	1.77	0.200	0.30	1536
H2	Step	5.22	109	109	692	1.82	0.222	0.28	1486
H2	Step	5.19	109	109	690	1.94	0.222	0.30	1529

H2	Step	5.12	114	114	687	2.01	0.229	0.30	1532
H2	Step	8.70	64	64	700	1.59	0.217	0.25	1422
H2	Step	8.70	63	63	696	1.65	0.216	0.26	1446
H2	Step	9.08	69	69	697	1.98	0.244	0.28	1485
H2	Step	9.20	82	82	710	2.02	0.294	0.24	1390
H2	Step	8.94	83	83	708	2.26	0.287	0.27	1476
H2	Step	8.98	93	93	714	2.33	0.323	0.25	1424
H2	Step	8.86	91	91	713	2.38	0.307	0.27	1469
H2	Step	9.17	99	99	716	2.38	0.352	0.23	1388
H2	Step	8.82	90	90	710	2.21	0.307	0.25	1418
H2	Step	9.24	96	96	713	2.28	0.345	0.23	1372

Hydrogen – Neutral Airfoil, Rotated Airfoil, and 0.50 Inch Cylinder

Fuel	Feature	Absolute Pressure (atm)	Mix. Vel. (m/s)	Edge Velocity (m/s)	Mix. Temp. (K)	Fuel Flow (g/s)	Air Flow (kg/s)	Equivalence Ratio	Adiabatic Flame Temp. (K)
H2	Airfoil	3.12	68	68	503	1.30	0.110	0.41	1613
H2	Airfoil	2.96	72	72	506	1.25	0.109	0.39	1585
H2	Airfoil	3.11	71	71	515	1.11	0.114	0.33	1459
H2	Airfoil	3.01	70	70	505	1.17	0.110	0.36	1521
H2	Airfoil	5.17	59	59	511	1.54	0.159	0.33	1450
H2	Airfoil	4.96	65	65	498	1.84	0.169	0.38	1539
H2	Airfoil	5.38	69	69	508	1.69	0.199	0.29	1349
H2	Airfoil	4.86	65	65	502	1.57	0.169	0.32	1411
H2	Airfoil	5.25	63	63	495	1.86	0.176	0.36	1508
H2	Airfoil	5.08	64	64	493	1.78	0.173	0.35	1485
H2	Airfoil	4.97	72	72	493	1.94	0.193	0.35	1467
H2	Airfoil	5.16	72	72	505	1.81	0.196	0.32	1410
H2	Airfoil	5.50	82	82	504	2.33	0.237	0.34	1459
H2	Airfoil	5.11	76	76	515	1.65	0.205	0.28	1322
H2	Airfoil	3.04	89	89	497	1.56	0.143	0.38	1539
H2	Airfoil	3.22	91	91	498	1.68	0.153	0.38	1542
H2	Airfoil	3.02	88	88	491	1.75	0.140	0.43	1655
H2	Airfoil	3.12	88	88	502	1.41	0.145	0.33	1448
H2	Airfoil	3.19	88	88	492	1.75	0.147	0.41	1606
H2	Airfoil	3.12	97	97	489	1.97	0.160	0.42	1638
H2	Airfoil	3.33	102	102	488	2.15	0.180	0.41	1611
H2	Airfoil	3.06	103	103	488	2.01	0.167	0.41	1616
H2	Airfoil	3.21	100	100	489	2.10	0.169	0.43	1646
H2	Airfoil	3.24	106	106	493	2.18	0.181	0.41	1621
H2	Airfoil	4.98	44	44	508	1.05	0.116	0.31	1397
H2	Airfoil	5.20	45	45	506	1.12	0.126	0.31	1383
H2	Airfoil	5.05	57	57	499	1.67	0.149	0.38	1562
H2	Airfoil	5.02	58	58	503	1.63	0.153	0.37	1523
H2	Airfoil	5.26	66	66	598	1.50	0.154	0.33	1529
H2	Airfoil	5.15	67	67	600	1.41	0.153	0.32	1490
H2	Airfoil	4.96	75	75	603	1.63	0.163	0.34	1558
H2	Airfoil	5.12	77	77	603	1.67	0.173	0.33	1528
H2	Airfoil	5.21	76	76	605	1.74	0.174	0.34	1558
H2	Airfoil	5.07	84	84	597	1.92	0.190	0.35	1563
H2	Airfoil	5.24	84	84	592	1.95	0.198	0.34	1538
H2	Airfoil	5.17	82	82	592	1.87	0.190	0.34	1534
H2	Airfoil	5.40	88	88	590	2.17	0.214	0.35	1555
H2	Airfoil	5.55	87	87	587	2.25	0.217	0.36	1571

H2	Airfoil	5.53	88	88	589	2.15	0.219	0.34	1532
H2	Rtd. Airfoil	5.00	74	74	598	1.70	0.163	0.36	1584
H2	Rtd. Airfoil	4.92	74	74	600	1.66	0.160	0.36	1584
H2	Rtd. Airfoil	4.98	74	74	600	1.72	0.161	0.37	1608
H2	Rtd. Airfoil	5.01	84	84	587	1.95	0.190	0.35	1566
H2	Rtd. Airfoil	5.03	80	80	582	1.90	0.183	0.36	1568
H2	Rtd. Airfoil	5.62	89	89	598	2.22	0.222	0.34	1551
H2	Rtd. Airfoil	5.64	89	89	608	2.14	0.220	0.33	1540
H2	0.50" Cyl.	5.01	75	75	604	1.57	0.166	0.32	1511
H2	0.50" Cyl.	5.04	72	72	603	1.56	0.159	0.34	1539
H2	0.50" Cyl.	4.94	73	73	603	1.56	0.159	0.34	1538
H2	0.50" Cyl.	4.97	85	85	603	1.72	0.188	0.32	1491
H2	0.50" Cyl.	5.08	83	83	599	1.88	0.187	0.34	1554
H2	0.50" Cyl.	5.11	82	82	598	1.82	0.187	0.33	1529
H2	0.50" Cyl.	5.11	93	93	599	2.12	0.211	0.34	1556
H2	0.50" Cyl.	5.18	93	93	596	2.21	0.214	0.36	1580
H2	0.50" Cyl.	5.20	95	95	598	2.21	0.219	0.35	1560
H2	0.50" Cyl.	5.40	103	103	619	1.51	0.251	0.21	1232
H2	0.50" Cyl.	5.36	96	96	601	2.27	0.226	0.35	1559
H2	0.50" Cyl.	5.43	96	96	598	2.43	0.230	0.36	1597

Appendix E – Test Feature Design Drawings

Elliot Sullivan-Lewis
esl@ucicl.uci.edu
Sheet 1/1

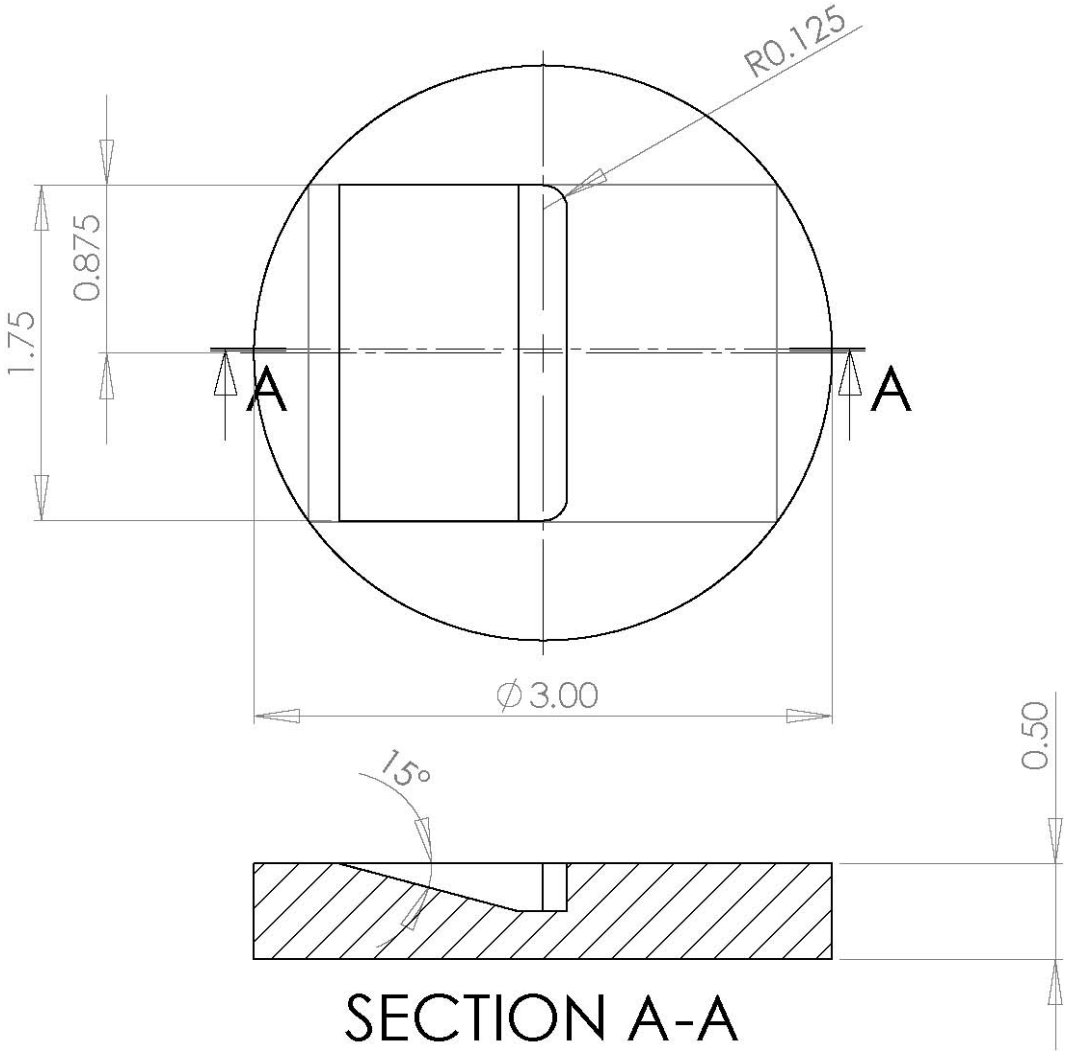

Inset Step
Scale 1:1
Tolerances are ± 0.001
Material: 304 SS
Dimensions are in inches

Elliot Sullivan-Lewis
esl@ucicl.uci.edu
Sheet 1/1

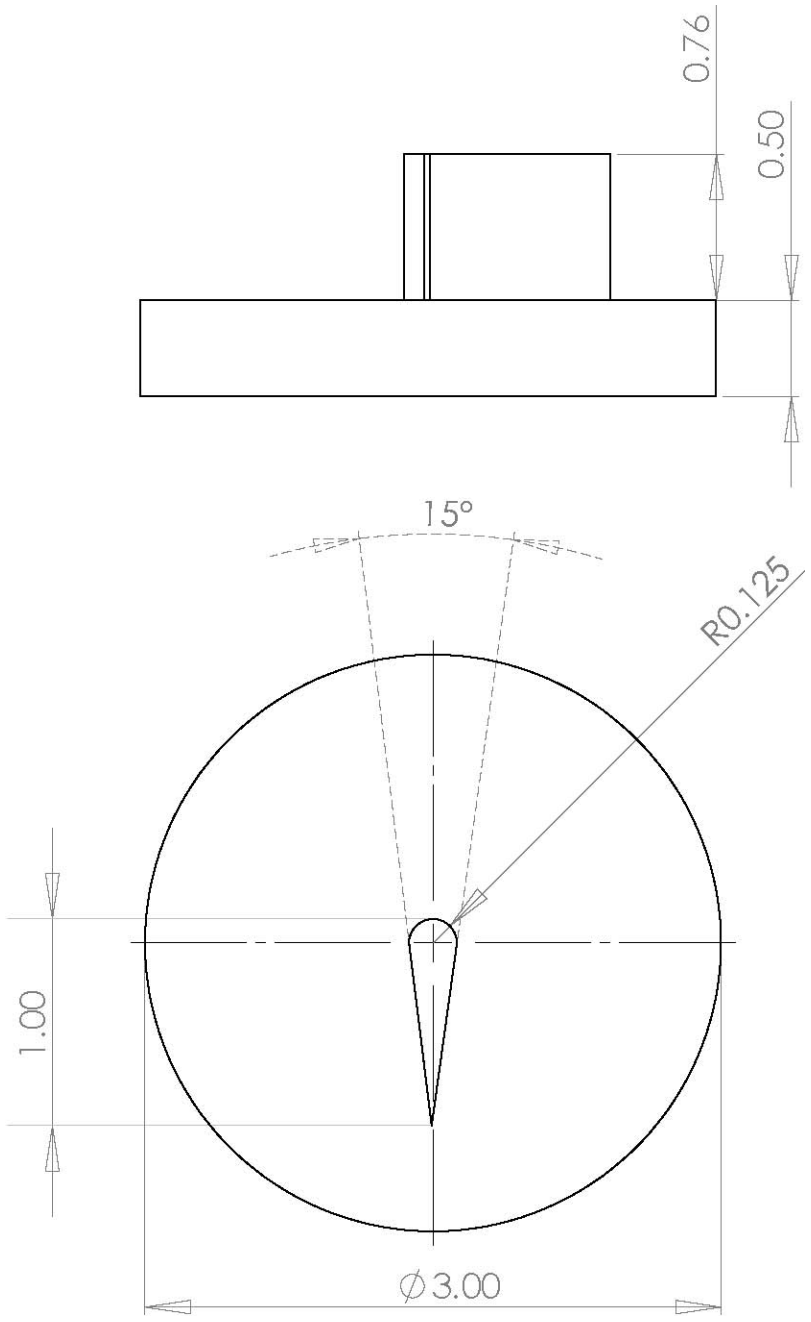

Symmetric Airfoil
Scale 1:1
Tolerances are ±0.001
Material: 304 SS
Dimensions are in inches

Elliot Sullivan-Lewis
esl@ucicl.uci.edu
Sheet 1/1

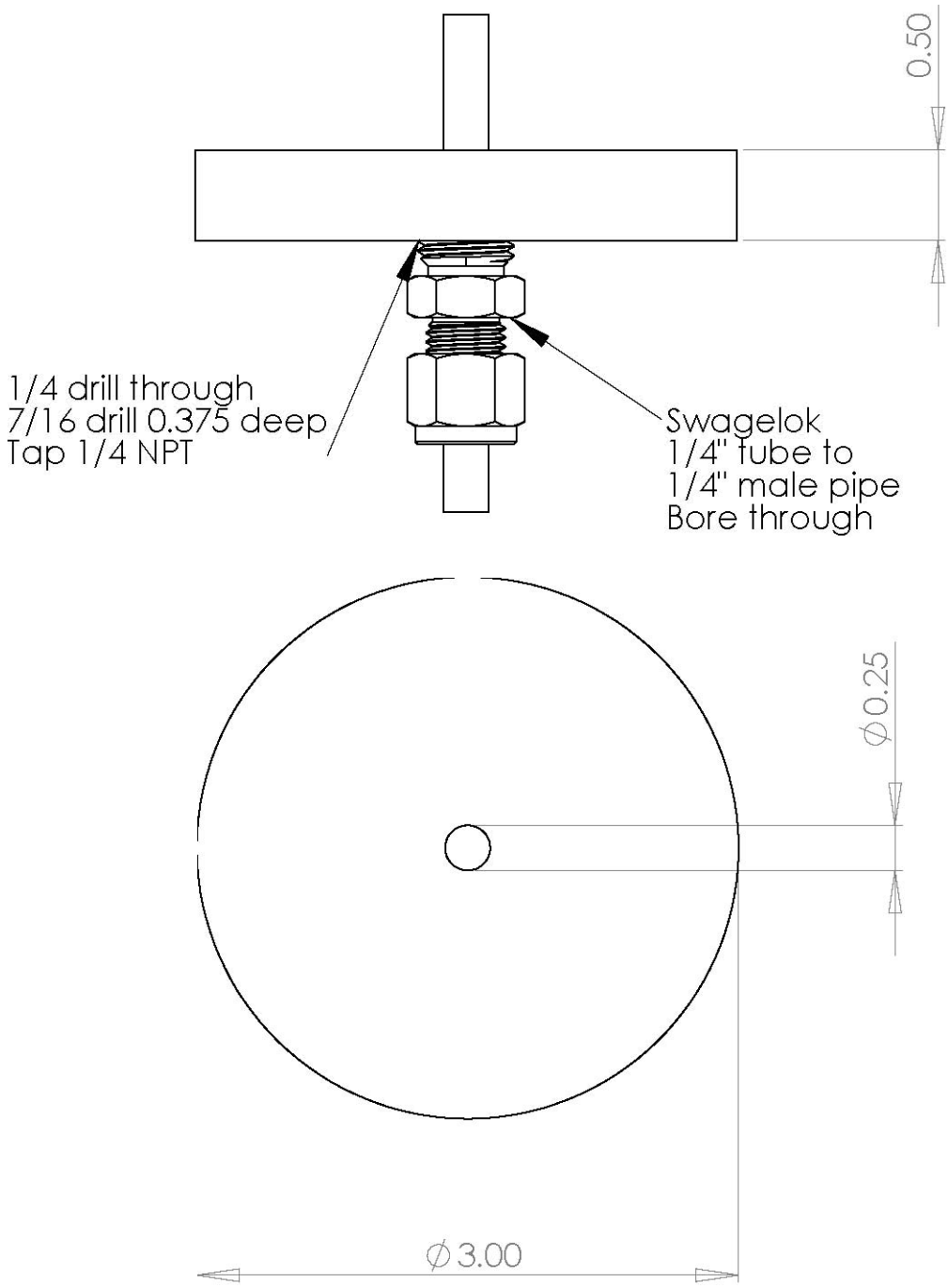

Cylinder
Scale: 1:1
Tolerances are ±0.001
Material: 304 SS
Dimensions are in inches

Elliot Sullivan-Lewis
esl@ucicl.uci.edu
Sheet 1/1

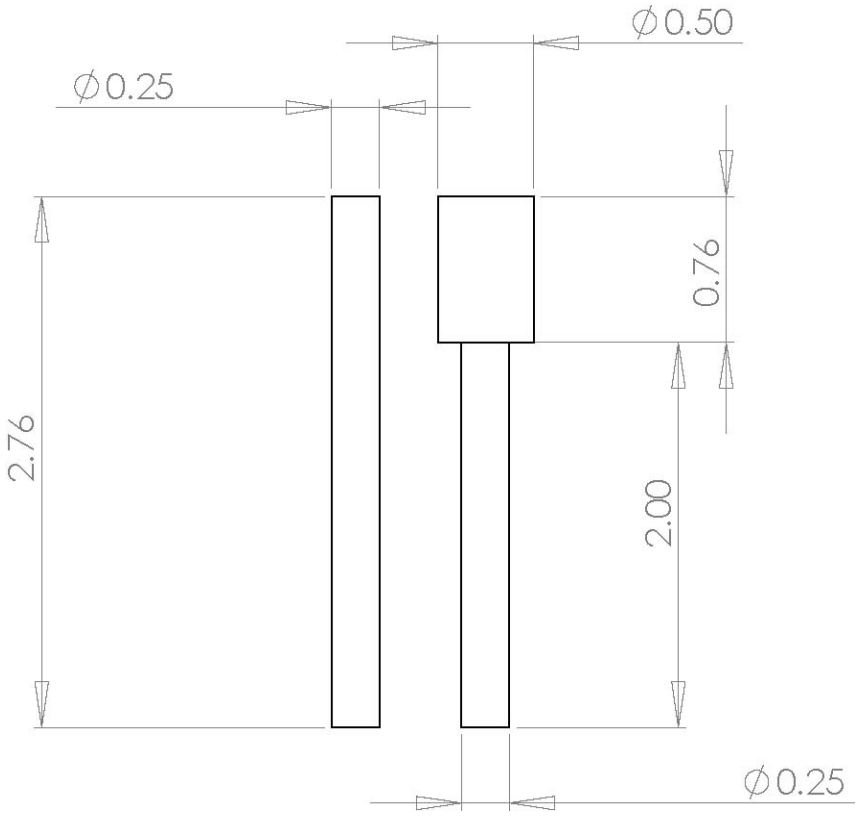

Cylindrical Flameholders
Scale: 1:1
Tolerances are ± 0.001
Material: 304 SS
Dimensions are in inches